REVIEW

Optical response of correlated electron systems

IOP Publishing Reports on Progress in Physics
Rep. Prog. Phys. **80** (2017) 026503 (31pp) doi:10.1088/1361-6633/80/2/026503

Review

Optical response of correlated electron systems

Dmitrii L Maslov[1] **and Andrey V Chubukov**[2]

[1] Department of Physics, University of Florida, PO Box 118440, Gainesville, FL 32611-8440, USA
[2] Department of Physics and William I. Fine Theoretical Physics Institute, University of Minnesota, Minneapolis, MN 55455, USA

E-mail: maslov@phys.ufl.edu and achubuko@umn.edu

Received 27 July 2016, revised 21 October 2016
Accepted for publication 28 October 2016
Published 21 December 2016

Corresponding Editor Laura Greene

Abstract

Recent progress in experimental techniques has made it possible to extract detailed information on dynamics of carriers in a correlated electron material from its optical conductivity, $\sigma(\Omega, T)$. This review consists of three parts, addressing the following three aspects of optical response: (1) the role of momentum relaxation; (2) Ω/T scaling of the optical conductivity of a Fermi-liquid metal, and (3) the optical conductivity of non-Fermi-liquid metals. In the first part (section 2), we analyze the interplay between the contributions to the conductivity from normal and umklapp electron–electron scattering. As a concrete example, we consider a two-band metal and show that although its optical conductivity is finite it does not obey the Drude formula. In the second part (sections 3 and 4), we re-visit the Gurzhi formula for the optical scattering rate, $1/\tau(\Omega, T) \propto \Omega^2 + 4\pi^2 T^2$, and show that a factor of $4\pi^2$ is the manifestation of the 'first-Matsubara-frequency rule' for boson response, which states that $1/\tau(\Omega, T)$ must vanish upon analytic continuation to the first boson Matsubara frequency. However, recent experiments show that the coefficient b in the Gurzhi-like form, $1/\tau(\Omega, T) \propto \Omega^2 + b\pi^2 T^2$, differs significantly from $b = 4$ in most of the cases. We suggest that the deviations from Gurzhi scaling may be due to the presence of elastic but energy-dependent scattering, which decreases the value of b below 4, with $b = 1$ corresponding to purely elastic scattering. In the third part (section 5), we consider the optical conductivity of metals near quantum phase transitions to nematic and spin-density-wave states. In the last case, we focus on 'composite' scattering processes, which give rise to a non-Fermi-liquid behavior of the optical conductivity at $T = 0$: $\sigma'(\Omega) \propto \Omega^{-1/3}$ at low frequencies and $\sigma'(\Omega) \propto \Omega^{-1}$ at higher frequencies. We also discuss Ω/T scaling of the conductivity and show that $\sigma'(\Omega, T)$ in the same model scales in a non-Fermi-liquid way, as $T^{4/3}\,\Omega^{-5/3}$.

Keywords: optical conductivity, non-Fermi-liquid systems, Fermi-liquid theory, quantum phase transitions

(Some figures may appear in colour only in the online journal)

1. Introduction

Optical spectroscopy of strongly correlated materials plays a crucial role in advancing our understanding of these complex systems [1, 2]. Recent progress in experimental techniques has made it possible to extract detailed information on two very important quantities: the dynamical effective mass and transport scattering rate of conduction electrons. The frequency and temperature dependences of these two quantities give one invaluable insights into the nature of the correlated electron state. A wide range of frequencies employed in optical spectroscopy allows one to extract the information both on the band structure, via studying inter-band transitions, and on dynamics of charge carriers within a given band (or several occupied bands). In this mini-review, we focus on the latter and discuss three particular aspects of intra-band optical response, which makes it distinct from other probes, such as angle-resolved photoemission (ARPES) and *dc* transport.

The first aspect is the role of momentum relaxation. Here, the optical probe occupies a special niche in between ARPES and *dc* transport. The width of the ARPES peak is given by the inverse quasiparticle relaxation time, which contains contributions from all kinds of scattering: elastic and inelastic, small- and large angle, momentum-conserving and momentum-relaxing, etc. Consequently, all sources of scattering, i.e. disorder, electron–phonon, and electron–electron (*ee*) interactions, etc contribute to the ARPES linewidth. The *dc* resistivity, on the other hand, is sensitive only to processes which are large-angle and momentum-relaxing at the same time. For *ee* interaction, a process of this type is umklapp scattering. Such scattering is effective for a sufficiently large Fermi surface (FS) [3] and not too long-range *ee* interaction [4]. However, if either of these two conditions is not satisfied, umklapp scattering is suppressed, and the *dc* resistivity is almost entirely determined by coupling of electrons to the 'sinks' of momentum, such as phonons or impurities. Note that this does not mean that *ee* interaction is weak but rather that it is of the 'wrong' type for transport.

The scattering rate probed by the optical conductivity is somewhat intermediate between those probed by ARPES and *dc* transport. As in the *dc* case, only large-angle scattering contributes to the optical scattering rate. Similar to the ARPES case, however, this scattering does not have to come from momentum-relaxing processes. As long as Galilean invariance is broken–by lattice or spin-orbit interaction–even momentum-conserving scattering gives a non-zero contribution to the optical scattering rate. In certain cases, this makes the optical conductivity amenable to hyperscaling analysis [5, 6], which does not rely on a specific scattering mechanism. Furthermore, at sufficiently high frequencies *ee* scattering is stronger than electron–phonon and electron-impurity ones, and the optical conductivity probes directly the transport rate of *ee* scattering. At the same time, the optical response at lower frequencies, including the *dc* limit, is controlled by momentum-relaxing processes, such as umklapp *ee* scattering or phonon/impurity scattering. This makes the optical response an effective tool for studying *ee* interaction even in cases when *dc* transport is controlled by scattering from phonons and/or impurities. A good example of the effectiveness of the optical probe is provided by classic studies of the optical conductivity of noble metals (Ag, Au, and Cu) [7, 8]. The temperature dependence of the *dc* resistivity in these metals is determined mostly by electron–phonon interaction, while the Fermi-liquid (FL), T^2 term due to *ee* interaction is virtually indiscernible. When probed at frequencies above the Debye frequency, the same metals show a different behavior. Indeed, the scattering rate due to phonons saturates at such frequencies, while the scattering rate due to *ee* interaction continues to grow with frequency all the way up to the bandwidth and determines the measured optical scattering rate.

In this review, we address several topics related to the role of momentum conservation in optical response. In particular, we discuss the interplay between contributions from normal and umklapp *ee* scattering to the optical conductivity, both at finite frequency and near the *dc* limit. We consider the optical conductivity of a two-band metal as the simplest example of a system with broken Galilean invariance. We also discuss how the FS geometry affects the behavior of the optical and *dc* conductivities.

The second aspect is Ω/T scaling of the optical conductivity, $\sigma(\Omega, T)$ [9–16]. The real part of the inverse optical conductivity is proportional to the optical scattering rate: $\mathrm{Re}\sigma^{-1}(\Omega, T) \propto 1/\tau(\Omega, T)$. For a FL, one generally expects the optical scattering rate due to *ee* interaction, $1/\tau_{ee}(\Omega, T)$, to scale quadratically with either of the variables, i.e. as $\max\{\Omega^2, T^2\}$. An explicit computation of $1/\tau_{ee}(\Omega, T)$ was performed in 1959 by Gurzhi [17], who showed that the prefactors of the Ω^2 and T^2 terms are related in a universal manner: $1/\tau_{ee}(\Omega, T) \propto \Omega^2 + 4\pi^2 T^2$. It was later realized [18–21] that a factor of $4\pi^2$ in front of T^2 appears there for a good reason: it reflects the fact that $1/\tau_{ee}(\Omega, T)$ must vanish upon analytic continuation to the first boson Matsubara frequency: $\Omega \to \pm 2\mathrm{i}\pi T$ (the 'first-Matsubara-frequency rule' for boson response). By a similar rule, the single-particle scattering rate in a FL behaves as $\Sigma''(\omega, T) \equiv \mathrm{Im}\Sigma(\omega, T) \propto \omega^2 + \pi^2 T^2$ and vanishes upon analytic continuation to the first fermion Matsubara frequency, $\omega \to \pm \mathrm{i}\pi T$.

However, recent studies of a number of materials, which might have been classified as FLs due to both Ω^2 and T^2 scalings of their *dc* and optical scattering rates, have found that $1/\tau(\Omega, T)$ often does not conform to the FL scaling form. Namely, a different scaling form, $1/\tau(\Omega, T) \propto \Omega^2 + b\pi^2 T^2$, with b ranging from 1 to about 6, has been observed [12–16]. One might be tempted to ignore this disagreement as it affects only a number. However, this number is quite important, because strong deviation of b from $b = 4$ implies that the optical scattering rate cannot be described by just *ee* interaction, although the overall behavior of a system resembles that of a canonical FL.

In this paper, we re-visit the Gurzhi formula for the optical scattering rate in a FL and discuss in some detail the 'first-Matsubara-frequency rule' (FMRF), first for the fermion self-energy and then for the optical conductivity. Explicitly, FMRF for the fermion self-energy states that the Matsubara self-energy, evaluated at $\omega_m = \pm\pi T$, does not contain the FL-like, T^2 term for $2 < D \leqslant 3$: $\Sigma(\pm\pi T, T) = \pm \mathrm{i}\pi\lambda T + 0 \times T^2 + O(T^D)$.

(In 2D, the self-energy does not contain the $T^2 \ln T$ term but does contain the T^2 one: $\Sigma(\pm\pi T, T) = \pm i\pi\lambda T + O(T^2)$). The remainder, which is generically of order T^D, is further reduced if a FL is of the Eliashberg type. The rule also applies to non-Fermi liquids (NFLs), with a proviso that the coefficient λ, which is constant in a FL, now depends on T. The corresponding rule for the optical scattering rate on the Matsubara axis is $1/\tau_{ee}(\pm 2\pi T, T) = 0 \times T^2 + O(T^D)$. We relate these two properties to the scaling forms of the self-energy and optical conductivity on the real axis. We also discuss recent experiments and the phenomenological model, proposed in [21] to explain the violation of Gurzhi scaling. In this model, one assumes that there are two channels of scattering. The first one is *ee* interaction, which does lead to the usual FL scaling form of the self-energy. The second one is an elastic scattering process with an effective cross-section, which depends on the electron energy but not on temperature. Consequently, this channel contributes an ω^2 but no T^2 term to the self-energy. This changes the balance between the Ω^2 and T^2 terms in the optical conductivity. As a result, the coefficient b is not equal to 4 but depends on the relative weights of the inelastic and elastic channels. In particular, the value of $b \approx 1$, observed in a number of rare-earth Mott insulators and heavy metals, implies that the elastic channel is much stronger than the *ee* one. As a particular example, we consider elastic scattering at resonance levels and show that this model is in reasonable agreement with the data on URu_2Si_2 [12].

The third aspect is the optical conductivity of a NFL metal. We consider two particular examples of a NFL, encountered in metals near nematic (Pomeranchuk) and spin-density-wave (SDW) instabilities. In the last case, we focus on a clean two-dimensional (2D) metal near a quantum-critical point (QCP) separating the paramagnetic and commensurate SDW phases. Critical magnetic fluctuations are known to destroy fermion coherence, but only at particular 'hot spots' (FS points connected by the ordering wavenumber, (π, π)). On the rest of the FS, quasiparticles are strongly renormalized compared to the non-interacting case, but still display a FL behavior at the lowest energies. Because $1/\tau_{ee}(\Omega) \propto \Omega^2$ for coherent quasiparticles and because the optical conductivity is obtained by averaging over the FS [22], it had long been believed that the conductivity at the SDW QCP retains its FL form: $\sigma'(\Omega) \equiv \mathrm{Re}\sigma(\Omega) \propto 1/\Omega^2\, \tau_{ee}(\Omega) = \mathrm{const}$. However, it has been argued recently [23, 24] that this is not the case because of composite scattering—a process in which fermions, located away from a hot spot, are scattered twice by (π, π) fluctuations and return to nearly the same points. It turns out that this scattering gives a larger contribution to $\sigma'(\Omega)$ than direct scattering by (π, π) fluctuations. As a result, the dissipative part of the conductivity displays a non-FL behavior at a QCP: $\sigma'(\Omega)$ scales as $\Omega^{-1/3}$ at asymptotically low frequencies and as Ω^{-1} at higher frequencies, nominally up to the bandwidth. The $1/\Omega$ scaling of $\sigma'(\Omega)$ is reminiscent of the behavior observed in the superconducting cuprates [1, 25–27]. We derive these results and also show that, at finite temperature, the optical conductivity is of the FL form at frequencies below certain T-dependent scale, but displays NFL-like Ω- and T-dependences at frequencies above this scale: $\sigma'(\Omega, T) \propto T^{4/3}\, \Omega^{-5/3}$.

Due to limited and focused scope of this review, we do not discuss several modern approaches to optical response of correlated electron systems, e.g. the holographic approach. We refer the reader to recent literature on this subject, e.g. [28–33].

The rest of the paper is organized as follows. In section 2, we address various aspects of momentum conservation for the optical conductivity. In section 3, we derive the Gurzhi formula for the optical scattering rate in a FL. In section 4, we discuss the first-Matsubara-frequency rule, both for the fermion self-energy (section 4.1) and optical conductivity (section 4.2). In section 4.3, we discuss recent experiments and the phenomenological model, proposed in [21] to explain the observed deviations from FL scaling. In section 5.1, we re-visit the optical conductivity of a metal near Pomeranchuk quantum criticality. In section 5.2, we consider a 2D metal near an SDW quantum phase transition, and show that its optical conductivity exhibits a non-FL behavior due to composite scattering of fermions away from hot spots.

2. Momentum conservation in optical response

2.1. Normal and umklapp scattering in the optical conductivity

2.1.1. Boltzmann equation and Kubo formula.

2.1.1.a. Optical conductivity of a non-Galilean-invariant system: Boltzmann equation. It is well-known that the *dc* conductivity of a single-band electron system is infinite in the absence of umklapp scattering processes and/or disorder, even if Galilean invariance is broken by lattice and/or spin-orbit interaction. Indeed, consider a linearized Boltzmann equation

$$e\mathbf{v}_{\mathbf{k}} \cdot \mathbf{E} = -\sum_{\mathbf{kpk'p'}} W_{\mathbf{k},\mathbf{p};\mathbf{k'p'}} \left(g_{\mathbf{k}} + g_{\mathbf{p}} - g_{\mathbf{k'}} - g_{\mathbf{p'}}\right) F_{\mathbf{kp};\mathbf{k'p'}}, \quad (2.1)$$

where $\mathbf{v}_{\mathbf{k}} = \boldsymbol{\nabla}_{\mathbf{k}} \varepsilon_{\mathbf{k}}$ is the group velocity of a Bloch electron with dispersion $\varepsilon_{\mathbf{k}}$, $\mathbf{E}$ is the external electric field, $g_{\mathbf{k}}$ is a non-equilibrium part of the distribution function, defined as $f_{\mathbf{k}} = f_{0\mathbf{k}} + g_{\mathbf{k}} \frac{\partial f_{0\mathbf{k}}}{\partial \varepsilon_{\mathbf{k}}}$, $f_{0\mathbf{k}}$ is the Fermi function for free electrons, $W_{\mathbf{k},\mathbf{p};\mathbf{k'p'}}$ is the *ee* scattering probability, and $F_{\mathbf{kpk'p'}}$ is a combination of the Fermi functions whose explicit form is not essential for the present discussion. In the absence of umklapp processes, the total momentum is conserved: $\mathbf{k} + \mathbf{p} = \mathbf{k'} + \mathbf{p'}$. Let $g_{\mathbf{k}}$ be a solution of equation (2.1). But then $\tilde{g}_{\mathbf{k}} = g_{\mathbf{k}} + \mathbf{C} \cdot \mathbf{k}$ with a $\mathbf{k}$-independent but otherwise arbitrary vector $\mathbf{C}$ is also a solution. Since $\mathbf{C}$ is arbitrary, the corresponding charge current

$$\mathbf{j} = 2e \sum_{\mathbf{k}} \mathbf{v}_{\mathbf{k}} f_{\mathbf{k}} = 2e \sum_{\mathbf{k}} \mathbf{v}_{\mathbf{k}} g_{\mathbf{k}} \frac{\partial f_{0\mathbf{k}}}{\partial \varepsilon_{\mathbf{k}}} \quad (2.2)$$

can be made arbitrarily large even by infinitesimally weak electric field, which means that the conductivity is infinite. In the memory-matrix formalism, the same result follows from the fact that the memory matrix has a zero mode in the absence of umklapp scattering [34, 35].

However, if the electric field oscillates in time, umklapp processes are not necessary for the conductivity to be finite at finite frequency: a violation of Galilean invariance suffices.

[17]. Let's see how this result follows from the Boltzmann equation. Adding the time derivative to the left-hand-side of equation (2.1), we obtain

$$-\mathrm{i}\,\Omega\, g_{\mathbf{k}} + e\mathbf{v}_{\mathbf{k}}\cdot\mathbf{E} = -\sum_{\mathbf{kpk'p'}} W_{\mathbf{k},\mathbf{p};\mathbf{k'p'}}\left(g_{\mathbf{k}} + g_{\mathbf{p}} - g_{\mathbf{k'}} - g_{\mathbf{p'}}\right) F_{\mathbf{kpk'p'}}. \tag{2.3}$$

Now the Boltzmann equation can be solved by iterations with respect to the collision integral:

$$g_{\mathbf{k}} = g^{(0)}_{\mathbf{k}} + g^{(1)}_{\mathbf{k}} + g^{(2)}_{\mathbf{k}} + \ldots \tag{2.4}$$

This expansion is valid in the 'collisionless' or 'high-frequency' regime, defined by the condition $\Omega\,\tau_{\mathrm{ee}} \gg 1$, where $1/\tau_{\mathrm{ee}}$ is the *ee* scattering rate obtained by some appropriate averaging of the collision integral. Within the semiclassical approximation, the frequency of light must be small compared to temperature; therefore, τ_{ee} in the solution of the semiclassical Boltzmann equation is a function of temperature but not frequency[3], which is what we will be assuming here and in section 2.2. The zeroth-order term in the expansion, $g^{(0)}_{\mathbf{k}} = e\mathbf{v}_{\mathbf{k}}\cdot\mathbf{E}/\mathrm{i}\,\Omega$, is independent of τ_{ee} and gives the imaginary, i.e. non-dissipative, part of the conductivity $\sigma''(\Omega) \propto 1/\Omega$. The first-order term is given by

$$g^{(1)}_{\mathbf{k}} = -\frac{e}{\Omega^2}\sum_{\mathbf{kpk'p'}} W_{\mathbf{k},\mathbf{p};\mathbf{k'p'}}(\Delta\mathbf{J}\cdot\mathbf{E})\, F_{\mathbf{kpk'p'}}, \tag{2.5}$$

where

$$\Delta\mathbf{J} \equiv \mathbf{v}_{\mathbf{k}} + \mathbf{v}_{\mathbf{p}} - \mathbf{v}_{\mathbf{k'}} - \mathbf{v}_{\mathbf{p'}} \tag{2.6}$$

is a change in the total particle flux due to an *ee* collision [36–38]. The correction $g^{(1)}_{\mathbf{k}}$ is real and, if non-zero, gives rise to a non-zero real, i.e. dissipative, part of the conductivity: $\sigma' \propto 1/\Omega^2\,\tau_{\mathrm{ee}}$. In a Galilean-invariant system, $\mathbf{v}_{\mathbf{k}} = \mathbf{k}/m$ and thus momentum conservation implies current conservation. In this case $\Delta\mathbf{J} = 0$, and the dissipative term in the conductivity is absent. (This is true for an arbitrary order in $1/\Omega\,\tau_{\mathrm{ee}}$.) If $\mathbf{v}_{\mathbf{k}} \neq \mathbf{k}/m$, which is the case in the presence of a lattice and/or spin-orbit interaction, $\Delta\mathbf{J}$ is non-zero, even though momentum is conserved. Consequently, the conductivity of a non-Galilean-invariant system contains the dissipative part.

There are two points which one needs to keep in mind, however. First, the conductivity at frequencies $\Omega \gg 1/\tau_{\mathrm{ee}}$ behaves as

$$\sigma(\Omega) = C_1\frac{\mathrm{i}}{\Omega} + C_2\frac{1}{\Omega^2\,\tau_{\mathrm{ee}}} \tag{2.7}$$

where $C_{1,2}$ are real constants. This form does coincide with the corresponding limit of the Drude formula

$$\sigma(\Omega) = \frac{\Omega_p^2}{4\pi}\frac{1}{{\tau_{\mathrm{ee}}}^{-1} - \mathrm{i}\,\Omega}, \tag{2.8}$$

[3] In the semiclassical Boltzmann equation, the frequency of the electric field enters only the left-hand-side. Correspondingly, the result for the conductivity contains the *ee* relaxation time, τ_{ee}, which depends on the temperature but not frequency. On the other hand, the Kubo formula treats the frequency and temperature on equal footing. The quantum Boltzmann equation remedies semiclassical limitation and the resulting conductivity coincides with the one given by the Kubo formula.

where Ω_p is the plasma frequency. At an arbitrary frequency, however, the conductivity is not described by equation (2.8). This follows already from the fact that equation (2.8) has a finite limit at $\Omega \to 0$, while we argued at the beginning of this section that the *dc* conductivity is infinite in the absence of umklapp/impurity scattering. In section 2.2, we discuss the actual behavior of $\sigma(\Omega)$ for a particular example of a non-Galilean-invariant system–a two-band metal.

Second, $1/\tau_{\mathrm{ee}}$ in the high-frequency tail of the conductivity does not always coincide with the quasiparticle scattering rate which, in a FL, scales as T^2 for $T \gg \Omega$. This implies that $\sigma'(\Omega)$ does not always scale as T^2/Ω^2 even for a FL. For certain FS geometries (see section 2.3), the prefactor of the leading, T^2 term in $1/\tau_{\mathrm{ee}}$ vanishes, and $1/\tau_{\mathrm{ee}}$ scales as T^4, which implies that the conductivity scales as T^4/Ω^2 [4, 35, 39–46].

Obviously, if umklapp scattering is allowed, it also contributes to the optical conductivity. There is a certain interplay between normal and umklapp scattering, which we discuss in sections 2.1.2 and 3.1.2.

2.1.1.b. Optical conductivity of a non-Galilean-invariant system: Kubo formula. One can arrive at the same result–that $\sigma'(\Omega)$ vanishes in the Galilean-invariant case but $\sigma'(\Omega) \propto 1/\Omega^2\,\tau_{ee} \neq 0$ if Galilean invariance is broken–by using the Kubo formula for the conductivity rather than the Boltzmann equation. Holstein [47] and a number of authors after him [34, 35, 38, 48, 49] demonstrated the cancellation of diagrams for the conductivity in the Galilean-invariant case in various physical contexts. Following the previous work, we show in appendix A that the combination of the diagrams for the conductivity in figure 1 can be reduced to a form that contains the same change in the total flux, $\Delta\mathbf{J}$, as in equation (2.5). For the current–current correlation function to second order in the static *ee* interaction $U_{\mathbf{l}}$, we find

$$\mathcal{K}(\mathrm{i}q_0) = \frac{1}{q_0^2}\sum_{P,K,L}\left(\mathbf{v}_{\mathbf{p}}\cdot\Delta\mathbf{J}\right)U^2_{\mathbf{l}}\big(2G_P G_{P+L} - G_P G_{P+L+Q} - G_{P+Q}G_{P+L}\big)G_K G_{K-L}, \tag{2.9}$$

where $P = (\mathbf{p}, \mathrm{i}p_0)$, $K = (\mathbf{k}, \mathrm{i}k_0)$, $L = (\mathbf{l}, \mathrm{i}l_0)$, $Q = (\mathbf{0}, \mathrm{i}q_0)$, $G_P = 1/(\mathrm{i}p_0 - \varepsilon_{\mathbf{p}})$ is the Green's function, and $\sum_K$ stands for $T\sum_{k_0}\int \mathrm{d}^D k/(2\pi)^D$, etc. The dissipative part of the conductivity is obtained as $\sigma'(\Omega) = e^2\mathrm{Im}\mathcal{K}(\mathrm{i}q_0 \to \Omega + \mathrm{i}0^+)/\Omega$. Because $\mathrm{Im}\mathcal{K}(\mathrm{i}q_0 \to \Omega + \mathrm{i}0^+)$ in equation (2.9) is proportional to $1/\Omega^2$ and contains the square of the *ee* interaction, it gives an $\mathcal{O}(1/\Omega^2\,\tau_{\mathrm{ee}})$ term in the conductivity. Whether $\sigma'(\Omega)$ is finite or zero is determined by whether $\Delta\mathbf{J}$ in equation (2.9) is finite or zero, which is the same result as obtained from the Boltzmann equation.

2.1.2. Similarity between the optical conductivity of a clean system and the ***dc*** *conductivity of a disordered system.* The situation with the optical conductivity is to a certain extent similar to that for the *dc* conductivity in the presence of both impurities and *ee* interaction. In the latter case, the impurity collision integral, $(f_{\mathbf{k}} - \langle f_{\mathbf{k}}\rangle)/\tau_{\mathrm{i}}$ with $\langle\ldots\rangle$ standing for averaging over the directions of $\mathbf{k}$, plays the role of the time derivative in the *ac* case, the zeroth-order solution is obtained in the presence

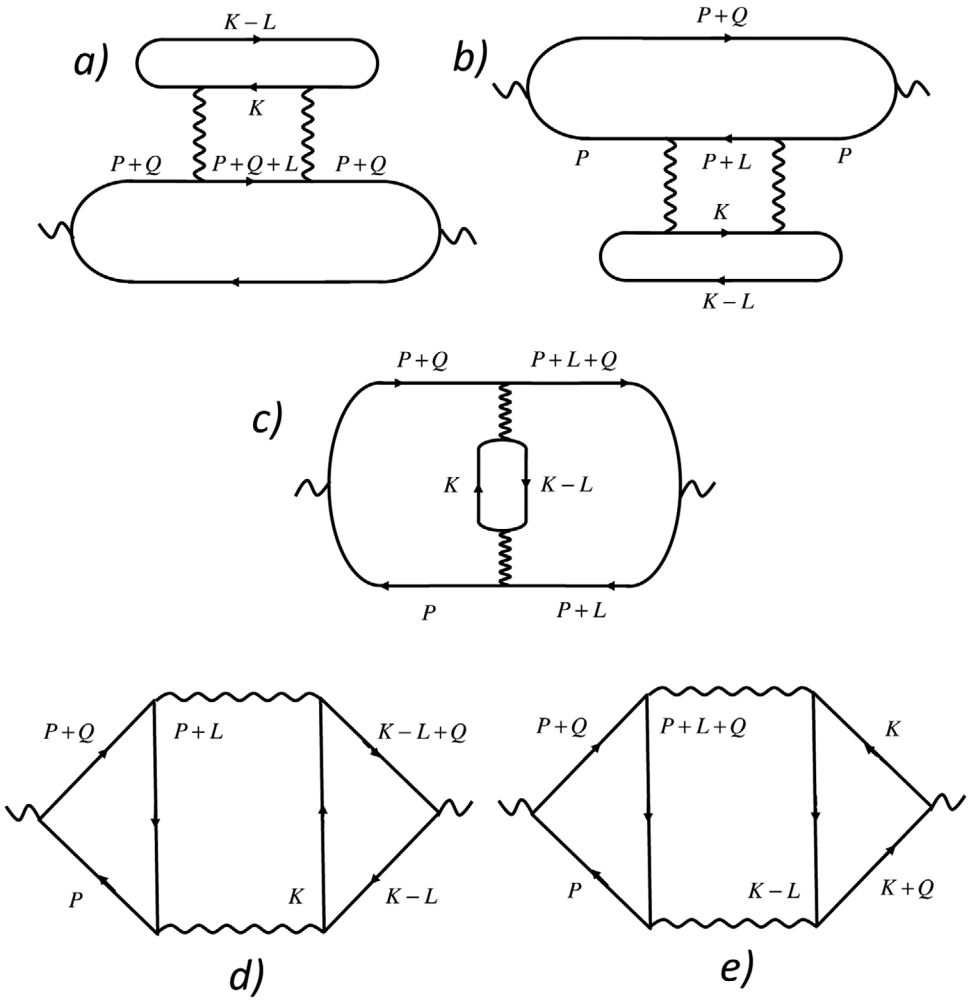

Figure 1. Feynman diagrams for the optical conductivity.

of impurities only, and higher orders are obtained by iterations with respect to the *ee* collision integral. In the Galilean-invariant case[4], the Boltzmann equation predicts that *ee* interaction does not affect the resistivity, i.e. the analog of $g_{\mathbf{k}}$ in equation (2.4) vanishes. If Galilean invariance is broken, the analog of $g^{(1)}_{\mathbf{k}}$ is non-zero, i.e. *ee* interaction contributes to the resistivity. Beyond the Boltzmann equation, *ee* interaction may affect the resistivity already in the Galilean-invariant case via, e.g. quantum-mechanical interference effects [50], superconducting fluctuations [51], and finite viscosity of the electron liquid [52, 53].

Another similarity between the *dc* and optical conductivities is in the interplay between normal *ee* scattering (with rate $1/\tau_{ee}$) and momentum-relaxing scattering (with rate $1/\tau_i$). For simplicity, we assume that the latter mechanism in the *dc* case is due to impurities. At low temperatures, when $\tau_{ee} \gg \tau_i$, the scattering rates of the two processes add up according to the Matthiessen rule:

$$1/\tau_{\rm eff} = 1/\tau_i + 1/\tau_{ee}. \qquad (2.10)$$

[4] Although impurities violate Galilean invariance, this effect is not captured by the Boltzmann equation for an average (over realizations of disorder) distribution function, which is still parametrized by momentum. In this case, it makes sense to speak about Galilean invariance of an electron system in the presence of impurities.

The Matthiessen rule, however, does not hold at all temperatures. In particular, at higher temperatures, when $\tau_{ee} \ll \tau_i$, the *ee* term in the resistivity does not become the dominant one. Instead, the resistivity saturates at a temperature-independent value, which is proportional to $1/\tau_i$ but, in general, differs from the residual resistivity at $T = 0$ [4, 45]. The physical reason for such saturation is that normal *ee* collisions by themselves cannot relax the current, no matter how frequent they are. This can be done only by impurities (and/or umklapps). All normal collisions can do is to modify the energy dependence of the distribution function, and it is this modification that changes the resistivity compared to the residual one. The ratio of the high-T to low-T saturation values is determined by the shape of the FS.

The interplay between normal and momentum-relaxing scattering in the optical conductivity is similar to the *dc* case in a sense that the Matthiessen rule is, in general, also violated. In the collisionless regime, $\sigma'(\Omega) \propto 1/\Omega^2\,\tau_{\rm eff}$, where $1/\tau_{\rm eff}$ is given by an equation similar to equation (2.10) but with, generally speaking, different weights of the $1/\tau_{ee}$ and $1/\tau_i$ terms (see equation (2.21) below). At lower frequencies, however, $1/\tau_{ee}$ and $1/\tau_i$ do not contribute additively to the frequency dependence of $\sigma'(\Omega)$.

In the next section, we analyze the optical conductivity of a two-band metal. The results of this section are not new: they

can be inferred from general formulas, derived, e.g. in [54]. We include this discussion for completeness and also because this simple case does give an idea of how the interplay between the normal and momentum-relaxing scattering mechanisms works.

2.2. Optical conductivity of a two-band metal

A two-band metal is the simplest example of a system with broken Galilean invariance. Even if each of the bands is parabolic, the system as a whole is not Galilean-invariant. The analysis of the conductivity in this model is usually associated with the name of Baber [55], who considered the effect of inter-band *ee* scattering. It is sometimes forgotten, however, that Baber analyzed only the case of a *compensated semimetal*, with equal numbers of electrons and holes. Only in this case, normal *ee* collisions alone render the *dc* resistivity finite. (This is also true also for Weyl/Dirac semimetals at the charge neutrality point [56]). If a metal is not compensated, one needs momentum-relaxing scattering to obtain a finite *dc* resistivity.

We now analyze how the optical conductivity of a two-band metal evolves as a function of frequency between the *dc* and high-frequency limits.

2.2.1. Momentum-conserving scattering only. At first, let momentum-relaxing scattering be absent. For a two-band metal with parabolic bands, the conductivity can be found by solving the semiclassical equations of motion [54]

$$\begin{aligned} -\mathrm{i}\,\Omega\, m_1 \mathbf{v}_1 &= e_1\mathbf{E} - \eta n_2(\mathbf{v}_1 - \mathbf{v}_2), \\ -\mathrm{i}\,\Omega\, m_2 \mathbf{v}_2 &= e_2\mathbf{E} - \eta n_1(\mathbf{v}_2 - \mathbf{v}_1), \end{aligned} \tag{2.11}$$

where $e_{1,2} = \pm e$, indices 1 and 2 denote the bands, $n_{1,2}$ is the number density[5], and $\eta > 0$ parametrizes inter-band *ee* scattering. (For parabolic bands, intra-band *ee* scattering conserves the in-band momentum and thus does enter the equations of motion.)[6] Solving these equations, we find the current $\mathbf{j} = e_1 n_1 \mathbf{v}_1 + e_2 n_2 \mathbf{v}_2$ and thus the conductivity at finite frequency $\Omega \neq 0$

$$\sigma(\Omega) = \frac{1}{4\pi}\frac{\Omega\,\Omega_p^2 + \mathrm{i}\tau_{ee}{}^{-1}\Omega_0^2}{\Omega(\tau_{ee}{}^{-1} - \mathrm{i}\,\Omega)} = \frac{\Omega_p^2 - \Omega_0^2}{4\pi}\frac{1}{\tau_{ee}{}^{-1} - \mathrm{i}\,\Omega} + \frac{\Omega_0^2}{4\pi}\frac{\mathrm{i}}{\Omega}, \tag{2.12}$$

where $\Omega_p^2 = \Omega_1^2 + \Omega_2^2$, $\Omega_{1,2}^2 = 4\pi e^2 n_{1,2}/m_{1,2}$ is the intra-band plasma frequency,

$$\Omega_0^2 = 4\pi\frac{(e_1 n_1 + e_2 n_2)^2}{n_1 m_1 + n_2 m_2} \tag{2.13}$$

is the 'compensation frequency', and we defined τ_{ee} as

[5] By assuming that the number density in each of the bands is finite, we exclude the case of a Weyl/Dirac semimetal at the charge neutrality point, which is the special limit of the Baber's case with zero band overlap.

[6] For parabolic bands, the phenomenological equations of motion are equivalent to the solution of the Boltzmann equation. What is left undetermined at the phenomenological level is an explicit form of the scattering time, which is to be found from the Boltzmann equation with a given collision integral. Solutions of the Boltzmann equation for two-band systems in particular physical contexts can be found in, e.g. [45, 141].

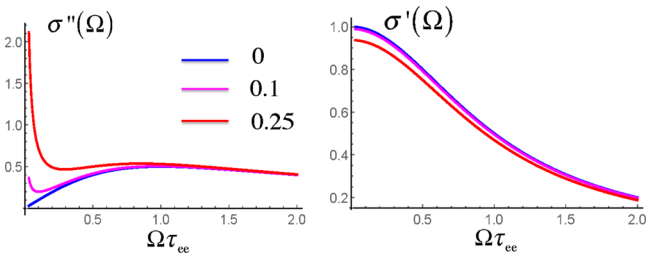

Figure 2. The imaginary (left) and real (right) parts of the conductivity of a two-band metal with interband *ee* scattering but without intra-band relaxation (equations (2.15) and (2.16), correspondingly). A degree of compensation, Ω_0/Ω_p (see equation (2.13)), is specified in the legend. The conductivity in measured in units of $\Omega_p^2\,\tau_{ee}/4\pi$. Only in the fully compensated case ($\Omega_0 = 0$), both the real and imaginary parts obey the Drude formula. Away from compensation, the real part of the conductivity $\sigma'(\Omega)$ also contains a $\delta(\Omega)$ term (not shown).

$$1/\tau_{ee} \equiv \eta\left(\frac{n_1}{m_2} + \frac{n_2}{m_1}\right). \tag{2.14}$$

As in the previous section, τ_{ee} depends on the temperature but not on frequency; for a FL, $1/\tau_{ee} \propto T^2$.

If the metal is compensated, i.e. $e_1 n_1 + e_2 n_2 = 0$, then $\Omega_0 = 0$ and the conductivity is described the Drude formula (equation (2.8)) at all frequencies, including $\Omega = 0$. This is the Baber's case [55]: σ' approaches a finite value $\sigma' = \Omega_p^2\,\tau_{ee}/4\pi$ in the limit of $\Omega \to 0$, while σ'' vanishes in this limit. However, if the metal is not compensated, $\sigma(\Omega)$ as a whole cannot be described by the Drude formula. Indeed, the imaginary part of $\sigma(\Omega)$

$$\sigma''(\Omega) = \frac{1}{4\pi}\frac{\Omega_p^2\,\Omega^2\,\tau_{ee}{}^2 + \Omega_0^2}{\Omega\,(\Omega^2\,\tau_{ee}{}^2 + 1)} \tag{2.15}$$

diverges as $1/\Omega$ at $\Omega \to 0$ (see figure 2, left). This divergence is the same as the diamagnetic term in the conductivity of an ideal metal. The real part of the conductivity at $\Omega \neq 0$ is

$$\sigma'(\Omega) = \frac{\Omega_p^2 - \Omega_0^2}{4\pi}\frac{\tau_{ee}}{\Omega^2\,\tau_{ee}{}^2 + 1} \tag{2.16}$$

is still of the Drude form with a renormalized plasma frequency, and it remains finite at $\Omega \to 0$ (see figure 2, right). Note that

$$\Omega_p^2 - \Omega_0^2 = \frac{4\pi n_1 n_2 m_1 m_2}{n_1 m_1 + n_2 m_2}\left(\frac{e_1}{m_1} - \frac{e_2}{m_2}\right)^2$$

is always positive.

So far, we have completely neglected momentum-relaxing scattering. Infinitesimally weak momentum-relaxing scattering can be accounted for by adding a small imaginary part to Ω in the denominator of the second term in equation (2.12): $\Omega \to \Omega + \mathrm{i}0^+$. Then the Kramers–Kronig transform of this term produces an additional $\delta(\Omega)$ term in $\sigma'(\Omega)$, which is the same as in the case of an ideal metal without any scattering. Finite momentum-relaxing scattering smears out the delta-function into a Drude peak, which will be described in the next section. At compensation, $\Omega_0 = 0$ and there is no $\delta(\Omega)$ term even in the absence of momentum relaxation.

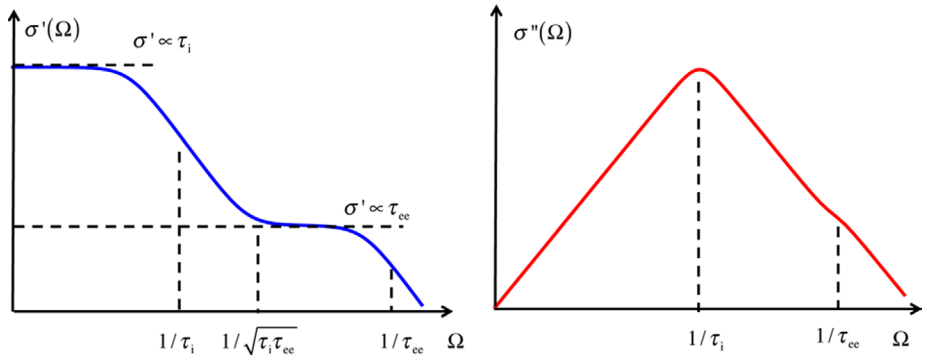

Figure 3. Left: $\sigma'(\Omega)$ of a two-band metal (equation (2.18)) in the hydrodynamic regime, where the momentum-relaxing scattering rate, $1/\tau_{\rm i}$, is much smaller than the rate of momentum-conserving *ee* scattering, $1/\tau_{\rm ee}$. Right: the same for $\sigma''(\Omega)$ (equation (2.19)). Both $\sigma'(\Omega)$ and $\sigma''(\Omega)$ are plotted on the log-log scale.

A non-Drude from of the conductivity affects the behavior of the reflection coefficient at low frequencies ($\Omega\,\tau_{\rm ee} \ll 1$). For a Drude metal, $1-R \propto \sqrt{\Omega}$ (the Hagen–Rubens relation). For $\sigma(\Omega)$ given by equation (2.12), $1-R$ scales instead as Ω^2:

$$1-R \approx 2\sqrt{2}\,\Omega^2\,\tau_{\rm ee}\frac{\Omega_p^2-\Omega_0^2}{\Omega_p^3}. \tag{2.17}$$

2.2.2. Both momentum-conserving and momentum-relaxing scattering. Now, let's add momentum-relaxing scattering due to disorder or umklapps. This can be modeled by adding the $-m_j\mathbf{v}_j/\tau_j$ terms ($j=1,2$) to the right-hand sides of the equations of motion (equation (2.11)), where $\tau_{1,2}$ are the momentum-relaxation times. (The rates $1/\tau_{1,2}$ are assumed to account for both intra- and inter-band momentum-relaxing processes.) Even in this case, however, the conductivity is not described by the Drude formula with the total relaxation rate given by the sum of partial rates, i.e. by $1/\tau_1+1/\tau_2+1/\tau_{\rm ee}$ because momentum-relaxing and momentum-conserving mechanisms are not additive. While the Drude formula has only one characteristic frequency scale ($1/\tau$), the actual conductivity in our case has three scales: the first two are given by the momentum-relaxing and momentum-conserving scattering rates, correspondingly, and the third one (roughly a geometric mean of the two previous ones) defines a crossover between the two regimes. Solving the modified equations of motion, we obtain

$$\sigma'(\Omega)=\frac{1}{4\pi}\frac{\gamma_0^2\left(\frac{\Omega_1^2}{\tau_2}+\frac{\Omega_2^2}{\tau_1}+\frac{\Omega_0^2}{\tau_{\rm ee}}\right)+\Omega^2\left(\frac{\Omega_1^2}{\tau_1}+\frac{\Omega_2^2}{\tau_2}+\frac{\Omega_p^2-\Omega_0^2}{\tau_{\rm ee}}\right)}{\left(\Omega^2-\gamma_0^2\right)^2+\left(\Omega/\tau_{\rm eff}\right)^2} \tag{2.18}$$

and

$$\sigma''(\Omega)=\Omega\frac{\frac{1}{\tau}\left(\frac{\Omega_1^2}{\tau_2}+\frac{\Omega_2^2}{\tau_1}+\frac{\Omega_0^2}{\tau_{\rm ee}}\right)+(\Omega_1^2+\Omega_2^2)(\Omega^2-\gamma_0^2)}{\left(\Omega^2-\gamma_0^2\right)^2+\left(\Omega/\tau_{\rm eff}\right)^2}, \tag{2.19}$$

where

$$\gamma_0^2=\frac{1}{\tau_1\tau_2}+\frac{1}{\tau_{\rm ee}}\left(\frac{1}{\tau_1}\frac{1}{1+\frac{n_2m_2}{n_1m_1}}+\frac{1}{\tau_2}\frac{1}{1+\frac{n_1m_1}{n_2m_2}}\right) \quad \text{and} \tag{2.20a}$$

$$\frac{1}{\tau_{\rm eff}}=\frac{1}{\tau_1}+\frac{1}{\tau_2}+\frac{1}{\tau_{\rm ee}}. \tag{2.20b}$$

The high-frequency tail of equation (2.18) is of the Drude form

$$\sigma'(\Omega)=\frac{1}{4\pi\,\Omega^2}\left(\frac{\Omega_1^2}{\tau_1}+\frac{\Omega_2^2}{\tau_2}+\frac{\Omega_p^2-\Omega_0^2}{\tau_{\rm ee}}\right), \tag{2.21}$$

while $\sigma''(\Omega)\propto 1/\Omega$. In the static limit, $\sigma'(\Omega=0)=\left(\frac{\Omega_1^2}{\tau_2}+\frac{\Omega_2^2}{\tau_1}+\frac{\Omega_0^2}{\tau_{\rm ee}}\right)/4\pi\gamma_0^2$ is finite, while $\sigma''(\Omega)$ vanishes.

In between the high- and low-frequency limits, however, the conductivity is not described by the Drude formula. To analyze the form of conductivity at intermediate frequencies, we focus on the *hydrodynamic* regime, when momentum-conserving scattering is stronger than momentum-relaxing one: $1/\tau_{\rm ee} \gg 1/\tau_1 \sim 1/\tau_2$ (here and thereafter, the $\sim$ sign means 'equal in order of magnitude'). This regime has received considerable attention recently in the context of both strongly-correlated systems and Weyl/Dirac metals [46, 53, 57–62]. We consider a generic case when $n_1 \sim n_2$ and $m_1 \sim m_2$; this implies that $\Omega_1 \sim \Omega_2 \sim \Omega_0 \sim \Omega_p$, and $\tau_1 \sim \tau_2$. In this case, the analysis of equation (2.18) shows that there are three crossover frequencies: (1) $1/\tau_{\rm i} \sim 1/\tau_1 \sim 1/\tau_2$, (2) $1/\tau_{\rm ee}$, and (3) the intermediate scale $1/\tau^* \sim 1/\sqrt{\tau_{\rm i}\tau_{\rm ee}} \sim \gamma_0$.

For $\Omega \ll 1/\tau^*$, $\sigma'(\Omega)$ has a Drude peak with relaxation time $\tau_{\rm i}$: in the *dc* limit, $\sigma'(\Omega)$ is proportional to $\tau_{\rm i}$; for $1/\tau_{\rm i} \ll \Omega \ll 1/\tau^*$, $\sigma'(\Omega) \propto 1/\Omega^2\,\tau_{\rm i}$. This is the smeared-out delta-function peak described in the previous section. The high-frequency tail of this peak is cut off at $\Omega \sim 1/\tau^*$, where $\sigma'(\Omega)$ saturates at a quasi-static value proportional to $\tau_{\rm ee}$. For $\Omega \gtrsim 1/\tau_{\rm ee}$, $\sigma'(\Omega)$ has a second Drude peak with relaxation time $\tau_{\rm ee}$. The two-peak structure of $\sigma'(\Omega)$ is depicted in figure 3, left.

For $\Omega \ll 1/\tau^*$, the imaginary part of $\sigma(\Omega)$ obeys the Drude formula with relaxation time $\tau_{\rm i}$: $\sigma''(\Omega)$ vanishes linearly with Ω for $\Omega \ll 1/\tau_{\rm i}$ and falls off as $1/\Omega$ for $\Omega \gg 1/\tau_{\rm i}$. In contrast to $\sigma'(\Omega)$, however, $\sigma''(\Omega)$ does not have the second Drude peak for $\Omega \gg 1/\tau^*$. Instead, the $1/\Omega$ tail of the first Drude peak matches smoothly with a non-Drude form in equation (2.15), parametrized by relaxation time $\tau_{\rm ee}$. Overall, $\sigma''(\Omega)$ behaves as $1/\Omega$ for $\Omega \gg 1/\tau_{\rm i}$, with different plasma frequencies in the prefactor of the $1/\Omega$ term. As a result, $\sigma''(\Omega)$ has a knee at $\Omega \sim 1/\tau_{\rm ee}$, see figure 3, right.

2.2.3. dc *limit.* We now briefly discuss the static limit, where equation (2.18) yields the *dc* resistivity in the following form

$$\rho = 1/\sigma'(0) = 4\pi \frac{\gamma_0^2}{\frac{\Omega_1^2}{\tau_2} + \frac{\Omega_2^2}{\tau_1} + \frac{\Omega_0^2}{\tau_{ee}}}. \tag{2.22}$$

Suppose that $1/\tau_{ee}$ is a monotonically increasing function of the temperature with $1/\tau_{ee}|_{T=0} = 0$, while τ_1 and τ_2 are T-independent. In the low-T regime, $1/\tau_{ee} \ll 1/\tau_1,\ 1/\tau_2$; in the high-$T$ regime, $1/\tau_{ee} \gg 1/\tau_1,\ 1/\tau_2$. The low- and high-$T$ limits of the resistivity are

$$\rho|_{T=0} = 4\pi \frac{1}{\Omega_1^2 \tau_1 + \Omega_2^2 \tau_2}, \tag{2.23a}$$

$$\rho|_{T\to\infty} = \frac{4\pi}{\Omega_0^2}\left(\frac{1}{\tau_1}\frac{1}{1+\frac{n_2 m_2}{n_1 m_1}} + \frac{1}{\tau_2}\frac{1}{1+\frac{n_1 m_1}{n_2 m_2}}\right). \tag{2.23b}$$

These results allow for a transparent physical interpretation. At $T = 0$, inter-band *ee* scattering is absent, the two bands conduct independently, and the total resistance is equal to that of a circuit with two bands connected in parallel. At $T \to \infty$, inter-band *ee* scattering is the strongest mechanism. Momentum gained from the electric field is re-distributed quickly between the bands and then relaxed slowly within each band. The effective circuit for this case corresponds to two bands connected in series, but with weights of the two resistances that depend on the number densities and masses of the two bands.

From equation (2.23*b*), we see that as long as a metal is not compensated, i.e. $\Omega_0 \neq 0$, the *ee* contribution to the resistivity does not grow unboundedly with temperature (as it does in the Baber case) but saturates at high temperatures. Both the low- and high-T limits of ρ are controlled by the momentum-relaxing scattering rate. The ratio $\rho|_{T\to\infty}/\rho|_{T=0}$ is determined by the ratio of the effective masses of the bands [4, 45] and can be large in transition and heavy-fermion metals, but is *finite*[7].

Recent experiments on a quantum paraelectric $SrTiO_3$ [63, 64] have posed an interesting puzzle: the *dc* resistivity has been found to have a very pronounced T^2 term even at very low doping, when umklapps are essentially impossible and only one of the three conduction bands is occupied. The magnitude of this term far exceeds the theoretical prediction for a single-band non-Galilean-invariant FL [65]. More work is needed, however, before one can say whether the T^2 term comes from *ee* interactions or has a different origin, such as scattering from soft phonons modes [66, 67], characteristic for this material.

2.3. Additional cancelations due to special geometry of the Fermi surface

In section 2.1, we argued that since the change in total particle flux (equation (2.6)) does not vanish identically in a non-Galilean-invariant system, normal *ee* scattering gives rise to a non-zero dissipative part of the conductivity, $\sigma'(\Omega, T) \propto 1/\Omega^2\, \tau_{ee}$. We now relax the semiclassical condition of Ω being the smallest energy scale in the problem and allow τ_{ee} to depend both on Ω and T. In a FL, the (inverse) relaxation time scales as $1/\tau_{sp} \propto \max\{\Omega^2, T^2\}$. If τ_{ee} entering the conductivity were the same as τ_{sp}, the optical conductivity of a non-Galilean-invariant system would behave as

$$\sigma'(\Omega, T) \propto \frac{\max\{\Omega^2, T^2\}}{\Omega^2}, \tag{2.24}$$

while the *dc* resistivity in the presence of disorder would be given by

$$\rho = \rho_i + 4\pi^2 A_{dc} T^2, \tag{2.25}$$

where ρ_i is the residual resistivity and the factor of $4\pi^2$ is singled-out for further convenience. This is not always the case, however, because the geometry of the FS may lead to additional cancelations of the leading, $\mathcal{O}(\max\{\Omega^2, T^2\})$ term in equation (2.24) and of the T^2 term in equation (2.25). The study of such 'geometrical' cancelations has a long history [4, 35, 39–46] and has been reviewed recently in [45]. Here, we only list the results. In 2D, the cancelation of the leading terms occurs for any convex and simply connected FS, such as the one in the tight-binding model with sufficiently weak next-to-nearest neighbor hopping. In this case, momentum conservation $\mathbf{k} + \mathbf{p} = \mathbf{k}' + \mathbf{p}'$ for electrons on the FS can only be satisfied in processes that either swap the initial and final states ($\mathbf{k}' = \mathbf{p}$, $\mathbf{p}' = \mathbf{k}$) or occur in the Cooper channel ($\mathbf{k} + \mathbf{p} = 0 = \mathbf{k}' + \mathbf{p}'$). In both cases, $\Delta\mathbf{J}$ in equation (2.6) vanishes. For a circular FS, this result is almost self-evident and hinges on a simple geometric fact that two circles can have at most two intersection points. But then the same is true for any convex contour in 2D, and hence $\Delta\mathbf{J}$ vanishes for a FS of this type. To get a non-zero result, one needs to include the states further away from the FS, which costs an extra factor of $\mathcal{O}(\max\{T^2, \Omega^2\}$, and the resulting contribution to the optical conductivity scales as $\max\{T^4, \Omega^4\}/\Omega^2$, while the T^2 term in the *dc* resistivity is replaced by T^4. In 3D, the restrictions are less severe: as long as one keeps quartic (and higher) terms in the dispersion, there is no cancelation. In what follows, we will assume that the FS is such that geometric cancelations of this kind do not happen.

3. Optical conductivity of Fermi-liquid metals

3.1. Gurzhi formula

3.1.1. Kubo formula without vertex corrections. As we showed in the previous section, the optical conductivity of a non-Galilean-invariant system is finite even in the absence of umklapp scattering: normal scattering suffices. In the previous section, however, we treated the *ee* scattering rate, $1/\tau_{ee}$, as a phenomenological parameter, borrowing the knowledge of its T- and Ω-dependences from the microscopic theories. In this section, we review the microscopic theory for the optical conductivity of a FL. The main result of this theory is that $1/\tau_{ee}$, which appears in the formula for optical conductivity at high frequencies, $\sigma'(\Omega, T) \propto 1/\Omega^2\, \tau_{ee}$, scales as $\max\{\Omega^2, T^2\}$ and, moreover, the two dependences are described by a universal form $1/\tau_{ee} \propto \Omega^2 + 4\pi^2 T^2$. This result follows from the formula

[7] Explanations of a large (compared to the residual resistivity) T-dependent part of the resistivity of multi-band but decompensated metals, e.g. $SrTiO_3$, by Baber scattering [142] do not take this point account.

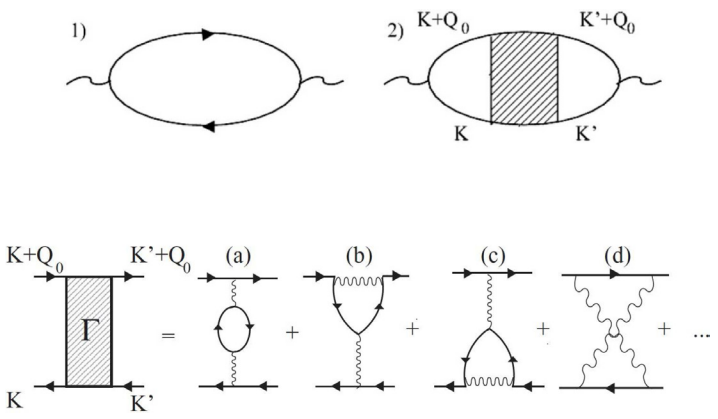

Figure 4. Top: diagrammatic representation of the Kubo formula for the conductivity. Bottom: examples of vertices contributing to diagram 2 on the top. Adapted with permission from [21]. Copyright by the American Physical Society.

for the optical conductivity of a FL [17], derived by Gurzhi in 1959 from the quantum Boltzmann equation:

$$\sigma'(\Omega) = \text{const} \times \frac{\Omega^2 + 4\pi^2 T^2}{\Omega^2} = \text{const}\left(1 + \frac{4\pi^2 T^2}{\Omega^2}\right). \tag{3.1}$$

To reproduce the Gurzhi result, we use the Kubo formula, which relates the conductivity to the current–current correlation function, $\mathcal{K}^R(\Omega, T)$ [68]:

$$\sigma'(\Omega) = \frac{e^2}{\Omega}\text{Im}\mathcal{K}^R(\Omega, T). \tag{3.2}$$

Here and thereafter, the superscript R denotes a retarded version of a certain quantity. For simplicity, we assume a cubic lattice in the D-dimensional space, so that the conductivity tensor, $\sigma_{ij}(\Omega)$, is diagonal and symmetric, and define $\sigma(\Omega) \equiv \sum_{i=1}^{D} \sigma_{ii}(\Omega)/D$. Diagrammatically, the current–current correlation function is given by a fully renormalized particle-hole bubble at zero momentum and finite frequency, with group velocities $\mathbf{v}_\mathbf{k}$ at the vertices. Without loss of generality, $\mathcal{K}^R(\Omega, T)$ can be split into parts: with and without vertex corrections, $\mathcal{K}_2^R(\Omega, T)$ and $\mathcal{K}_1^R(\Omega, T)$, correspondingly (see figure 4, top). The lines in these diagrams denote full Green's functions, with self-energy corrections included.

First, we compute $\mathcal{K}_1^R(\Omega, T)$ and then show that the functional form of $1/\tau_{ee}(\Omega, T)$ does not change if vertex corrections are included. To obtain $\text{Im}\mathcal{K}_1^R(\Omega, T)$, we first find the current–current correlation function $\mathcal{K}_1(\Omega_n, T)$ at the discrete Matsubara frequencies, $\Omega_n = 2\pi nT$, and then obtain $\mathcal{K}_1^R(\Omega, T)$ by analytic continuation, $\Omega_n \to -\text{i}\,\Omega + \text{i}0^+$. Along the Matsubara axis, we have

$$\mathcal{K}_1(\Omega_n, T) = -\frac{2}{(2\pi)^D D} T\sum_{\omega_m} \int \text{d}\varepsilon_\mathbf{k} \oint \text{d}a_\mathbf{k} v_\mathbf{k} G_\mathbf{k}(\omega_m) G_\mathbf{k}(\omega_m + \Omega_n), \tag{3.3}$$

where $\omega_m = \pi(2m+1)T$ and $\text{d}a_\mathbf{k}$ is the element of an isoenergetic surface ($\text{d}^D k = \text{d}\varepsilon_\mathbf{k}\text{d}a_\mathbf{k}/v_\mathbf{k}$ with $v_\mathbf{k} = |\mathbf{v}_\mathbf{k}|$). Note that we define the self-energy with the sign opposite to that in the traditional definition, e.g. in our definition $G_\mathbf{k}(\omega_m) = [\text{i}\omega_m - \varepsilon_\mathbf{k} + \Sigma_\mathbf{k}(\omega_m, T)]^{-1}$.

For definiteness, we consider a 3D FL, the self-energy of which at low frequencies and temperatures is given by

$$\begin{aligned} \text{Re}\Sigma_\mathbf{k}^R(\omega) &= \omega(Z_\mathbf{k}^{-1} - 1), \\ \text{Im}\Sigma_\mathbf{k}^R(\omega, T) &= A_\mathbf{k}(\omega^2 + \pi^2 T^2), \end{aligned} \tag{3.4}$$

where $Z_\mathbf{k}$ is the quasiparticle renormalization factor at point $\mathbf{k}$ on the FS. The real part of the self-energy may also contain a term which depends linearly on the quasiparticle dispersion $\varepsilon_\mathbf{k}$. Such a term, however, accounts only for an overall renormalization of the conductivity, and we neglect it. Transforming the Matsubara sum in equation (3.3) into the integral over the real axis and integrating over $\varepsilon_\mathbf{k}$, we obtain

$$\sigma'(\Omega) = \frac{8e^2}{D(2\pi)^D} \oint \text{d}a_\mathbf{k}\, v_\mathbf{k} \int_{-\infty}^{\infty} \frac{\text{d}\omega}{\Omega} \frac{[n_\text{F}(\omega) - n_\text{F}(\omega + \Omega)][\text{Im}\Sigma_\mathbf{k}^R(\omega, T) + \text{Im}\Sigma_\mathbf{k}^R(\omega + \Omega, T)]}{[\Omega + \text{Re}\Sigma_\mathbf{k}^R(\omega + \Omega, T) - \text{Re}\Sigma_\mathbf{k}^R(\omega, T)]^2 + [\text{Im}\Sigma_\mathbf{k}^R(\omega + \Omega, T) + \text{Im}\Sigma_\mathbf{k}^R(\omega, T)]^2}, \tag{3.5}$$

where $n_\text{F}(\omega)$ is the Fermi function. In a FL, $\Omega/Z_\mathbf{k} \gg \text{Im}\Sigma_\mathbf{k}^R(\Omega, T)$. Then one can neglect the imaginary parts of the self-energy in the denominator of equation (3.5). After averaging the imaginary parts of the self-energies in the numerator of equation (3.5) with the Fermi functions, we arrive at

$$\begin{aligned} \sigma'(\Omega) &= \frac{8e^2}{D(2\pi)^D} \oint \text{d}a_\mathbf{k}\, v_\mathbf{k} Z_\mathbf{k}^2 \int_{-\infty}^{\infty} \text{d}\omega \frac{n_\text{F}(\omega) - n_\text{F}(\omega + \Omega)}{\Omega^3} [\text{Im}\Sigma_\mathbf{k}^R(\omega, T) + \text{Im}\Sigma_\mathbf{k}^R(\omega + \Omega, T)] \\ &= \frac{8e^2}{D(2\pi)^D} \oint \text{d}a_\mathbf{k}\, v_\mathbf{k} Z_\mathbf{k}^2 A_\mathbf{k} \int_{-\infty}^{\infty} \text{d}\omega \frac{n_\text{F}(\omega) - n_\text{F}(\omega + \Omega)}{\Omega^3} [2\pi^2 T^2 + \omega^2 + (\Omega + \omega)^2] \\ &= \sigma_0 \frac{\Omega^2 + 4\pi^2 T^2}{\Omega^2}, \end{aligned} \tag{3.6}$$

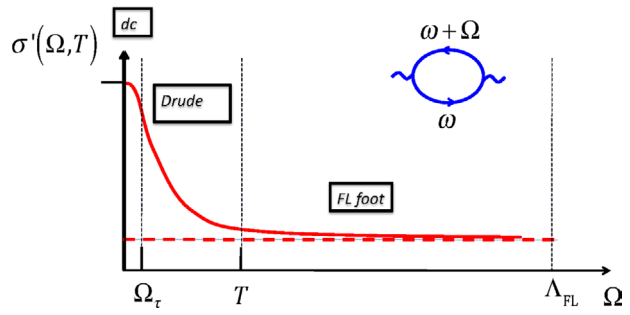

Figure 5. Optical conductivity of a Fermi liquid. $\Omega_\tau \sim 1/\tau_{ee}(\Omega=0,T) \propto T^2$.

where $\sigma_0 = (16e^2/3D)\oint da_{\mathbf{k}} v_{\mathbf{k}} Z_{\mathbf{k}}^2 A_{\mathbf{k}}$. For $\Omega \ll T$, $\sigma'(\Omega,T)$ assumes a Drude form ($\sigma' \propto 1/\Omega^2\tau_{ee}$) with $1/\tau_{ee} = 2\langle \mathrm{Im}\Sigma^R_{\mathbf{k}}(0,T)\rangle \propto T^2$, where $\langle\ldots\rangle$ indicates averaging over the FS. For $\Omega \gg T$, the Ω^2 term in the self-energy cancels with the Ω^2 term in the denominator, and σ' saturates at a frequency-independent value (the 'FL foot', see figure 5). The foot continues up to frequency Λ_{FL} at which the FL description breaks down. At higher frequencies, the behavior of σ' is non-universal [69]; at even higher frequencies, comparable to the bandwidth, the situation is further complicated by interband transitions, which can sometimes mimic a non-FL behavior [70]. The FL foot is seen, for example, in the optical conductivity of a heavy-fermion material UPd_2Al_3 [69, 71], and organic conductors β-(BEDT-TTF)$_2$AuI$_2$/I$_2$Br [72] and κ-(BEDT-TTF)$_2$Cu[N(CN)$_2$]Br$_x$Cl$_{1-x}$ [73, 74].

3.1.2. Vertex corrections.

3.1.2.a. Vertex-correction diagrams. While neglecting the vertex corrections simplifies the derivation of the Gurzhi formula, it is by no means a necessary condition for its validity. Originally, the Gurzhi formula was derived from the quantum Boltzmann equation, which takes into account vertex corrections automatically [17]. In the diagrammatic approach, one can show that any vertex-correction diagram for the conductivity, such as the ones in the bottom panel of figure 4, produces a contribution of the same form as in equation (3.5). Indeed, diagram 2 in figure 4, top) reads

$$\mathcal{K}_2(\Omega_n,T) = \frac{2}{D(2\pi)^{\{2D\}}}T^2\sum_{\omega_m,\omega_{m'}}\oint\frac{da_{\mathbf{k}}}{v_{\mathbf{k}}}\oint\frac{da_{\mathbf{k}'}}{v_{\mathbf{k}'}}\ \mathbf{v}_{\mathbf{k}}\cdot\mathbf{v}_{\mathbf{k}'}G_{\mathbf{k}}(\omega_m)G_{\mathbf{k}}(\omega_m+\Omega_n)G_{\mathbf{k}'}(\omega_{m'})G_{\mathbf{k}'}(\omega_{m'}+\Omega_n)\times\Gamma_{\mathbf{k},\mathbf{k}'}(\omega_m,\omega_{m'},\Omega_n), \quad (3.7)$$

where $\Gamma_{\mathbf{k},\mathbf{k}'}(\omega_m,\omega_{m'},\Omega_n)$ is the four-leg vertex, which we assume to depend on the directions of $\mathbf{k}$ and $\mathbf{k}'$ but not on their magnitudes. Employing the Eliashberg procedure of analytic continuation [75], integrating over $\varepsilon_{\mathbf{k}}$ and $\varepsilon_{\mathbf{k}'}$ with the assumption of a local self-energy, and neglecting the imaginary parts of the self-energies in the numerators of the resulting integrals (this corresponds to the same assumption that we used to arrive at equation (3.6)), we obtain for the vertex part of the conductivity

$$\sigma'_V(\Omega) = \mathrm{const}\times\oint da_{\mathbf{k}}\oint da_{\mathbf{k}'}\frac{\mathbf{v}_{\mathbf{k}}\cdot\mathbf{v}_{\mathbf{k}'}}{v_{\mathbf{k}}v_{\mathbf{k}'}}Z_{\mathbf{k}}Z_{\mathbf{k}'}\int_{-\infty}^{\infty}\frac{d\omega}{\Omega^3}$$
$$\times\int_{-\infty}^{\infty}d\omega'[n_F(\omega)-n_F(\omega+\Omega)]\mathrm{Im}\Gamma_{\mathbf{k},\mathbf{k}'}(\omega,\omega',\Omega), \quad (3.8)$$

where

$$\Gamma_{\mathbf{k},\mathbf{k}'}(\omega,\omega',\Omega) = \coth\frac{\omega'-\omega}{2T}(\Gamma^{\mathrm{II}}_{\mathbf{k},\mathbf{k}'}-\Gamma^{\mathrm{III}}_{\mathbf{k}\mathbf{k}'})$$
$$+\coth\frac{\omega+\omega'+\Omega}{2T}(\Gamma^{\mathrm{III}}_{\mathbf{k},\mathbf{k}'}-\Gamma^{\mathrm{IV}}_{\mathbf{k},\mathbf{k}'})-\tanh\frac{\omega'}{2T}\Gamma^{\mathrm{II}}_{\mathbf{k},\mathbf{k}'}$$
$$+\tanh\frac{\omega'+\Omega}{2T}\Gamma^{\mathrm{IV}}_{\mathbf{k},\mathbf{k}'}. \quad (3.9)$$

Vertices $\Gamma^{\mathrm{II-IV}}_{\mathbf{k},\mathbf{k}'}$ (which are functions of ω, ω', and Ω) are obtained by analytically continuing the Matsubara vertex into the corresponding regions of the $(\mathrm{Im}\omega,\mathrm{Im}\omega')$ plane for $\mathrm{Im}\,\Omega>0$, as shown in figure 6(a). As an example, diagram (a) in the bottom panel of figure 4 gives

$$\mathrm{Im}\Gamma_{\mathbf{k}\mathbf{k}'}(\omega,\omega',\Omega) = -2U^2_{\mathbf{k}-\mathbf{k}'}\mathrm{Im}\Pi^R_{\mathbf{k}-\mathbf{k}'}(\omega-\omega')$$
$$\times[2n_B(\omega'-\omega)+n_F(\omega')+n_F(\omega'+\Omega)], \quad (3.10)$$

where $U_{\mathbf{q}}$ is the (static) interaction corresponding to the wavy line, $n_B(\omega)$ is the Bose function, and

$$\Pi^R_{\mathbf{q}}(\Omega) = \frac{2}{(2\pi)^D}\oint\frac{da_{\mathbf{k}}}{v_{\mathbf{k}}}\int d\varepsilon_{\mathbf{k}}\frac{n_F(\varepsilon_{\mathbf{k}})-n_F(\varepsilon_{\mathbf{k}+\mathbf{q}})}{\Omega-\varepsilon_{\mathbf{k}+\mathbf{q}}+\varepsilon_{\mathbf{k}}+i0^+} \quad (3.11)$$

is the particle-hole polarization bubble. Now we recall that $\mathrm{Im}\Pi^R_{\mathbf{q}}(\Omega)\propto\Omega$ for $\Omega\ll v_F q$, relabel $\Omega'=\omega'-\omega$, and rewrite the double integral over ω and ω' in equation (3.8) as

$$\int_{-\infty}^{\infty}d\omega\,[n_F(\omega)-n_F(\omega+\Omega)]\,[S(\omega)+S(\omega+\Omega)], \quad (3.12)$$

where

$$S(\epsilon)\equiv\int_{-\infty}^{\infty}d\Omega'\Omega'[n_B(\Omega')+n_F(\epsilon+\Omega')] = \frac{1}{2}(\epsilon^2+\pi^2T^2) \quad (3.13)$$

is the same integral that appears in the imaginary part of the self-energy, equation (4.20). Therefore, the contribution from diagram (a) has the same dependence on Ω and T as equation (3.6). The remaining diagrams can also be shown to give the same contribution [21]. Following the Eliashberg's proof that an arbitrary order diagram for the self-energy produces the combination of $\omega^2+\pi T^2$ [76], one can also prove that any diagram for the conductivity scales with Ω and T as specified by equation (3.6) [21].

3.1.2.b. Physical consequences of vertex corrections. Because vertex corrections do not seem to affect the scaling form of the conductivity, it is widely accepted [77] that to get a reasonably accurate (within a 'factor of two') description of the conductivity, one can consider only the bare bubble diagram for the current–current correlator (diagram 1 in figure 4). This

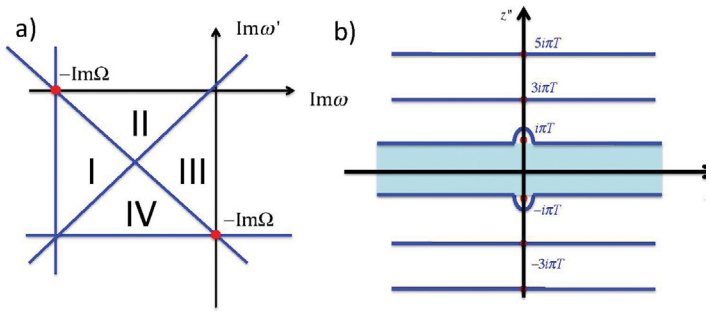

Figure 6. (a) Regions in the complex plane in which the vertex functions $\Gamma^{\mathrm{I-IV}}_{\mathbf{k},\mathbf{k}'}$ are defined. (b) Analytic structure of the imaginary part of the self-energy continued to the complex plane. Adapted with permission from [20] and [21]. Copyright by the American Physical Society.

is generally true, but there are two caveats, which we discuss below.

First, we recall that $\mathrm{Im}\Sigma^R \propto (\omega^2 + \pi^2 T^2)\ln(\omega^2 + \pi^2 T^2)$ in 2D contains an extra logarithm compared to the expression for $\mathrm{Im}\Sigma^R$ in 3D. This extra logarithm comes from a special subset of scattering processes, which are essentially one-dimensional (1D) [78–80]: the two interacting fermions move on either almost parallel or antiparallel trajectories both before and after the collision. However, a change in total current due to such processes ($\Delta\mathbf{J}$ in equation (2.6)) is negligibly small, and thus these almost 1D processes should not contribute to the conductivity. It turns out that it is the vertex corrections that cancel the contribution to $\sigma'(\Omega)$ from 1D processes [21]. As a result, $\sigma'(\Omega)$ of a 2D FL still scales as Ω^2 and T^2, as in the Gurzhi formula, equation (3.1), without extra logarithmic factors.

Second, equation (3.5) formally predicts a finite conductivity with the relaxation time $1/2\langle \mathrm{Im}\Sigma^R_{\mathbf{k}}(0,T)\rangle$ even at $\Omega = 0$. This is an artifact of neglecting the vertex corrections. If only normal processes are allowed, the *dc* conductivity is infinite. The deviations from the behavior predicted by equation (3.5) occur at $\Omega \lesssim \Omega_\tau$, where $\Omega_\tau \sim \langle \mathrm{Im}\Sigma^R_{\mathbf{k}}(0,T)\rangle \propto T^2$. (In section 2.2 we discussed these deviations for the case of a two-band metal.) In the presence of umklapp scattering, however, the *dc* conductivity is finite, and then equation (3.5) is qualitatively correct at all frequencies, provided that $\mathrm{Im}\Sigma^R_{\mathbf{k}}(\omega,T)$ is replaced by the transport scattering rate. One needs to keep in mind, however, that the coupling constants of *e-e* interaction entering the conductivity in the *dc* ($\Omega \ll \Omega_\tau$) and high-frequency ($\Omega \gg \Omega_\tau$) limits are, in general, different. Indeed, the *dc* conductivity is finite only in the presence of umklapp processes but, once they are allowed, normal processes can also contribute [35]. The Matthiessen rule in this regime in violated because the total scattering rate is not the sum of the umklapp and normal contributions. The *dc* resistivity can be written as $\rho_{\mathrm{dc}} = A_{\mathrm{dc}} 4\pi^2 T^2$, where A_{dc} depends on the effective coupling constants for normal and umklapp scattering (g_{n} and g_{u}, correspondingly) as

$$A_{\mathrm{dc}} = \mathrm{const} \times g_{\mathrm{u}} f\left(\frac{g_{\mathrm{n}}}{g_{\mathrm{u}}}\right), \tag{3.14}$$

where $f(x)$ takes constant and, in general, different values at $x \to 0$ and $x \to \infty$. On the contrary, the high-frequency conductivity contains contributions of both umklapp and normal scattering processes, which add up in a Matthiessen-like way, so that the optical resistivity

$$\rho_{\mathrm{opt}}(\Omega,T) \equiv \mathrm{Re}\sigma^{-1}(\Omega,T) \tag{3.15}$$

can be written as

$$\rho_{\mathrm{opt}}(\Omega,T) = A_{\mathrm{opt}}(\Omega^2 + 4\pi^2 T^2) \tag{3.16}$$

with $A_{\mathrm{opt}} = \mathrm{const} \times \max\{(g_{\mathrm{n}}, g_{\mathrm{u}}\}$. This means that the prefactors of the T^2 terms in the *dc* and optical resistivities, in general, are supposed to be different. In some cases, e.g. in $Nd_{1-x}TiO_3$ [81] and $CaRuO_3$ [82], the slopes of the T^2 terms in the *dc* and optical resistivities are indeed markedly different. However, this difference may be partially due by a systematic error in the absolute value of the *dc* resistivity, related to uncertainties in the sample size and shape [83].

4. First-Matsubara-frequency rules

Comparing the scaling forms of the self-energy and optical resistivity (equations (3.4) and (3.16)), one notices that they are *not* identical: the universal numerical prefactor of the T^2 term in the self-energy is π^2, whereas that in the optical resistivity is $(2\pi)^2 = 4\pi^2$. In this section we argue that this difference is not coincidental. Specifically, we show that the T-dependent part of $\mathrm{Im}\Sigma^R_{\mathbf{k}}(\omega,T)$, which measures the decay rate of fermion quasiparticles, contains the square of first fermion Matsubara frequency ($= \pi T$), while the T-dependent part of $\rho_{\mathrm{opt}}(\Omega,T)$, which measures the decay rate of current fluctuations, which are bosons, contains the square of the first non-zero boson Matsubara frequency ($= 2\pi T$). Also not coincidentally, equation (3.16) is of the same form as the sound absorption rate in a FL [84].

In more general terms, we argue that the scaling forms, given by equations (3.4) and (3.16), are manifestations of quite general 'first-Matsubara-frequency rules' (FMFR) that must be satisfied by the self-energy and optical conductivity of any electron system, not necessarily of a FL [19–21]. In the context of electron–phonon interaction, such a rule for the fermion self-energy is known as the 'Fowler-Prange theorem' [18, 85–87]. In sections 4.1 and 4.2, we analyze FMFR from the theoretical point of view. In section 4.3, we discuss the

experimental status of the Gurzhi formula for the optical conductivity, which is a consequence of FMFR.

4.1. First-Matsubara-frequency rule for the self-energy

4.1.1. Self-energy on the Matsubara axis.

4.1.1.a. Formulation of the rule. For a FL in $D > 2$, the FMFR states that the Matsubara self-energy, evaluated at the first fermion frequency $\omega = \pm\pi T$, contains a linear-in-T term but no T^2 term:

$$\Sigma_{\mathbf{k}}(\pm\pi T, T) = \pm \mathrm{i}\pi\lambda_{\mathbf{k}} T + 0 \times T^2 + R(T), \qquad (4.1)$$

where $\lambda_{\mathbf{k}}$ is related to the quasiparticle residue as $Z_{\mathbf{k}} = 1/(1+\lambda_{\mathbf{k}})$. In general, the remainder $R(T)$ scales as T^D, but the prefactor of the T^D term vanishes in the 'local approximation' [20], in which the fully renormalized interaction between quasiparticles is replaced by its value for the initial and final fermion states right on the Fermi surface. In $D = 2$, rule (4.1) is modified to the extent that $\Sigma_{\mathbf{k}}(\pm\pi T, T)$ contains a T^2 term but no $T^2 \ln T$ term.

For all but the first Matsubara frequencies, $\Sigma_{\mathbf{k}}(\omega_m, T)$ contains a T^2 term in $D > 2$ and a $T^2 \ln T$ term in $D = 2$. Equation (4.1) is also applicable to NFLs, the only difference is that the coefficient $\lambda_{\mathbf{k}}$ in a NFL itself depends on the temperature, and the form of the remainder changes. Two particular cases of NFLs, a marginal FL [88, 89] and a Hertz–Millis–Moriya quantum-critical metal [90–92], are discussed later in this section and in appendix B, correspondingly.

In dimensions $1 < D < 2$, FMFR is not satisfied even for FLs: the next-to-linear term in $\Sigma_{\mathbf{k}}(\pm\pi T, T)$ is of the same order as in $\Sigma_{\mathbf{k}}(\omega_m, T)$ with $m \neq 0, -1$.

4.1.1.b. One-loop order. The analysis of the remainder $R(T)$ requires special care and is presented in appendix B, but the derivation of the leading term in equation (4.1) is quite straightforward. For example, a one-loop diagram for the Matsubara self-energy (figure 7(a)) reads

$$\Sigma_{\mathbf{k}}(\omega_m, T) = T\sum_{\Omega_n} \int \frac{\mathrm{d}^D q}{(2\pi)^D} G_{\mathbf{q}}(\omega_m + \Omega_n)\chi(\mathbf{q}, \Omega_n), \quad (4.2)$$

where $\chi(\mathbf{q}, \Omega_n)$ is some dynamic interaction (double wavy line), which can represent, e.g. a phonon, screened Coulomb potential, spin fluctuation, etc. Suppose that χ decreases dramatically for q above some scale Λ, then typical momentum transfers are $\lesssim \Lambda$. We are interested in the low-energy dynamics, when $\max\{\omega, T\} \ll v_{\mathrm{F}}\Lambda$. Then the projection of $\mathbf{q}$ on the normal to the FS, $q_\perp$, is on the order of $\max\{\omega, T\}/v_{\mathrm{F}}$, and is thus smaller that than the projection on a plane tangential to the FS, $q_\parallel \sim \Lambda$. Since $q_\parallel \gg q_\perp$, the leading term in the self-energy can be obtaining by replacing q by $q_\parallel$ in $\chi(\mathbf{q}, \Omega_n)$. Consequently,

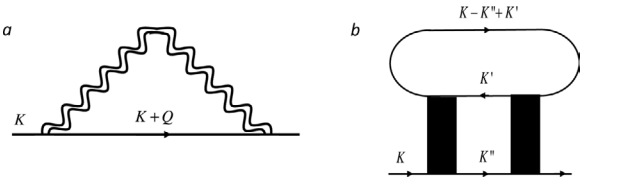

Figure 7. (a) One-loop self-energy in equation (4.2). (b) A general self-energy diagram with $K = (\mathbf{k}, \omega_m)$, $K' = (\mathbf{k}, \omega_{m'})$, and $K'' = (\mathbf{k}'', \omega_m + \Omega_n)$.

the integral over $\mathbf{q}$ factorizes into a one-dimensional integral over $q_\perp$ and a $D-1$-dimensional integral over the plane. The 1D integral involves only the Green's function and gives

$$\int \frac{\mathrm{d}q_\perp}{2\pi} G_{\mathbf{k}+\mathbf{q}}(\omega_m + \Omega_n) = \int \frac{\mathrm{d}q_\perp}{2\pi} \frac{1}{\mathrm{i}(\omega_m + \Omega_n) - \varepsilon_{\mathbf{k}} - v_{\mathrm{F}} q_\perp - q_\parallel^2/2m^*}$$
$$= -\frac{\mathrm{i}}{2v_{\mathrm{F}}} \mathrm{sgn}(\omega_m + \Omega_n), \qquad (4.3)$$

where v_{F} and m^* are the Fermi velocity and effective mass at point $\mathbf{k}$, correspondingly. The $D-1$-dimensional integral over $q_\parallel$ gives a local form of the interaction:

$$\chi_{\mathrm{loc}}(\Omega_n) = \int \frac{\mathrm{d}^{D-1} q_\parallel}{(2\pi)^{D-1}} \chi(\mathbf{q}_\parallel, \Omega_n). \qquad (4.4)$$

We thus arrive at

$$\Sigma_{\mathbf{k}}(\omega_m, T) = -\frac{\mathrm{i}}{2v_{\mathrm{F}}} T\sum_{\Omega_n} \mathrm{sgn}(\omega_m + \Omega_n)\chi_{\mathrm{loc}}(\Omega_n). \qquad (4.5)$$

For the remainder of the proof it matters only that χ_{loc} is an even function of Ω_n. Using this property and singling out the $\Omega_n = 0$ term, we re-arrange the sum in the equation above as

$$\Sigma_{\mathbf{k}}(\omega_m, T) = -\frac{\mathrm{i}}{2v_{\mathrm{F}}} \mathrm{sgn}\omega_m T\left[\chi_{\mathrm{loc}}(0) + 2\sum_{\Omega_n = 2\pi T}^{|\omega_m| - \pi T} \chi_{\mathrm{loc}}(\Omega_n)\right]. \qquad (4.6)$$

For $\omega_m = \pm\pi T$, the sum vanishes and

$$\Sigma_{\mathbf{k}}(\pm\pi T, T) = \mp \frac{\mathrm{i}}{2v_{\mathrm{F}}} T\chi_{\mathrm{loc}}(0), \qquad (4.7)$$

which yields the leading term in equation (4.1) with $\lambda_{\mathbf{k}} = -\chi_{\mathrm{loc}}(0)/2\pi v_{\mathrm{F}}$. For other ω_m, the sum in equation (4.6) does not vanish and gives rise to additional terms in $\Sigma_{\mathbf{k}}(\omega_m, T)$ besides the $\pm\mathrm{i}\pi\lambda_{\mathbf{k}} T$ one.

4.1.1.c. Examples. FMRF can be verified for a number of specific models with different forms of $\chi_{\mathrm{loc}}(\Omega_n)$. For example, if the boson in equation (4.2) corresponds to an Einstein phonon with frequency Ω_0, then $\chi_{\mathrm{loc}}(\Omega_n) = \mathrm{const}/(\Omega_n^2 + \Omega_0^2)$. (In this and other examples, we assume that the FS is isotropic, and suppress the dependence of the self-energy on the direction of $\mathbf{k}$.) The Matsubara sum in equation (4.6) in this case can be calculated exactly [93]:

$$\Sigma(\omega_m,T)=\text{const}\times\text{sgn}\omega_m\left[-\mathrm{i}\pi\coth\frac{\Omega_0}{2T}+\Psi\left(\frac{1}{2}+\mathrm{i}\frac{\Omega_0}{2\pi T}+\frac{|\omega_m|}{\pi T}\right)-\Psi\left(\frac{1}{2}-\mathrm{i}\frac{\Omega_0}{2\pi T}+\frac{|\omega_m|}{\pi T}\right)\right]$$
$$=\text{const}\times\text{sgn}\omega_m\left[\frac{2\pi T}{|\omega_m|-\pi T+\mathrm{i}\,\Omega_0}+\Psi\left(\mathrm{i}\frac{\Omega_0}{2\pi T}+\frac{|\omega_m|-\pi T}{2\pi T}\right)-\Psi\left(\mathrm{i}\frac{\Omega_0}{2\pi T}-\frac{|\omega_m|-\pi T}{2\pi T}\right)\right], \tag{4.8}$$

where $\Psi(x)=\mathrm{d}\ln\Gamma(x)/\mathrm{d}x$ is the digamma function. (We used the identity $\Psi(1-z)=\Psi(z)+\pi\cot(\pi z)$ to obtain the result shown in the second line). For $|\omega_m|=\pi T$, the two last terms cancel each other, whereas the first term reduces to a linear T dependence.

Another familiar example is a FL with *ee* interaction, where bosons correspond to particle-hole excitations. The frequency dependence of χ comes from Landau damping: $\chi_{\rm loc}(\Omega_n)=\text{const}_1+\text{const}_2\times|\Omega_n|$. The first term ($\text{const}_1$) gives an ω_m term in the self-energy, which is non-zero for all ω_m. The second term gives a T^2,ω_m^2 contribution, which vanishes for $\omega_m=\pm\pi T$:

$$\Sigma(\omega_m,T)=\mathrm{i}\lambda\omega_m-\frac{\mathrm{i}\text{const}_2}{2v_{\rm F}}T\sum_{\Omega_n=2\pi T}^{|\omega_m|-\pi T}|\Omega_n|$$
$$=\mathrm{i}\lambda\omega_m-\mathrm{i}\frac{\text{const}_2}{4\pi v_{\rm F}}(\omega_m^2-\pi^2T^2). \tag{4.9}$$

4.1.1.d. Beyond the one-loop order. In fact, the FL case allows for a more rigorous treatment than the one presented above just for the one-loop diagram. Following the arguments by Luttinger [94] and Eliashberg [76], one can show that any diagram for the self-energy gives a contribution that scales with ω_m and T as specified by equation (4.9). Details of the derivation are given in [20]; here we just outline the main idea. First, one realizes that a FL contribution to the self-energy comes from any diagram that contains three internal fermions with energies close to the Fermi energy. All other fermions, which are away from the Fermi energy, renormalize the interaction between these three low-energy fermions. All diagrams of this type can be represented by diagram (b) in figure 7, in which the shaded rectangles denote the exact interaction vertices. Since the dynamics in the problem is already coming from the three Green's functions, the vertices can be taken as static. After this simplification, diagram (b) is reduced to

$$\Sigma(\omega_m,T)=T^2\sum_{\omega_{m'},\Omega_n}\int\frac{\mathrm{d}^Dk'}{(2\pi)^D}\int\frac{\mathrm{d}^Dk''}{(2\pi)^D}G(\mathbf{k}',\omega_{m'})$$
$$G(\mathbf{k}'',\omega_m+\Omega_n)G(\mathbf{k}-\mathbf{k}''+\mathbf{k}',\omega_{m'}-\Omega_n)\Gamma^2(\mathbf{k},\mathbf{k}',\mathbf{k}''). \tag{4.10}$$

Dispersions $\varepsilon_{\mathbf{k}'}$, $\varepsilon_{\mathbf{k}''}$, and $\varepsilon_{\mathbf{k}-\mathbf{k}''+\mathbf{k}'}$ are assumed to be small, of order ω_m or T. Within the same local approximation already employed for diagram (a), the vertices can be then assumed to depend only on the directions of the incoming and outgoing momenta but not on their magnitudes. The condition of a small $\varepsilon_{\mathbf{k}-\mathbf{k}''+\mathbf{k}'}$ imposes a geometrical constraint on the angles between the momenta, e.g. on the angle between $\mathbf{k}'$ and $\mathbf{k}-\mathbf{k}''$. We thus have three 'infrared' integrals–over $\varepsilon_{\mathbf{k}'}$, $\varepsilon_{\mathbf{k}''}$, and over the angle–which are carried out in infinite limits and produce signs of the corresponding Matsubara frequencies, similar to the integral over $q_\perp$ in equation (4.3). Integrating over $\varepsilon_{\mathbf{k}'}$ and over the angle, we obtain a combination $\text{sgn}\omega_{m'}\text{sgn}(\omega_{m'}-\Omega_n)$. Upon summation over $\omega_{m'}$, this combination produces a term, which can absorbed into the linear-in-ω_m part of the self-energy, and an $|\Omega_n|$ term. The latter comes in a combination

$$\int\mathrm{d}\theta_{\mathbf{k}''}\left[T\sum_{\Omega_n}|\Omega_n|\int\mathrm{d}\varepsilon_{\mathbf{k}''}G(\mathbf{k}'',\omega_m+\Omega_n)\right]\Gamma^2(\mathbf{k},\mathbf{k}'\{\mathbf{k},\mathbf{k}''\},\mathbf{k}''), \tag{4.11}$$

where the notation $\mathbf{k}'\{\mathbf{k},\mathbf{k}''\}$ means that the constraint on the angles has already been taken into account. The square brackets in the equation above give a factor of $\omega_m^2-\pi T^2$, which means that this part of the self-energy vanishes at $\omega_m=\pm\pi T$, and thus the FMFR is satisfied.

4.1.1.e. Partial self-energy. Notice that the combination $\omega_m^2-\pi T^2$ occurs *before* integrating over $\theta_{\mathbf{k}''}$. This means that FMFR can also be formulated for a *partial self-energy*, defined in the same way as the usual self-energy but without the last angular integration:

$$\mathcal{S}_{\mathbf{k},\mathbf{k}''}(\omega_m,T)=N_{\rm F}T^2\sum_{\omega_{m'},\Omega_n}\int\mathrm{d}\varepsilon_{\mathbf{k}''}\int\frac{\mathrm{d}^Dk'}{(2\pi)^D}G(\mathbf{k}',\omega_{m'})$$
$$\times G(\mathbf{k}'',\omega_m+\Omega_n)G(\mathbf{k}-\mathbf{k}''+\mathbf{k}',\omega_{m'}-\Omega_n)\Gamma^2(\mathbf{k},\mathbf{k}',\mathbf{k}'') \tag{4.12}$$

where the density of states ($N_{\rm F}$) was introduced for $\mathcal{S}_{\mathbf{k},\mathbf{k}''}(\omega_m,T)$ to have units of energy. The usual self-energy is obtained by averaging the partial one over the direction of $\mathbf{k}''$. Restoring anisotropy of FS, the relation between the partial and usual self-energies can be written as

$$\Sigma_{\mathbf{k}}(\omega_m,T)=\frac{1}{N_{\rm F}(2\pi)^D}\int\frac{\mathrm{d}a_{\mathbf{k}''}}{v_{\mathbf{k}''}}\mathcal{S}_{\mathbf{k},\mathbf{k}''}(\omega_m,T). \tag{4.13}$$

FMFR for the partial self-energy implies that

$$\mathcal{S}_{\mathbf{k},\mathbf{p}}(\pm\pi T)=\pm\mathrm{i}T\mu_{\mathbf{k},\mathbf{p}}+0\times T^2. \tag{4.14}$$

Averaging $\mu_{\mathbf{k},\mathbf{p}}$ over the direction of $\mathbf{p}$ gives $\lambda_{\mathbf{k}}$ in equation (4.1). FMRF for the partial self-energy will be important for deriving the analogous rule for the optical conductivity, see section 4.2.

4.1.1.f. Physical consequences. In physical terms, FMFR says that $\Sigma_{\mathbf{k}}(\pm\pi T,T)$ does not contain a part which, if continued to real frequencies, would correspond to damping of quasiparticles. This, by itself, has important physical consequences, especially for thermodynamic quantities, which can be calculated entirely in the Matsubara representation. For example, the effect of many-body interactions on the

amplitude of de Haas-van Alphen (dHvA) oscillations, $A(T)$, is encapsulated by the Matsubara self-energy:

$$A(T) = \frac{4\pi^2 T}{\omega_c} \sum_{\omega_m = \pi T}^{\infty} \exp\left[-2\pi \frac{\omega_m - \mathrm{i}\Sigma(\omega_m, T)}{\omega_c}\right], \tag{4.15}$$

where ω_c is the cyclotron frequency. If $T \gtrsim \omega_c$, one can keep only the first term in the sum which, thanks to equation (4.1), is reduced to

$$A(T) = \frac{4\pi^2 T}{\omega_c} \exp\left[-2\pi \frac{\pi T - \mathrm{i}\Sigma(\pi T, T)}{\omega_c}\right] = \frac{4\pi^2 T}{\omega_c} \exp\left(-2\pi^2 \frac{T}{\omega_c^*}\right), \tag{4.16}$$

where $\omega_c^* = \omega_c/(1+\lambda)$. Therefore, the effect of interactions on dHvA amounts only to mass renormalization while damping disappears [18, 19, 85–87, 95]. (Damping by disorder is still present because the corresponding self-energy $\Sigma(\omega_m, T) = \text{const} \times i\text{sgn}\,\omega_m$ is not a subject to FMFR.)

Another example is superconductivity mediated by soft boson modes near a quantum phase transition in $D < 3$. In this case, fermions are strongly scattered by the same near-critical bosons that provide the glue for superconductivity. It might seem that this scattering would impede superconductivity. As in the previous example, however, the effect of fermion damping on T_c is embodied by the Matsubara self-energy, which does not contain the damping part at $\omega_m = \pm\pi T$. It turns out [96] that the vanishing of the damping part of the self-energy at these two frequencies renders T_c finite, even if damping at other Matsubara frequencies is very strong.

4.1.2. Self-energy on the real axis.

4.1.2.a. Analytic structure of the self-energy in the complex plane. For other observables, such as photoemission intensity and optical conductivity, one would like to know the constraints on the real and imaginary parts of the self-energy. For positive (negative) Matsubara frequencies, the Matsubara self-energy can be obtained by analytic continuation of the retarded (advanced) self-energy from the real axis to the complex plane (which is opposite to usual analytic continuation, in which the Matsubara self-energy is continued to the real axis). Let $S_R(z,T)$ and $S_I(z,T)$ be analytic continuations of the real and imaginary parts of the retarded self-energy into the complex plane, correspondingly. For $\omega_m > 0$, FMRF implies that

$$\Sigma(\pi T, T) = S_R(\mathrm{i}\pi T, T) + \mathrm{i}S_I(\mathrm{i}\pi T, T) = \mathrm{i}\lambda T. \tag{4.17}$$

In the FL regime, the real part of the self-energy can be written as $\mathrm{Re}\Sigma^R(\omega, T) = \lambda\omega + \mathrm{Re}\tilde{\Sigma}^R(\omega, T)$, where $\mathrm{Re}\tilde{\Sigma}^R(\omega, T)$ contains higher-order terms in ω and T. The function $S_R(z, T)$ can be likewise separated into the linear part and the remainder: $S_R(z, T) = \lambda z + \tilde{S}_R(z, T)$. After that, equation (4.17) is reduced to

$$\tilde{S}_R(\mathrm{i}\pi T, T) + \mathrm{i}S_I(\mathrm{i}\pi T, T) = 0. \tag{4.18}$$

Equation (4.18) does not imply that $S_R(\mathrm{i}\pi T, T)$ and $S_I(\mathrm{i}\pi T, T)$ must vanish separately. However, they do in all particular cases that we know of. The best-known case is the conventional FL, where

$$\mathrm{Im}\Sigma^R(\omega, T) = \text{const} \times (\omega^2 + \pi^2 T^2) \tag{4.19}$$

on the real axis. Obviously, $\mathrm{Im}\Sigma^R(\pm\mathrm{i}\pi T, T) = 0$.

One might argue that the vanishing of $\mathrm{Im}\Sigma^R(\pm\mathrm{i}\pi T, T)$ is a general property. Indeed, within the local approximation $\mathrm{Im}\Sigma^R(\omega, T)$ can be written as an integral

$$\mathrm{Im}\Sigma^R(\omega, T) = -\frac{1}{2\pi\nu_F} \int_{-\infty}^{\infty} \mathrm{d}\,\Omega[n_B(\Omega) + n_F(\omega + \Omega)]\mathrm{Im}\chi^R_{\mathrm{loc}}(\Omega), \tag{4.20}$$

where $\chi^R_{\mathrm{loc}}(\Omega)$ is obtained by analytic continuation of equation (4.4) and $n_B(\Omega)$ is the Bose function. Substituting $\omega = \pm\,\mathrm{i}\pi T$ directly into the Fermi function in equation (4.20) and noting that

$$n_F(\Omega \pm \mathrm{i}\pi T) = -n_B(\Omega), \tag{4.21}$$

we see that $\mathrm{Im}\Sigma^R(\pm\,\mathrm{i}\pi T, T) = 0$.

The argument leaves unclear, however, why $\mathrm{Im}\Sigma^R(\omega, T)$ vanishes only at the first but not all Matsubara frequencies, whereas the identity

$$n_F(\Omega + \mathrm{i}\omega_m) = -n_B(\Omega), \tag{4.22}$$

holds for any ω_m. To understand why analytic continuation of $\mathrm{Im}\Sigma^R(\omega, T)$ does not vanish at all Matsubara frequencies, one needs to look more carefully into the analytic structure of the function $f(z) \equiv \mathrm{Im}\Sigma^R(z, T)$ in the complex plane. In fact, this function is multi-valued, and analytic continuation of $\mathrm{Im}\Sigma^R(z, T)$, i.e. function $S_I(z,T)$, corresponds to a particular branch that coincides with $\mathrm{Im}\Sigma^R(\omega, T)$ on the real axis. In the FL case, the result for $f(z)$, which is valid for any complex z, is especially simple:

$$f(z) = \text{const} \times T^2\left[\pi^2 + (\ln \mathrm{e}^{z/T})^2\right]. \tag{4.23}$$

On the real axis, equation (4.23) gives obviously the same result as equation (4.19). In the complex plane, however, $\ln\exp(z)$ is a multi-valued function: $\ln\exp(z) = z - 2\pi\mathrm{i}n$, with $n = 0, \pm 1, \ldots$ Single-valued branches are selected by cutting the plane by horizontal lines at $\mathrm{Im}z = \mathrm{i}\pi(2m+1)T$, that is, exactly at the Matsubara frequencies (see figure 6(b)). Analytic continuation of equation (4.19) is achieved by choosing the branch of $\ln\exp(z)$ with $n = 0$, which coincides with equation (4.19) on the real axis: $f(z) = \text{const} \times [\pi^2 T^2 + z^2]$. This branch obviously vanishes only at $z = \pm\mathrm{i}\pi T$ but not at any other Matsubara frequency. Therefore, the first Matsubara rule for the retarded the self-energy can be formulated as follows: the analytic continuation of $\mathrm{Im}\Sigma^R(\omega, T)$ vanishes at $\omega \to \pm\mathrm{i}\pi T$. Equation (4.18) implies then that the same holds for analytic continuation of $\mathrm{Re}\tilde{\Sigma}^R(\omega, T) = \mathrm{Re}\Sigma^R(\omega, T) - \lambda\omega$.

4.1.2.b. Example: marginal Fermi liquid. As an example when the implementation of FMFR leads to non-trivial results, we consider the marginal Fermi liquid (MFL) model [88, 89]. The MFL model was introduced phenomenologically to explain the ubiquitously observed linear scaling of the scattering rate with temperature and frequency. In this model, the scattering rate is identified with the imaginary part of the self-energy. The required behavior of $\mathrm{Im}\Sigma^R(\omega, T)$, i.e. $\mathrm{Im}\Sigma^R(\omega, T) = \text{const} \times \max\{\omega, T\}$, is

achieved by choosing $\mathrm{Im}\chi^R_{\mathrm{loc}}(\Omega,T)$ to be a scaling function of Ω/T with the limits given by $\mathrm{Im}\chi^R_{\mathrm{loc}}(\Omega,T)\propto \mathrm{sgn}\,\Omega$ for $T\ll\Omega\leqslant\Omega^*$ and $\mathrm{Im}\chi^R_{\mathrm{loc}}(\Omega,T)\propto\Omega/T$ for $\Omega\ll T$, where Ω^* is the high-energy cutoff of the model. A convenient choice that satisfies these conditions is

$$\mathrm{Im}\chi^R_{\mathrm{loc}}(\Omega,T)=\mathrm{const}\times\tanh(\Omega/T). \tag{4.24}$$

With this choice, equation (4.20) gives

$$\mathrm{Im}\Sigma^R(\omega,T)=\mathrm{const}\times TF\left(\frac{\omega}{T}\right), \tag{4.25}$$

where

$$F(x)=\frac{\pi}{2}\left(1+\frac{1}{\cosh x}\right)+x\tanh x. \tag{4.26}$$

(Note that this result is different from the often used empirical form $\mathrm{Im}\Sigma^R(\omega,T)=\mathrm{const}\times\sqrt{\omega^2+\pi^2T^2}$.)

From the mathematical point of view, equation (4.26) is different from the corresponding result for a FL (equation (4.19)) not only in the overall linear versus quadratic scaling with ω and T, but also in that $\mathrm{Im}\Sigma^R(\omega,T)$ of a MFL vanishes not only at the first but also at any Matsubara frequency, if one formally sets $\omega=\mathrm{i}\pi T(2m+1)$ in equation (4.26). Nevertheless, one can show that the correct self-energy on the Matsubara axis, obtained by the analytic continuation of $\mathrm{Im}\Sigma^R(\omega,T)$, vanishes only at the first Matsubara frequency, in agreement with FMRF. The Matsubara self-energy at $\omega_m=\pm\pi T$ is given by equation (4.7) with $\chi_{\mathrm{loc}}(0)$ related to $\mathrm{Im}\chi^R_{\mathrm{loc}}(\Omega,T)$ by the spectral representation

$$\chi_{\mathrm{loc}}(0)=\frac{2}{\pi}\int^{\Omega^*}\frac{\mathrm{d}\,\Omega}{\Omega}\mathrm{Im}\chi^R_{\mathrm{loc}}(\Omega,T). \tag{4.27}$$

Using the MFL form of $\mathrm{Im}\chi^R_{\mathrm{loc}}(\Omega,T)$ (equation (4.24)), we obtain

$$\Sigma(\pm\pi T,T)=\pm\mathrm{i}\ \mathrm{const}\times T\ln\left(\frac{4e^{\gamma}\Omega^*}{\pi T}\right), \tag{4.28}$$

where $\gamma=0.577\ldots$ is the Euler constant. A $T\ln T$-scaling of the Matsubara self-energy (as opposed to a T-scaling in a FL) is what makes this model 'marginal'.

Other examples of the same kind are encountered, for example, for electrons interacting with both optical and acoustic phonons, with the corresponding self-energies given by

$$\text{Opt.phonons}:\ \mathrm{Im}\Sigma^R(\omega,T)=\mathrm{const}\times[n_B(\Omega_0)+n_{\mathrm{F}}(\omega+\Omega_0)-n_B(-\Omega_0)-n_{\mathrm{F}}(\omega-\Omega_0)], \tag{4.29a}$$

$$\text{Ac.phonons}:\ \mathrm{Im}\Sigma^R(\omega,T)=\mathrm{const}\times T^3[2\zeta(3)-\mathrm{Li}_3(-\mathrm{e}^{\omega/T})-\mathrm{Li}_3(-\mathrm{e}^{-\omega/T})], \tag{4.29b}$$

where $\zeta(x)$ is the Riemann ζ-function and $\mathrm{Li}_n(x)=\sum_{k=1}^{\infty}x^k/k^n$ the polylogarithmic function. In both cases, $\mathrm{Im}\Sigma^R(\omega,T)$ also vanishes at $\omega=\mathrm{i}\pi T(2m+1)$ with any integer m. However the correct $\Sigma(\omega_m,T)$ vanishes only at the first Matsubara frequency.

Recent photoemission study of a HTC cuprate ($Bi_2Sr_2CaCu_2O_{8+\delta}$) [16] used a phenomenological form $\mathrm{Im}\Sigma^R(\omega,T)=\mathrm{const}(\omega^2+\beta^2T^2)^{\alpha}$ (the 'power-law liquid') to describe the observed scaling of the momentum distribution peak with ω and T over a wide range of doping. The coefficient β was found to be near π without a systematic variation with doping, which means that FMFR is satisfied. On the other hand, the exponent α was found to vary across the phase diagram from $\alpha\approx0.3$ (underdoped) to $\alpha\approx0.6$ (overdoped). To explain the values of $\alpha<0.5$ within the MFL model, one would need to modify the Ansatz for the local susceptibility as $\mathrm{Im}\chi_{\mathrm{loc}}(\Omega,T)=\mathrm{const}\times|\Omega|^{-(1-2\alpha)}\tanh(\Omega/T)$.

4.2. First-Matsubara-frequency rule for the optical conductivity

4.2.1. Optical conductivity on the Matsubara axis. Similarly to the self-energy considered in the previous section, the optical conductivity also satisfies FMRF, which can be formulated both on the Matsubara and real axes. First, we consider the Matsubara axis and define the 'Matsubara conductivity' as

$$\sigma(\Omega_n,T)=-\frac{e^2}{\Omega_n}\mathcal{K}(\Omega_n,T). \tag{4.30}$$

Analytic continuation of $\sigma(\Omega_n,T)$ gives the usual conductivity on the real axis. The first Matsubara rule for $\sigma(\Omega_n,T)$ can be formulated as

$$\sigma(\pm2\pi T,T)=\frac{\mathcal{D}}{T}+R_\sigma(T). \tag{4.31}$$

In a FL, the 'Drude weight' $\mathcal{D}$ is independent of the temperature. The remainder $R_\sigma(T)$ is related to $R(T)$ in equation (4.1) and will be discussed below.

We split the proof of equation (4.31) into two steps. At the first step, we consider only the bare bubble diagram for the conductivity (diagram 1 in figure 4, top). In this case, equation (4.31) follows directly from FMRF for the self-energy, equation (4.1). To see this, we assume again that the self-energy is local and recall that $\mathrm{sgn}\Sigma_{\mathbf{k}}(\omega_m)=\mathrm{sgn}\omega_m$. Integrating over $\varepsilon_{\mathbf{k}}$ in equation (3.3), we then obtain for $\Omega_n>0$

$$\mathcal{K}_1(\Omega_n,T)=-\frac{2\mathrm{i}T}{D(2\pi)^{D-1}}\oint\mathrm{d}a_{\mathbf{k}}v_{\mathbf{k}}\sum_{\omega_m=-\Omega_n+\pi T}^{\omega_m=-\pi T}\frac{1}{\mathrm{i}\,\Omega_n+\Sigma_{\mathbf{k}}(\omega_m+\Omega_n)-\Sigma_{\mathbf{k}}(\omega_m)}. \tag{4.32}$$

For $\Omega_n=2\pi T$, only the $\omega_m=-\pi T$ term survives in the sum and

$$\mathcal{K}_1(2\pi T,T)=-\frac{2\mathrm{i}T}{D(2\pi)^D}\oint\mathrm{d}a_{\mathbf{k}}v_{\mathbf{k}}\frac{1}{2\pi\mathrm{i}T+\Sigma_{\mathbf{k}}(\pi T)-\Sigma_{\mathbf{k}}(-\pi T)}. \tag{4.33}$$

Thanks to FMFR for the self-energy (equation (4.1)), we have $\Sigma_{\mathbf{k}}(\pi T)-\Sigma_{\mathbf{k}}(-\pi T)=2\pi\mathrm{i}T\lambda_{\mathbf{k}}+\mathcal{O}(T^D)$. Therefore, we arrive at equation (4.31) with $\mathcal{D}=-[2/D(2\pi)^D]\oint\mathrm{d}a_kv_{\mathbf{k}}Z_{\mathbf{k}}$ and $R_\sigma(T)=\mathcal{O}(T^{D-2})$.

At the second step, we consider the vertex corrections to the conductivity. This step is more involved and requires the

use of the first Matsubara rule for the *partial* self-energy, equation (4.14). Although there is no Ward identity for the current vertex in in the absence of Galilean invariance, some Ward-type relations between the vertices and partial self-energies can still be derived within the local approximation. This procedure is described in appendix C. The result is that the vertex part of the conductivity also obeys FMRF in equation (4.31).

4.2.2. Optical conductivity on the real axis. On the real axis, FMRF for the optical conductivity states that its real part vanishes at $\Omega = \pm 2\pi \mathrm{i}T$ up to subleading terms:

$$\mathrm{Re}\sigma(\pm 2\pi \mathrm{i}T, T) = 0 + \tilde{R}_\sigma(T), \tag{4.34}$$

with $\tilde{R}_\sigma(T) = \mathcal{O}(T^D)$. This rule follows from substituting $\Omega = \pm 2\pi \mathrm{i}T$ directly into the self-energy (equation (3.6)) and vertex (equation (3.8)) parts of the conductivity and noticing that $n_\mathrm{F}(\omega \pm 2\pi \mathrm{i}T) = n_\mathrm{F}(\omega)$. As in the case of the self-energy (see section 4.1.2), the functions defined by equations (3.6) and (3.8) have branch-cut singularities in the complex plane, and thus analytic continuation is possible only to the first (boson) frequency but not to the higher ones.

As we mentioned in section 4.1.2, gauge invariance makes the conductivity to be more robust with respect to infrared singularities, which modify the canonical FL scaling in $D \leqslant 2$. In 2D, for example, only $\mathcal{O}(T^2 \ln T)$ terms in the self-energy vanish at $\omega = \pm \mathrm{i}\pi T$, while $\mathcal{O}(T^2)$ terms survive. This is not the case for the conductivity, which does not have $\mathcal{O}(T^2 \ln T)$ terms.

4.3. Experimental verification of the Gurzhi formula

4.3.1. Review of recent experiments. In this section, we discuss the experimental status of the Gurzhi formula, equation (3.1), for the optical conductivity of a Fermi liquid. Although it seems to be most natural to verify this formula in conventional metals, which are expected to obey the FL-theory predictions, it is very hard to detect the FL, T^2 term in $\tau^{-1}(\Omega, T)$ because it is masked by the electron–phonon interaction at any temperatures except for very low ones. On the other hand, the FL part of the Ω-dependence can be verified because the electron–phonon contribution to $\tau^{-1}(\Omega, T)$ saturates at frequencies above the characteristic phonon scale ('Debye frequency'), whereas the *ee* contribution continues to grow as Ω^2 until interband transitions become important. Indeed, the Ω^2 dependence of $\tau^{-1}(\Omega, T)$ was convincingly demonstrated for a number of conventional metals (Au,Ag, and Cu) [7, 8]. As expected, however, the T dependence of $\tau^{-1}(\Omega, T)$ was found to result from the electron–phonon rather than *ee* interaction. To the best of our knowledge, the $\Omega^2 + 4\pi^2 T^2$ scaling form has not been verified in conventional metals.

On the other hand, Ω/T scaling of the optical conductivity in strongly correlated metals has been studied quite extensively in the past [73, 74, 81, 97, 98] and the interest to this subject has been reignited recently by a detailed study of the optical conductivity of a 'hidden order' heavy-fermion compound URu_2Si_2 [12]. By now, the Gurzhi formula has been checked for several classes of materials: heavy fermions, [12, 97] doped Mott insulators [81, 98], organic materials of the BEDT-TTF family [73, 74], underdoped cuprates [13], Sr_2RuO_4 [14], and iron-based superconductors [15].

It is customary to use a particular parametrization of $\sigma(\Omega, T)$, called an 'extended Drude formula' [1, 2]:

$$\sigma(\Omega, T) = \frac{\Omega_p^2}{4\pi} \frac{1}{1/\tau(\Omega, T) - \mathrm{i}\,\Omega\,[1 + \lambda_\mathrm{tr}(\Omega, T)]}, \tag{4.35}$$

where Ω_p is the plasma frequency, $1/\tau(\Omega, T)$ is the optical scattering rate, and $1 + \lambda_\mathrm{tr}(\Omega, T)$ is the ratio of the 'transport effective mass' to the band one. In general, the transport mass differs from the quasiparticle one. This can be seen already from the fact that, in a Galilean-invariant interacting system, the former coincides with the bare mass but the latter does not. In this parametrization,

$$\tau^{-1}(\Omega, T) \equiv \frac{\Omega_p^2}{4\pi} \mathrm{Re}\sigma^{-1}(\Omega, T). \tag{4.36}$$

The Gurzhi formula implies that

$$\tau^{-1}(\Omega, T) \propto \Omega^2 + 4\pi^2 T^2. \tag{4.37}$$

In an experiment, one fits the data to a phenomenological form

$$\frac{1}{\tau(\Omega, T)} = \mathrm{const} \times (\Omega^2 + b\pi^2 T^2), \tag{4.38}$$

where b is treated as a fitting parameter. The theoretical value is $b = 4$. The results from a number of studies are summarized in table 1, which is an updated version of table I in [12]. As one can see, the discrepancy between the experimental and theoretical values is quite significant in most cases, except for Sr_2RuO_4 [14]. The discrepancy is especially pronounced in doped rare-earth Mott insulators and heavy-fermion materials, where b is smaller than 2 and remarkably close to 1 in some cases, e,g. in URu_2Si_2 [12]. The cuprates and iron pnictides occupy an intermediate niche with $2 < b < 3$.

4.3.2. Phenomenological model: elastic and inelastic scattering. A quantitative analysis of Ω/T scaling of the optical conductivity is a difficult task, as one needs to make sure that the data are taken over regions of comparable Ω and T [99]. In addition, Gurzhi scaling is expected to work only at the lowest frequencies and temperatures, which is not necessarily the case in all of the experiments cited in table 1. Nevertheless, it is interesting to ask whether there are fundamental reasons for the coefficient b to deviate from the theoretical value of 4. If the $\pi^2 T^2$ and Ω^2 terms in the scattering rate come from the same mechanism, namely, from *ee* interaction of any sort, the relative weight of these terms should be equal exactly to 4. However, if there are other, non-electron mechanisms which contribute extra T^2 and Ω^2 terms, the relative weight of these terms in the total scattering rate may be different from 4.

One example of such a situation is the low-temperature (Nozières) regime of the Kondo effect [100], where electrons interact with screened magnetic impurities and also with electrons forming the screening clouds. The first mechanism is elastic, which means that the corresponding part of $\mathrm{Im}\Sigma^R$ does not depend on temperature but does depend on frequency, as ω^2 at the lowest ω. The second mechanism is inelastic and

Table 1. Measured values of parameter b in the Gurzhi formula for the optical scattering rate (equation (4.38)) and phenomenological parameter a, defined by equation (4.41) and related to b via equation (4.43). Parameter a measures the relative strength of an elastic contribution to the self-energy (equation (4.41)). * indicates that the slope of the T^2 term was taken from the *dc* resistivity, which may not be an accurate procedure due to a difference in the normal and umklapp contributions to the *dc* and optical resistivities, see section 3.1.2.

Material	b	Reference for raw data	Reference for b	a
UPt_3	<1	[97]	[97]	$\to\infty$[a]
$CePd_3$	1.3*	[97]	[12]	9.0
doped $CeTiO_3$	1.8*	[98]	[98]	2.8
doped $NdTiO_3$	1.0	[81]	[81]	$\to\infty$
κ-BEDT-TTF	5.6*	[73, 74]	[12, 69]	-0.3
URu_2Si_2	1.0 ± 0.1	[12]	[12]	$\to\infty$
Hg1201, YBCO, Bi2201	2.3	[13]	[13]	1.3
Sr_2RuO_4	4[b]	[14]	[14]	0
Co-doped $BaFe_2As_2$	2.16	[15]	[15]	1.58

[a] $a\to\infty$ indicates that the elastic contribution exceeds by far the inelastic one. A precise determination of a is impossible given the accuracy of the reported values of b.
[b] Extrapolated value.

contributes a FL-like, $\omega^2+\pi^2T^2$ combination to $\mathrm{Im}\Sigma^R$. In the unitary limit, the prefactor of the elastic ω^2 term is twice larger than that of the inelastic one [100], so the total $\mathrm{Im}\Sigma^R$ is given by

$$\mathrm{Im}\Sigma^R(\omega,T)=\mathrm{const}+\frac{2}{3}\mathrm{const}'\left(\omega^2+\frac{1}{2}[\omega^2+\pi^2T^2]\right)$$
$$=\mathrm{const}+\mathrm{const}'\left(\omega^2+\frac{1}{3}\pi^2T^2\right), \quad (4.39)$$

where $\mathrm{const}>0$ is the ω-independent part of the elastic contribution and $\mathrm{const}'<0$ in the dilute limit. Substituting equation (4.39) into Kubo formula (3.6), we obtain for the optical scattering rate

$$\frac{1}{\tau(\Omega,T)}=\mathrm{const}+\frac{2}{3}\mathrm{const}'(\Omega^2+2\pi^2T^2). \quad (4.40)$$

A reduced weight of the T^2 term in $\mathrm{Im}\Sigma^R$ is reflected in the corresponding reduction of the T^2 term in the optical scattering rate, where now the coefficient b is equal to 2 rather than 4. Thus the local (Kondo) FL belongs to a different universality class compared to the usual (itinerant) FL. Of course, the Kondo model (in the dilute limit) cannot explain the experiment because, first of all, $1/\tau(\Omega,T)$ in equation (4.40) *decreases* with Ω and T, while it increases with Ω and T in the experiment. However, this example gives one an idea to address the issue phenomenologically, by asking what form of the self-energy would produce the measured scattering rate.

Suppose that there are two scattering channels in a system. The first one is the conventional channel of inelastic *ee* scattering, which gives an $\omega^2+\pi^2T^2$ contribution to $\mathrm{Im}\Sigma^R(\omega,T)$ with a positive prefactor, and the second one is the elastic channel that contributes an ω^2 but no T^2 term to the self-energy. The total self-energy is then given by

$$\mathrm{Im}\Sigma^R(\omega,T)=\mathrm{const}+\mathrm{const}''\,[a\omega^2+(\omega^2+\pi^2T^2)] \quad (4.41)$$

with $\mathrm{const}''>0$. Substituting this form into the Kubo formula, we find the corresponding optical rate

$$\frac{1}{\tau(\Omega,T)}=\mathrm{const}+\mathrm{const}''(a+1)\,[\Omega^2+b\pi^2T^2] \quad (4.42)$$

with

$$b=\frac{a+4}{a+1}. \quad (4.43)$$

The (itinerant) FL value of $b=4$ corresponds to $a=0$. The opposite limit of $a\to\infty$ (and thus of $b\to1$) corresponds to purely elastic scattering. The range $0<a<\infty$ yields $1<b<4$. This corresponds to a mixture of elastic and inelastic mechanisms, with a 'metallic' sign ($\partial_\omega\mathrm{Im}\Sigma^R>0$) of the elastic contribution to the self-energy. For $-1<a<0$, the elastic contribution to the self-energy has a 'non-metallic' sign ($\partial_\omega\mathrm{Im}\Sigma^R<0$), although the Ω and T dependences of $1/\tau(\Omega,T)$ are still metallic-like. This interval of a corresponds to $b>4$. The special case of $a=-1$ corresponds to $\mathrm{Im}\Sigma^R(\omega,T)$ that depends only on T but not on Ω. For $a<-1$, the Ω dependence of $1/\tau(\Omega,T)$ has a non-metallic sign. Such a behavior was not observed in the experiments discussed here.

According to this classification scheme, the value of $b\approx1$ observed in U, Ce, and Nd-based compounds [12, 81, 97, 98] indicates that a purely elastic scattering mechanism is the dominant one in these materials ($a\to\infty$). The values of $b\approx2.3$ and 2.16 observed in the cuprates [13] and pnictides [15], correspondingly, points at a mixture of elastic and inelastic mechanisms with a metallic sign of the elastic contribution. Finally, $b\approx5.6$ in BEDT-TTF [73, 74] also corresponds to a mixture of two mechanisms with a non-metallic sign of the elastic contribution to the self-energy.

Elastic scattering from resonant levels is one example where $b\approx1$ [21]. If the resonant level is described by a Lorentzian centered at $\omega=\varepsilon_F+\omega_0$ and of width γ, the imaginary part of the self-energy also has a Lorentzian form:

$$\mathrm{Im}\Sigma^R_{\mathrm{el}}(\omega)=\mathrm{const}\times\frac{\gamma}{(\omega-\omega_0)^2+\gamma^2}. \quad (4.44)$$

Expanding equation (4.44) to $\mathcal{O}(\omega^2)$ and substituting the result into the Kubo formula, we obtain for the Ω- and T- dependent parts of the optical scattering rate:

$$\frac{1}{\tau(\Omega,T)}=\mathrm{const}\times\frac{\gamma(3\omega_0^2-\gamma^2)}{(\omega_0^2+\gamma^2)^3}(\Omega^2+\pi^2T^2), \quad (4.45)$$

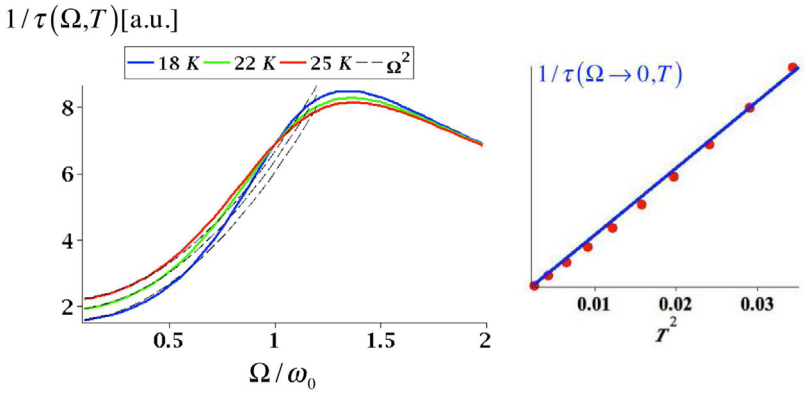

Figure 8. Left: optical scattering rate in the resonant-impurity model as a function of frequency at several temperatures. The absolute scale of temperature is fixed by choosing $\omega_0 = 12.5$ meV and $\gamma = 0.2\omega_0$. The dashed lines are the Ω^2 fits of the actual dependences. Right: the zero-frequency intercept, $1/\tau(\Omega \to 0, T)$, in the resonant-impurity model as a function of $(T/\omega_0)^2$. Adapted with permission from [21]. Copyright by the American Physical Society.

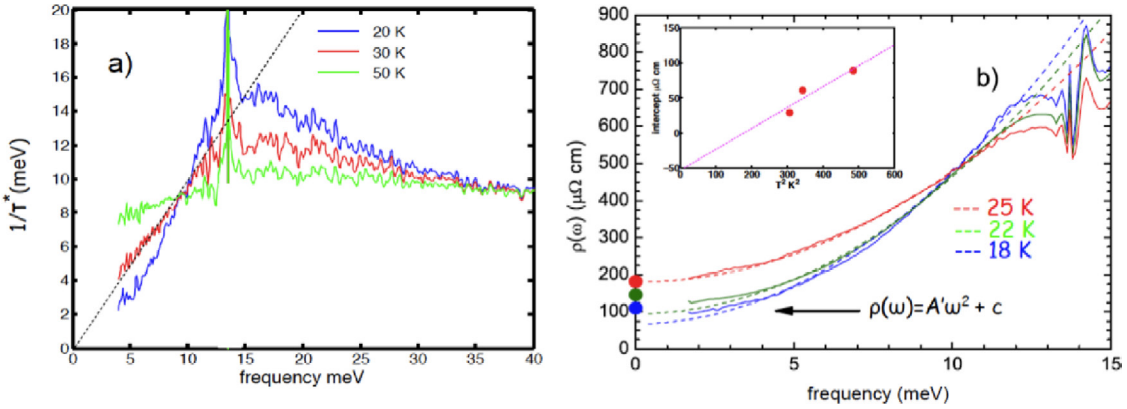

Figure 9. Experimental results for URu_2Si_2 from [12]. (a) Optical scattering rate $1/\tau(\Omega, T)$. (b) The optical resistivity at lower frequencies from the refined reflectivity. Reproduced with permission from [12]. Copyright by National Academy of Sciences.

which corresponds to $b = 1$. The full optical scattering rate, obtained from the self-energy in equation (4.44) without expanding in ω, is shown in figure 8, left. The quadratic Ω dependence at the lowest Ω is followed by a maximum at $\Omega \approx \omega_0$. The T-dependence of $1/\tau(\Omega, T)$ at the lowest Ω is almost quadratic, see figure 8, right. The overall shape of the Ω and T dependences in this model reproduce some subtle features of the experimental data for URu_2Si_2 [12] (figure 9), including an isosbestic point at $\Omega \approx 10$ meV.

The microscopic origin of resonant levels is not clear at the moment. It is very unlikely, however, that clean samples of materials with $b \approx 1$ contain considerable amounts of *extrinsic* resonant impurities. Therefore, resonant states must be *intrinsic* to these compounds. We surmise that localized *f*-electrons of U, Ce, and Nd atoms may play the role of *incoherent* resonant levels at sufficiently high energy scales probed in optical measurements. On the other hand, materials with itinerant *d*-orbitals (cuprates and pnictides) tend to have b closer to the theoretical value of 4. The 124 strontium ruthenate, which exhibits a robust FL behavior at low enough temperatures (below 30 K and above the superconducting transition at $\approx$1 K) [101], comes also the closest to the theoretical prediction in its optical conductivity. Apparently, more data need to be accumulated before one can say that the materials with b in the intermediate range between 1 and 4 represent a new universality class.

5. Optical conductivity of non-Fermi liquids

5.1. Pomeranchuk criticality

5.1.1. Model. A Pomeranchuk instability is a quantum phase transition that breaks rotational but not translational symmetries of a Fermi liquid [102]. The most common example of a Pomeranchuk instability is a ferromagnetic phase transition in the $\ell = 0$ angular momentum channel. Nematic instability in channels with $\ell \geqslant 1$ [103] is currently a subject of considerable interest stimulated, in part, by observations of nematic phases in $Sr_3Ru_2O_7$ [104], iron-based superconductors [105–107], and high-T_c cuprates [108].

The order parameter in the ordered phase is spatially uniform ($q = 0$). At the critical point, the propagator of order-parameter fluctuations (the dynamical susceptibility) is assumed to be Landau overdamped and, at weak coupling, has the form

$$\chi(\mathbf{q},\Omega)=\frac{\bar{g}}{q^2+\gamma d(\mathbf{q})\frac{|\Omega|}{q}}, \tag{5.1}$$

where $\bar{g}$ is the coupling constant of the effective 4-fermion interaction, mediated by critical bosons, and $d(\mathbf{q})$ is the form-factor, determined by the angular momentum of the critical channel. Below, we will focus of the simplest case of $\ell=0$ instability, when $d(\mathbf{q})=1$. Because typical Ω in equation (5.1) scale as q^3, Pomeranchuk criticality belongs to the Hertz–Millis–Moriya class [90–92] with the dynamical exponent $z=3$. In the single-band case, the damping parameter γ is related to $\bar{g}$ via $\gamma\sim\bar{g}N_{\mathrm{F}}/v_{\mathrm{F}}$ [109], where N_{F} is the density of states.

A singular form of the critical propagator leads to a breakdown of the FL, which is manifested by a NFL behavior of the self-energy. In 2D,

$$\Sigma'(\omega)\sim\Sigma''(\omega)=\omega_0^{1/3}\omega^{2/3}, \tag{5.2}$$

where $\omega_0\sim\bar{g}^2/\varepsilon_{\mathrm{F}}$ (in this case, $\bar{g}$ has units of energy). In 3D,

$$\Sigma'(\omega)\sim\frac{\bar{g}}{v_{\mathrm{F}}}\omega\ln\frac{\varepsilon_{\mathrm{F}}}{\omega},\quad \Sigma''(\omega)\sim\frac{\bar{g}}{v_{\mathrm{F}}}\omega \tag{5.3}$$

(in this case, $\bar{g}$ has units of velocity). A necessary (but not sufficient) condition for a controllable theory with the interaction of this type is the requirement that the coupling is weak, i.e. $\bar{g}\ll\varepsilon_{\mathrm{F}}$ in 2D and $\bar{g}\ll v_{\mathrm{F}}$ in 3D. This ensures that the low-energy sector, where the behavior is universal, and the high-energy sector, where it is not, are not mixed by the interaction.

5.1.2. Optical conductivity. As is typical for a $q=0$ criticality, characteristic momentum transfers $q\sim(\gamma\omega)^{1/3}$ near Pomeranchuk criticality are small compared to k_{F}. Correspondingly, the transport time is much longer than the quasiparticle lifetime, given by $1/\Sigma''(\omega)$. Yet, the real part of the self-energy is larger than the frequency below certain energy scale (ω_0 in 2D and $\varepsilon_{\mathrm{F}}\exp(-v_{\mathrm{F}}/\bar{g})$ in 3D), which marks the onset of the NFL behavior. To account for the effect of small-angle scattering quantitatively, one needs to consider the set of diagrams shown in figure 10 [38]. This set is similar to the one considered in section 2.1 and appendix A (figure 1), except for that now the Green's functions, depicted by thick solid lines in figure 10, in are not free but satisfy the Dyson equation with one-loop self-energy, figure 10(e). After analytic continuation, one can expand the Green's functions in diagram (a) to first order in the *imaginary* part of the self-energy. In the rest of the diagrams, which contain additional interaction lines, one can neglect the imaginary parts of the self-energy in the Green's functions. The sum of the four diagrams treated in this way contains the square of the change in total current due to collisions, $(\Delta\mathbf{J})^2=(\mathbf{v_k}+\mathbf{v_p}-\mathbf{v_q}-\mathbf{v_{p+q}})^2$, see equation (2.6). Since $q\ll k_{\mathrm{F}}$, we have $(\Delta\mathbf{J})^2\propto q^2$. This is an analog of the 'transport factor' encountered in the context of impurity scattering [68]. Qualitatively, the effect can be captured by introducing the 'transport self-energy', whose imaginary part differs from the usual one by an extra factor of q^2 under the integral:

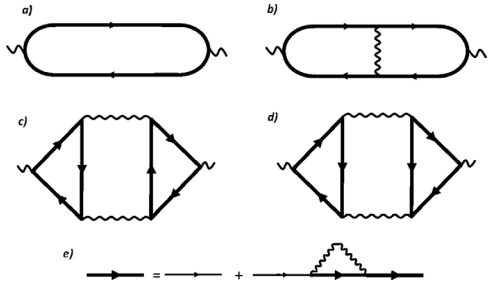

Figure 10. ((a)–(d)) Feynman diagrams for the optical conductivity in the boson-fermion model. The wavy line denotes the dynamic susceptibility of the order-parameter fluctuations, equation (5.1). (e) The Dyson equation for the Green's function.

$$\Sigma''_{\mathrm{tr}}(\omega,T)=\int\frac{\mathrm{d}^Dq}{(2\pi)^D}\int_{-\infty}^{\infty}\frac{\mathrm{d}\,\Omega}{\pi}[n_B(\Omega)+n_{\mathrm{F}}(\omega+\Omega)]\times\mathrm{Im}G^R(\mathbf{q},\omega+\Omega)\mathrm{Im}\chi^R(\mathbf{q},\Omega)\frac{q^2}{2k_{\mathrm{F}}^2}. \tag{5.4}$$

At $T=0$, this gives [110–112]

$$\Sigma''_{\mathrm{tr}}(\omega)=\begin{cases}\omega_1^{-1/3}\omega^{4/3}, & (2\mathrm{D})\\ \omega_1^{-2/3}\omega^{5/3}, & (3\mathrm{D})\end{cases} \tag{5.5}$$

where $\omega_1\sim\varepsilon_{\mathrm{F}}^5/\bar{g}^4$ and $\omega_1\sim\varepsilon_{\mathrm{F}}(v_{\mathrm{F}}/\bar{g})^{5/2}$, in 2D and 3D correspondingly. Since $\omega_1\gg\varepsilon_{\mathrm{F}}$ in the weak-coupling regime, $\Sigma''_{\mathrm{tr}}(\omega)\ll\omega$ for $\omega\ll\varepsilon_{\mathrm{F}}$. *A posteriori*, this justifies an expansion in the imaginary part of the self-energy. More specifically, each diagram in figure 10 is proportional to Σ'', which is not small compared to $\max\{\omega,\Sigma'\}$, but their sum is proportional to Σ''_{tr}, which is small[8]. If the FS satisfies the conditions specified in section 2.3, the conductivity can be described by the Drude formula with $1/\tau(\Omega,0)=\Sigma''_{\mathrm{tr}}(\Omega)$:

$$\sigma'(\Omega)=\frac{\Omega_p^2}{4\pi}\frac{\Sigma''_{\mathrm{tr}}(\Omega)}{\Omega^2+[\Sigma''_{\mathrm{tr}}(\Omega)]^2}\approx\frac{\Omega_p^2}{4\pi}\frac{\Sigma''_{\mathrm{tr}}(\Omega)}{\Omega^2}. \tag{5.6}$$

In accord with the argument given above, we neglected $\Sigma''_{\mathrm{tr}}(\Omega)$ in the denominator at the last step. It is tempting to include mass renormalization into this procedure, i.e. to replace Ω in the denominator of equation (5.6) by $\Omega/Z(\Omega)$, but it can be shown that, near a nematic QCP, the Z-factor is canceled out by vertex corrections [113].

In a FL, $\Sigma''_{\mathrm{tr}}(\Omega)\sim\Sigma''(\Omega)\propto\Omega^2$, and $\sigma'(\Omega)$ does not depend on Ω. This is the FL foot discussed in section 3.1.1. The result for a NFL is different because of NFL scaling of Σ''_{tr} with Ω. Substituting the 2D form of $\Sigma''_{\mathrm{tr}}(\Omega)\propto\Omega^{4/3}$ into equation (5.6), one obtains [6, 111]

$$\sigma'(\Omega)\propto\frac{1}{\Omega^{2/3}} \tag{5.7}$$

This behavior of $\sigma'(\Omega)$ was interpreted in [6] as a violation of hyperscaling, because hyperscaling implies that the

[8] The series for the self-energy does not converge in 2D due to so-called planar diagrams, which are not small in $1/N$, where N is the number of fermion flavors [143]. It can be surmised, however, that planar diagrams, which correspond to almost 1D scattering processes [144], should not affect the conductivity [145].

conductivity is independent of Ω in 2D. We note in passing that hyperscaling would be satisfied if one would replace Ω by $\Omega/Z(\Omega)$ in equation (5.6) and use the fact that $Z(\Omega) \propto \Omega^{1/3}$ at a nematic QCP in 2D.

In 3D, the same reasoning gives

$$\sigma'(\Omega) \propto \frac{1}{\Omega^{1/3}}. \tag{5.8}$$

5.1.3. dc *limit.* The T-dependence of *dc* resistivity of quantum-critical metals had long been believed to arise from scattering of electrons from fluctuations of the order parameter [38, 110, 114–117]. Since such a mechanism by itself cannot provide current relaxation, it had been assumed implicitly that umklapp processes quickly relax the momentum gained by small-q fluctuations. It was shown in [4, 45], however, that umklapp scattering is suppressed near a $q = 0$ criticality [4, 45], where scattering is predominantly of the small-angle type, while umklapp processes require momentum transfers comparable to the reciprocal lattice constant. In this case, the only effective mechanism of current relaxation in scattering by impurities. As was discussed in section 2.1, normal (as opposed to umklapp) scattering by fluctuations of the order parameter modifies the electron distribution function but in such a way that the momentum is still conserved. Nevertheless, if the FS satisfies certain conditions specified in section 2.3, normal scattering does give rise to a temperature-dependent (inelastic) term in the resistivity. In the single-band case, such a term cannot exceed substantially the residual resistivity, but it can happen if a metal has several bands with substantially different effective masses (see section 2.2.3).

The T-dependence of the inelastic term in the resistivity is obtained by substituting ω by T in the transport self-energy (equation (5.5)), which leads to $\rho \propto T^{4/3}$ and $\rho \propto T^{5/3}$ in 2D and 3D, correspondingly. The 5/3 scaling (or numerically close 3/2 one) was observed in a number of weak ferromagnets close to the quantum critical point, e.g. UGe_2 [118], Ni_xPd_{1-x}, [119], Ni_3Al [120], and $NbFe_2$ [121] (for a more complete list, see [122])[9]. Additional evidence for the quantum-critical nature of this scaling comes from the concomitant logarithmic divergence of the specific heat coefficient. To the best of our knowledge, however, quantum-critical scaling of the optical conductivity in 3D (equation (5.8)) has never been verified experimentally[10]. Such an experiment is very much desirable. In 2D, the situation is not clear even as far as *dc* resistivity is concerned: to the best of our knowledge, the 4/3 scaling of ρ has not been yet observed experimentally.

[9] In some materials, e.g. helimagnetic MnSi [146] and ferromagnetic $ZrZn_2$ [147], the 5/3 (3/2) scalings are observed in wide regions of the phase diagrams, and are therefore not likely to manifest quantum-critical physics [122].

[10] NFL scaling of the optical conductivity in $SrRuO_3$ and $CaRuO_3$ [10, 11, 148, 149] is not consistent with the predictions of the quantum-critical theory. Recently, this behavior has been attributed to minigaps produced by rotational and tilting distortions of the lattice [70].

5.2. Quantum phase transition at finite q

5.2.1. Hot and cold regions. As was pointed out several times in this paper, a conventional FL is characterized by two properties: (i) the Z-factor is finite and independent of the frequency and (ii) the scattering rate scales as $\max\{\omega^2, T^2\}$. The combination of these two properties results in a FL foot (see figure 5): a wide region of frequencies in which the real part of the conductivity is independent of the frequency.

However, this is not what the experiment shows in many cases. Of particular importance is a violation of the expected FL behavior in under- and optimally doped superconducting cuprates, where $\sigma'(\Omega)$ scales as $1/\Omega^d$ with $d > 0$. The exponent d was found to be close to 0.7 in the intermediate frequency range ($\Omega \sim 100$–500 meV) [123, 124] and close to 1 in a wider frequency range (from 100 meV to about 1 eV) [1, 25–27]. At the same time, the optical scattering rate scales roughly linearly with Ω at sufficiently high frequency, both in the cuprates [1, 123] and iron-based superconductors [125]. This scaling appears to be dual to enigmatic linear scaling of the *dc* resistivity with temperature, observed in many classes of strongly correlated materials [126].

Phenomenologically, one can argue that both linear dependences represent two limiting cases of the same scattering rate. This assumption is employed in the marginal FL model [88, 89], which postulates that the transport scattering rate is identical to the single-particle self-energy $\Sigma''(\omega, T) = \text{const} \times \max\{\omega, T\}$, while the latter does not vary significantly over the FS. However, it is generally problematic to justify these assumptions within a microscopic theory, which considers explicitly coupling between fermions and boson degrees of freedom. Indeed, if bosons represent long-wavelength fluctuations of the incipient order parameter, the transport scattering rate is reduced compared to the single-particle self-energy, and its Ω and T dependences differ, in general, from those of $\Sigma''(\omega, T)$ (this case was discussed in section 5.1). If bosons represent fluctuations of a spin- or charge-density-wave order parameter, one runs into a different kind of problem known as the 'Hlubina–Rice conundrum' [22]: the self-energy acquires a NFL form only near the special points of the FS ('hot spots') that are connected by the nesting wavenumber, while the rest of the FS stays cold. The *dc* conductivity contains an average of the scattering time over the FS. This average is dominated by the cold regions of the FS, where the scattering time is long, and the conductivity retains its FL form: $\sigma(T) \propto 1/T^2$. A number of ways out of the Hlubina–Rice conundrum were proposed in the past, either by introducing anisotropic scattering rates phenomenologically [127, 128] or by invoking impurity scattering, which effectively smears out the boundaries between the hot and cold regions [129].

In the optical conductivity, one averages the scattering rate instead of the scattering time, which at first glance implies that the optical conductivity should be dominated by hot regions, where the scattering rate is the highest. However, a small size of hot spots diminishes their contribution. The hot-spot contribution to the optical conductivity near an SDW QCP in 2D has been calculated explicitly in several recent papers [5, 23], where it was found that $\sigma'(\Omega) = \text{const}$. The same

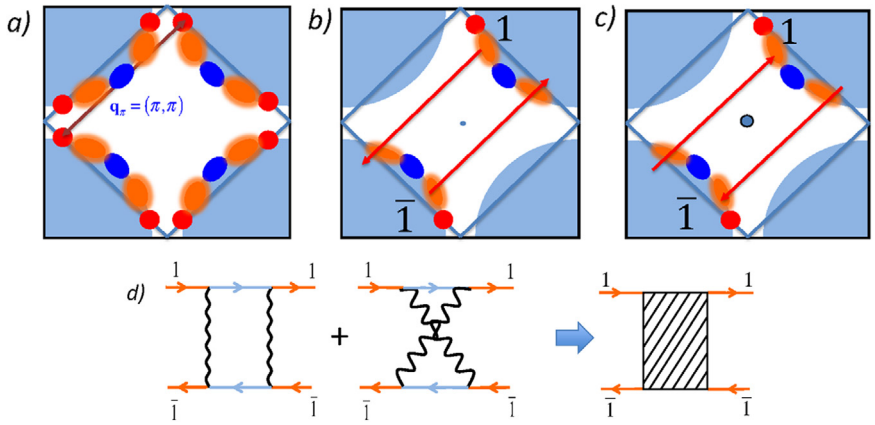

Figure 11. (a) A cuprate-like FS with hot (red), cold (blue), and lukewarm (orange) regions. Hot spots are connected by the spin-density-waver ordering vector $\mathbf{q}_\pi = (\pi, \pi)$. (b) The first step of the composite scattering process: a lukewarm fermion near hot spot 1 is scattered by q_π from its original position and lands away from the FS; simultaneously, another lukewarm fermion, located near the mirror image of hot spot 1 ($\bar{1}$), is scattered into a state also away from the FS. (c) The second step of the composite process: lukewarm fermions return to their original positions. (d) Diagrammatic representation of the composite scattered process. The internal Green's functions (solid blue lines) correspond to off-shell intermediate states. The wave line is the spin-density wave propagator, equation (5.10).

result can be obtained from the extended Drude formula, which does take into account mass renormalization. Indeed, generalizing equation (4.35) for an anisotropic FS, replacing $1/\tau$ by $\Sigma''(\Omega, \mathbf{k})$ and $1 + \lambda_{\rm tr}$ by $\approx 1/Z(\Omega, \mathbf{k})$, and expanding in Σ'', we obtain

$$\sigma'(\Omega) = \frac{2e^2}{D(2\pi)^D\,\Omega^2} \oint {\rm d}a_{\mathbf{k}} v_{\mathbf{k}} \Sigma''(\Omega, \mathbf{k}) Z^2(\Omega, \mathbf{k}). \quad (5.9)$$

In 2D, both $\Sigma''(\Omega, \mathbf{k})$ and $Z(\Omega, \mathbf{k})$ at the hot spot scale as $\Omega^{1/2}$, while the width of the hot spot scales as $\Omega^{1/2}$. This gives $\sigma'(\Omega) = {\rm const}$, which coincides with the hyperscaling prediction [5]. As we mentioned in the previous section, this may be an indication of a relation between hyperscaling and renormalization of the optical conductivity by the real part of the self-energy, i.e. by the Z-factor. Regardless of an interpretation, however, what matters is that the hot-spot contribution in the 2D case, which is relevant to cuprate and iron-based superconductors, is indistinguishable from the cold-region contribution, which remains of the FL-type even right at the QCP.

In 3D, $\Sigma''(\Omega, \mathbf{k}) \propto \Omega$ and $Z(\Omega, \mathbf{k}_{\rm hs}) = 1/|\ln \Omega|$, while the width of the hot line still scales as $\Omega^{1/2}$. This implies that $\sigma'(\Omega) \propto 1/\Omega^{1/2}$ in 3D (modulo logarithmic renormalization).

As written, equation (5.9) is valid if $\Sigma''(\Omega, \mathbf{k})$ is small compared to $\Omega/Z(\Omega, \mathbf{k})$. In 3D, this condition is satisfied both inside and outside the quantum-critical regime, because $\Sigma''(\Omega, \mathbf{k})$ is parametrically smaller than $\Omega/Z(\Omega, \mathbf{k})$. In 2D, the condition $\Sigma''(\Omega, \mathbf{k}) \ll \Omega/Z(\Omega, \mathbf{k})$ is, strictly speaking, satisfied only above the boundary of the quantum-critical region, but equation (5.9) is still valid in order of magnitude even well inside the quantum-critical region, because in this case $\Sigma''(\Omega, \mathbf{k})$ and $\Omega/Z(\Omega, \mathbf{k}) = \Omega + \Sigma'(\Omega, \mathbf{k})$ are of the same order.

5.2.2. Composite scattering, $T = 0$. A new microscopic approach to the optical conductivity near SDW criticality has recently been put forward by Hartnoll, Hofman, Metlitski, and Sachdev (HHMS) [23], who noticed that the interaction between 'lukewarm fermions', occupying an intermediate portion of the FS in between the hot and cold regions, may affect the optical conductivity significantly. This paper and the subsequent one by the two of us and Yudson [24] considered a particular case of finite-q instability—a (π, π) spin-density-wave (SDW) on a 2D square lattice—and we focus on this case below.

An SDW instability occurs in systems where the FS crosses the magnetic Brillouin zone boundary. The intersection points–the hot spots–are connected by the SDW ordering wavenumber, $\mathbf{q}_\pi = (\pi, \pi)$ (the lattice constant is set to unity). For a FS in figure 11, there are eight such spots (red circles). The interaction between fermions located in the vicinity of hot spots is mediated by exchange of SDW fluctuations with a propagator

$$\chi(\mathbf{q}, \Omega) = \frac{\bar{g}}{\xi^{-2} + (\mathbf{q} - \mathbf{q}_\pi)^2 - {\rm i}\gamma\Omega}, \quad (5.10)$$

where $\gamma = 4\bar{g}/\pi v_{\rm F}^2$ [109]. At criticality, i.e. at $\xi = \infty$, the one-loop self-energy of a fermion located at point $k_\parallel$ on the FS (measured from the hot spot) is [109]

$$\Sigma^{(1)}_{\mathbf{k}}(\omega) = {\rm i}\frac{3\bar{g}}{2\pi v_{\rm F}\gamma}\left(\sqrt{-{\rm i}\gamma\omega + k_\parallel^2} - |k_\parallel|\right). \quad (5.11)$$

The asymptotic limits of equation (5.11) allows one to identify different regions of the FS. For $\omega \ll \bar{g}$, each quadrant of the FS can be partitioned into hot, lukewarm, and cold regions (depicted by the red, orange, and blue areas in figure 11(a), correspondingly.) The characteristic scales for $k_\parallel$ are

$$k_1 = \sqrt{\bar{g}\omega}/v_{\rm F} \text{ and } k_2 = \bar{g}/v_{\rm F} \quad (5.12)$$

(the assumption of $\omega \ll \bar{g}$ ensures that $k_1 \ll k_2$). The hot region corresponds to $|k_\parallel| \ll k_1$. In this region, the self-energy is of a NFL form: ${\rm Re}\Sigma^{(1)}_{\mathbf{k}}(\Omega) = {\rm Im}\Sigma^{(1)}_{\mathbf{k}}(\omega) \sim \sqrt{\bar{g}\omega}$ and $Z_{\mathbf{k}}(\omega) \propto (\omega/\bar{g})^{1/2} \ll 1$. The cold region is the farthest one from the hot spot: $|k_\parallel| \gg k_2$. In there, we have a weakly renormalized FL with the Z-factor close to unity and

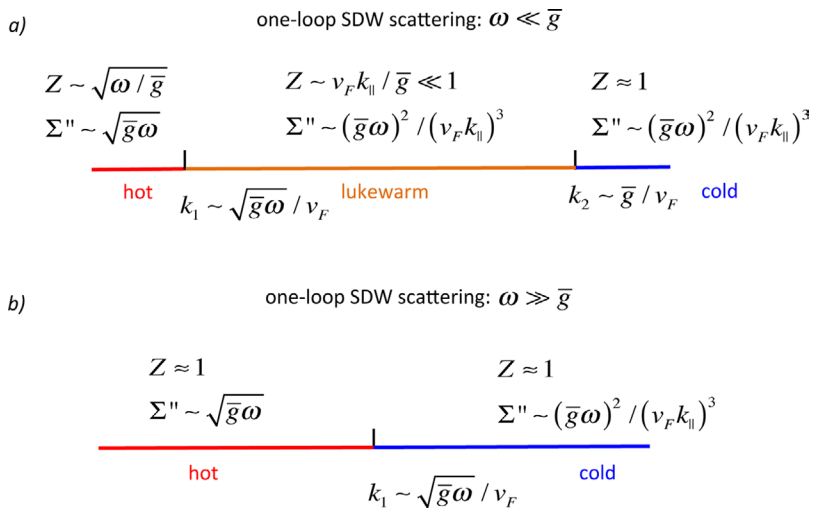

Figure 12. Partitioning of the FS into hot, lukewarm, and cold regions at one-loop order in SDW scattering.

$$\mathrm{Im}\Sigma^{(1)}_{\mathbf{k}}(\omega) \sim \bar{g}^2\omega^2/(v_F|k_\parallel|)^3. \tag{5.13}$$

The lukewarm region occupies the intermediate range $k_1 \ll |k_\parallel| \ll k_2$. In there, we have a strongly renormalized FL with the Z-factor that scales linearly with $k_\parallel$

$$Z_{\mathbf{k}} \sim v_F|k_\parallel|/\bar{g} \tag{5.14}$$

and approaches zero and unity at the two opposite ends of the lukewarm region, correspondingly. At the same time, $\mathrm{Im}\Sigma^{(1)}_{\mathbf{k}}(\Omega)$ is still given by equation (5.13). If $\omega \gg \bar{g}$ (but still smaller than the bandwidth), there is no lukewarm region: the hot are cold region are adjacent to each other.

Another characteristic energy scale is set by the curvature of the fermion dispersion $\varepsilon_{\mathbf{k}} = v_F k_\perp + k_\parallel{}^2/(2m^*)$, where m^* is inversely proportional to the local curvature of the FS at point $k_\parallel$. This scale can be deduced from comparing different parts of the Green's function of a lukewarm fermion with the Z-factor from equation (5.14):

$$G_{\mathbf{k}}(\omega) = \left(\frac{\bar{g}\omega}{v_F|k_\parallel|} - v_F k_\perp - \frac{k_\parallel{}^2}{2m^*}\right)^{-1}. \tag{5.15}$$

If the last term in the denominator of equation (5.15) is larger than the first one, curvature is important, and the FS must be treated as a 2D object. In the opposite case, the last term can be neglected and the FS becomes essentially 1D. As one moves along the FS away from the hot spot, one first enters the 1D region and then the 2D region. The crossover between the two occurs at $|k_\parallel| \sim k_3$, where

$$k_3 = (\bar{g}\varepsilon^*_F\omega)^{1/3}/v_F \tag{5.16}$$

and $\varepsilon^*_F = m^* v_F^2/2$. Depending on ω, k_3 can be either smaller or larger than the other two crossover scales (k_1 and k_2), and this complicates the partitioning scheme in figure 12 significantly. A detailed description of the self-energy with both 1D and 2D regions taken into account can be found in [24].

To one-loop order in SDW scattering, the optical conductivity of both cold and lukewarm fermions is independent of frequency (the FL foot). This is not immediately obvious for lukewarm fermions, as $\sigma'(\Omega)$ in equation (5.9) with Σ_{tr} replaced by the self-energy from equation (5.13) and with the Z-factor from equation (5.14) appears to have a logarithmic dependence on Ω: $\sigma'(\Omega) \propto \Omega^{-2}\int_{k_1} dk_\parallel k_\parallel{}^2\,\Omega^2/k_\parallel{}^3 \sim \ln\Omega$. However, a correction to the current vertex cancels the logarithmic singularity [23], and the conductivity reduces a constant, which is what one would expect in the FL regime.

Going beyond one-loop order, HHMS considered a composite process depicted in panels (b) and (c) of figure 11. At the first step, two lukewarm fermions located near diametrically opposite hot spots (1 and $\bar{1}$) are scattered by SWD fluctuations with ordering wavenumber $\mathbf{q}_\pi$ (panel (b)). Because lukewarm fermions are not located at hot spots, the final states after scattering are away from the FS. At the second step, fermions are scattered again by SDW fluctuations are return close to where they started from (panel (c)). The corresponding diagrams for the vertex are shown in panel (d). The intermediate states (light blue lines) are severely off-shell, and therefore their Green's functions can be approximated by the inverse dispersions. For the initial states at momenta $k_\parallel$ and $p_\parallel$ away from the corresponding hot spots, the product of the two Greens function then reduces to $1/v_F k_\parallel p_\parallel$. The rest of the diagram contains a product of two SDW propagators integrated over one of the two sets of the boson energy and momentum (the other set gives the energy and momentum transfers of incoming This integral depends logarithmically on the distance from the hot spots. Collecting everything together, we obtain the composite vertex

$$\Gamma^c(k_\parallel, p_\parallel; \Omega_m, q) = \frac{\bar{g}}{16\pi}\frac{1}{|k_\parallel p_\parallel|}\ln\frac{\Lambda^2}{q^2 + \gamma|\Omega_m|}, \tag{5.17}$$

where $\Lambda = \min\{k_\parallel, p_\parallel\}$. The most important feature of this result is its strong dependence on the distance from the hot spot: for $k_\parallel \sim p_\parallel$, $\Gamma^c \propto k_\parallel^{-2}$. This dependence continues down to the boundary between the lukewarm and hot regions located at $k_\parallel \sim k_1$ (equation (5.12)). Treating Γ^c as a new effective interaction of the theory, one can consider self-energy at one- and two-loop orders in this interaction (figures 13(a) and (b), correspondingly).

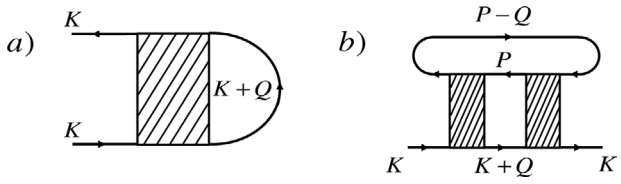

Figure 13. Self-energy at one-loop (a) and two-loop (b) orders in composite scattering. The shaded box is defined in figure 11(d).

Already at one-loop order, one gets something interesting: the self-energy of lukewarm fermions acquires a non-analytic frequency dependence

$$\mathrm{Im}\Sigma_{\mathbf{k}}^{(1c)}(\omega) \sim (\bar{g}\omega)^{3/2}/(v_{\mathrm{F}}k_{\|})^2, \tag{5.18}$$

which exceeds the ω^2 term from one-loop SDW scattering (equation (5.13)). This does not mean a FL breakdown: the quasiparticles are still well-defined in a sense that $\omega + \mathrm{Re}\Sigma \gg \mathrm{Im}\Sigma$, i.e. the quasiparticle energy is still larger than its linewidth. One can say that the lukewarm FL is a FL of the unconventional type because $\mathrm{Im}\Sigma$ decreases with ω slower than ω^2 but still faster than ω. By naive power counting, the corresponding optical conductivity should scale as $\Omega^{-1/2}$, which would signal a strong deviation from the FL picture. However, this does not happen, again because of the vertex correction. Note that double scattering by (large) SDW momentum is subsumed into the composite vertex which, by itself, corresponds to scattering by small momentum: $q \sim \sqrt{\gamma\Omega}$. The correct expression for the conductivity must include the current imbalance factor, $(\Delta\mathbf{J})^2 = (\mathbf{v_k} + \mathbf{v_p} - \mathbf{v_q} - \mathbf{v_{p-q}})^2$, which is of order $q^2 \propto \Omega$. This additional factor factor of Ω leads to a $\sqrt{\Omega}$ term in the conductivity, which is a subleading to the FL (constant) term from one-loop SDW scattering.

A more interesting effect occurs at two-loop order in composite scattering (figure 13(b))—this process gives rise to another non-analytic frequency dependence of $\mathrm{Im}\Sigma_{\mathbf{k}}(\omega)$, which does lead to a NFL behavior of the optical conductivity. This behavior is different in 1D and 2D regimes, which are defined by whether characteristic momenta $k_{\|}$ (proportional to the frequency of light) are smaller or larger than k_3 in equation (5.16), respectively.

In the 2D regime, the self-energy is the same as in a 2D FL liquid with an effective interaction given by equation (5.17):

$$\mathrm{Im}\Sigma_{\mathbf{k}}^{(2c)}(\omega) \sim \frac{\bar{g}^2}{(v_{\mathrm{F}}|k_{\|}|)^3}\frac{\varepsilon_{\mathrm{F}}^*}{v_{\mathrm{F}}|k_{\|}|}\omega^2 \ln^3\frac{Z_{\mathbf{k}}v_{\mathrm{F}}|k_{\|}|}{\omega}. \tag{5.19}$$

The prefactor of $k_{\|}^{-4}$ came from the square of the vertex in equation (5.17)–this is the most important part of the result as it will lead to a NFL behavior of the optical conductivity. The origin of the $\log^3\omega$ factor is also easy to trace down: two out of three logs came again from the square of the vertex while the third one is the conventional feature of a 2D FL. Depending on whether one is in the lukewarm or cold region, the Z-factor under the log is either given by equation (5.14) or almost equal to 1.

The 1D regime requires a more detailed analysis [24]. In a true 1D system, the self-energy is a highly singular function of the 'distance' to the mass shell, $\zeta \equiv \omega \mp v_{\mathrm{F}}(k \mp k_{\mathrm{F}})$, where $\mp$ corresponds to right/left-moving fermions: the self-energy from forward scattering has a pole at $\zeta = 0$ while that from backscattering vanishes at $\zeta = 0$. But our system is not really 1D in a sense that even if the $k_{\|}^2/2m^*$ term in the Green's function (5.15) is neglected, the information about the 2D nature of the FS still enters through the $k_{\|}$-dependence of the Z-factor. As a result, none of the two 1D singularities occur in our case but the self-energy is still of the 1D type, in a sense that it scales linearly with ω:

$$\mathrm{Im}\Sigma_{\mathbf{k}}^{(2c)}(\omega) \sim \left(\frac{\bar{g}}{v_{\mathrm{F}}k_{\|}}\right)^2 Z_{\mathbf{k}}\omega. \tag{5.20}$$

A crossover between the 1D and 2D regimes occurs at $|k_{\|}| \sim k_3$ (equation (5.16)). For $\omega \ll \bar{g}^2/\varepsilon_{\mathrm{F}}^*$, k_3 divides the lukewarm region (from k_1 to k_2) into two parts, such that the 1D part is closer to the hot spot while the 2D part is closer to the cold region. For $\omega \gg \bar{g}^2/\varepsilon_{\mathrm{F}}^*$, the 1D part extends over the entire lukewarm region. Notice that that 1D regime can be classified as a MFL: since $\mathrm{Im}\Sigma$ scales linearly with ω, quasiparticles are just barely defined, in a sense that $\omega + \mathrm{Re}\Sigma \sim \mathrm{Im}\Sigma$. However, in contrast to the traditional MFL phenomenology [88, 89], only a fraction of the FS exhibits such a behavior. The 2D regime corresponds to a conventional but strongly renormalized and anisotropic FL.

We now turn to the optical conductivity. For $\omega \ll \bar{g}^2/\varepsilon_{\mathrm{F}}^*$, the integral over $k_{\|}$ in equation (5.9) is controlled by $|k_{\|}| \sim k_3$, which means that either 1D or 2D forms of the self-energy can be used to estimate the conductivity. Using the 2D form (equation (5.19)) and setting the lower limit of the integral at $k_{\|} \sim k_3$, we obtain

$$\sigma'_{\Sigma}(\Omega) \sim \sigma_0\left[\frac{(\varepsilon_{\mathrm{F}}^*)^2}{\bar{g}\,\Omega}\right]^{1/3}\ln^3\frac{(E_{\mathrm{F}}^*)^2}{\bar{g}\,\Omega}. \tag{5.21}$$

Here $\sigma_0 = e^2N_{\mathrm{hs}}/4\pi^2c$ sets the overall scale of the conductivity (N_{hs} is the total number of hot spots and c is the lattice constant along the c-axis) and the subscript Σ indicates that we have not taken into account the vertex corrections yet. At higher frequencies, the 1D form of the self-energy (equation (5.20)) dominates the integral, which yields

$$\sigma'_{\Sigma}(\Omega) \sim \sigma_0\frac{\bar{g}}{\Omega}. \tag{5.22}$$

At first glance, the vertex corrections may modify the results for the optical conductivity significantly. Indeed, fermions involved in composed scattering belong to the vicinities of either the same or diametrically opposite hot spots, and are displaced only a little along the FS in the process of scattering. This seems to make the change in total current (equation (2.6)) small. However, the velocities entering $\Delta\mathbf{J}$ are the *renormalized* rather than the bare ones: $v_{\mathbf{k}} = Z_{\mathbf{k}}v_{\mathbf{k}}^0$. While the bare Fermi velocities may be assumed to vary slowly along the FS, the renormalized ones vary rapidly, following the rapid variation of the Z-factor. Replacing the slowly varying bare Fermi velocity by a constant ($= v_{\mathrm{F}}$) and using the lukewarm form of the Z-factor (equation (5.14)), we obtain for the current imbalance factor

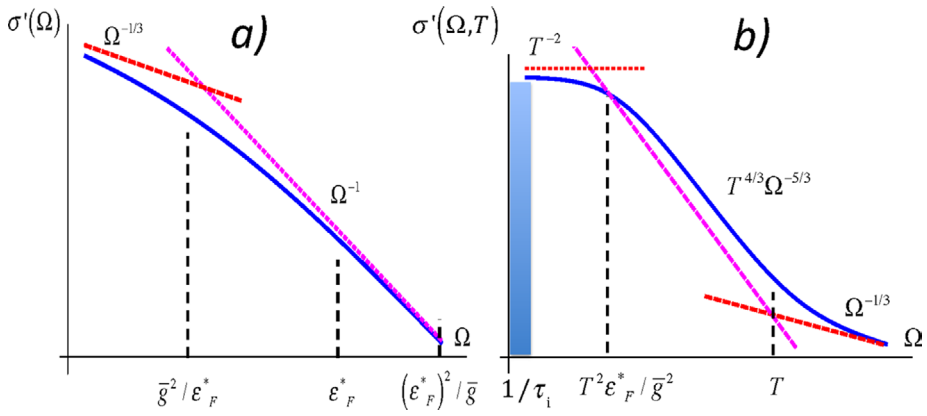

Figure 14. Schematic: real part of the conductivity (on a double-log scale) of a 2D metal at a spin-density-wave critical point. (a) $T = 0$. (b) same at finite T and in the hydrodynamic regime, where (momentum-conserving) composite scattering is stronger than (momentum-relaxing) umklapp or impurity scattering. The temperature is finite but sufficiently low: $T \ll \bar{g}^2/\varepsilon_F^*$. The high-frequency range ($\Omega \gg \bar{g}^2/\varepsilon_F^*$) is not shown here. $1/\tau_i$ is the momentum-relaxation rate. The shaded region corresponds to frequencies $\lesssim \gamma$, where momentum-relaxing scattering needs to be considered explicitly.

$$(\Delta\mathbf{J})^2 = (v_F^2/\bar{g})\Big(|k_\parallel| + |p_\parallel| - |k_\parallel + q_\parallel| - |p_\parallel - q_\parallel|\Big)^2. \qquad (5.23)$$

The momenta in the equation above are small compared to the size of the Brillouin zone. However, typical $q_\parallel$ are *not* small compared to $k_\parallel$ and $p_\parallel$, in fact $q_\parallel \sim k_\parallel \sim p_\parallel$[11]. The overall smallness of $|\Delta\mathbf{J}|$ reflects the smallness of the Z-factor, which has been already taken into account when deriving equations (5.21) and (5.22). The vanishing of $(\Delta\mathbf{J})^2$ at $q_\parallel = 0$ has only one effect: it regularizes the infrared singularity which gave rise to the logarithmic factors in equation (5.21), and the correct expression for the conductivity in the 2D regime does not have these factors. In the 1D regime, the only effect of this vanishing is a change in the numerical prefactor. However, the power-law dependences in equations (5.21) and (5.22) remain intact.

These hand-waving arguments are confirmed by considering a full set of the diagrams for the conductivity–which is the same set as in figure 1 but with the wavy lines replaced by the composite vertices [24]. The boundaries of the 2D and 1D regimes are identified by comparing the regions of validity of the approximations made in the process of deriving the corresponding formulas. The final result for the optical conductivity reads

$$\sigma'(\Omega) \sim \sigma_0 \times \begin{cases} [(\varepsilon_F^*)^2/\bar{g}\,\Omega]^{1/3}, & \text{for } \Omega \ll \bar{g}^2/\varepsilon_F^*; \\ \bar{g}/\Omega, & \text{for } \bar{g}^2/\varepsilon_F^* \ll \Omega \ll \varepsilon_F^*. \end{cases} \qquad (5.24)$$

The first (second) equation corresponds to the 2D (1D) regime. (Formally, the upper limit of 1D scaling is $(\varepsilon_F^*)^2/\bar{g} \gg \varepsilon_F^*$ but we replaced it by ε_F^* as the model considered here cannot be trusted at energies above ε_F^*.) In addition to $\Omega^{-1/3}$ scaling at lower frequencies, the conductivity also exhibits $1/\Omega$ scaling in a parametrically wide interval at higher frequencies (see figure 14(a)). The latter is reminiscent of scaling observed in the cuprates [1, 25–27, 123, 124].

[11] Note that the situation here is different compared to one-loop composite scattering, where typical $q_\parallel$ are small compared to $k_\parallel$.

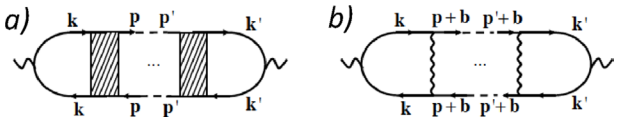

Figure 15. Normal (a) and umklapp (b) contributions to the conductivity.

The final result (equation (5.24)) should be taken with a number of warnings. First, the exponents 1/3 and 1 are evaluated at two-loop order in composite scattering. Contributions from higher-loop orders are likely to change these values [23]. One can show that higher-loop terms are on the same order as the one-loop result in the 2D regime and are larger by a $\ln\Omega$ factor in the 1D regime [24]. At best, one can hope to have two regions of scaling with exponents smaller than one (2D regime) and closer to one (1D regime). In addition, the low-frequency part of the 2D regime may be expected to be cut by either charge-density-wave or superconducting instabilities arising in the same model. Finally, our analysis was based on the assumption of $\bar{g}$ being smaller than ε_F^*, while in reality these two energies are on the same order, and thus one can only hope that a fortunate game of numbers will separate the low- and high-frequency regimes in the conductivity. Nevertheless, it is still encouraging to have a microscopic model that, with all the limitations described above, predicts a NFL behavior of the optical conductivity.

5.2.3. Composite scattering, $T \neq 0$. A natural question is: can composite scattering of lukewarm fermions also lead to NFL scaling of the *dc* conductivity with temperature? Unfortunately, this does not seem to be the case because the effective low-energy theory operating with lukewarm fermions does not explicitly contain umklapp processes [130, 131]. As we discussed in section 2.1, the main difference between the optical and *dc* conductivities is that the dissipative part of the former is finite even in the absence of umklapp scattering but the latter is finite only in the presence of umklapp scattering. Umklapp

scattering (by momentum $\mathbf{q}_\pi$) is subsumed into the composite vertex (figure 11(d)), and the total momentum of its initial states is conserved in the same way as for normal scattering (see figure 15(a)). This is to be contrasted with true umklapp scattering (see figure 15(b)), in which the momenta of the initial and final states differ by an integer multiple of the reciprocal lattice vector. Therefore, composite scattering on its own cannot render the *dc* conductivity finite, which means that the optical conductivity has a delta-function peak at $\Omega = 0$.

Suppose however that the momentum-relaxing process (be it umklapp or impurity scattering) is much weaker than the momentum-conserving one, i.e. that we are in the hydrodynamic regime. As we saw in section 2.1, for frequencies higher than the rate of a momentum-relaxing process ($1/\tau_i$), the conductivity takes a quasi-Drude form (see equation (2.12)): although its imaginary part scales as $1/\Omega$ (as if there is no relaxation), the real part behaves in a Drude-like way with the rate of the momentum-conserving process playing the role of the inverse relaxation time. One can ask then how this quasi-Drude form will look like at finite T in a metal at an SDW instability.

To be on the realistic side, we assume that $T \ll \bar{g}^2/\varepsilon^*$. For $T \ll \Omega \ll \bar{g}^2/\varepsilon^*_{\rm F}$, $\sigma'(\Omega)$ scales as $1/\Omega^{1/3}$. For $\Omega \ll T$, the frequency dependence of the self-energy is replaced by the temperature dependence. Since we are in the 2D regime, it amounts to replacing the Ω^2 factor in equation (5.19) by T^2. Because $\mathrm{Im}\Sigma$ is finite as Ω goes to zero at finite T, one cannot expand the denominator of the Drude formula in $\mathrm{Im}\Sigma$. Up to an overall factor, the conductivity is now given by

$$\sigma'(\Omega, T) \propto \int \mathrm{d}k_\parallel \frac{\mathrm{Im}\Sigma_{\mathbf{k}}(T)}{(\Omega/Z_{\mathbf{k}})^2 + [\mathrm{Im}\Sigma_{\mathbf{k}}(T)]^2}, \qquad (5.25)$$

where $\mathrm{Im}\Sigma_{\mathbf{k}}(T) \sim \bar{g}^2 \varepsilon^*_{\rm F} T^2/(v_{\rm F} k_\parallel)^4$. Assuming that the relevant $k_\parallel$ in this integral are within the lukewarm region and thus the Z-factor is given by equation (5.14), we find that the integral is dominated by such $k_\parallel$ that the two terms in the denominator of the equation above are of the same order, i.e. $k_\parallel \sim k_T \sim (T^2 \varepsilon^*_{\rm F} \bar{g}/\Omega)^{1/3}/v_{\rm F}$, and the conductivity is given by

$$\sigma'(\Omega, T) \sim \sigma_0 \frac{(\varepsilon^*_{\rm F})^{2/3}}{\bar{g}^{1/3}} \frac{T^{4/3}}{\Omega^{5/3}}. \qquad (5.26)$$

This expression matches with the first line of equation (5.24) at $\Omega \sim T$, as it should. As we see, the conductivity depends both on T and Ω in a NFL way (for a FL, we would have $\sigma'(\Omega, T) \propto T^2/\Omega^2$ in a similar interval of Ω and T). Equation (5.26) is valid at not too low frequencies, such that k_T is still smaller than the upper boundary of the lukewarm region, k_2 in equation (5.12). At lower frequencies, the integral over $k_\parallel$ in equation (5.25) is controlled by the cold region, where the Z-factor is close to one, while $\mathrm{Im}\Sigma \propto T^2$. This gives a conventional, FL form of the conductivity, $\sigma(\Omega, T) \propto T^{-2}$. The crossover between this form and the one in equation (5.26) occurs at $\omega \sim T^2 \varepsilon^*_{\rm F}/\bar{g}^2 \ll T$. The behavior of $\sigma'(\Omega, T)$ is sketched in figure 14(b). We remind the reader that the analysis above is valid only at frequencies above the momentum-relaxation rate ($1/\tau_i$); correspondingly, the region $\Omega \lesssim 1/\tau_i$ is masked by a box in the sketch.

6. Conclusions

In this review, we discussed three particular aspects of optical response of correlated electron systems. The first one is the role of momentum relaxation, the second one is Ω/T scaling of the optical conductivity of a Fermi-liquid metal, and the third one is the optical conductivity of a non-Fermi liquid metal. We argued that, in each of these three aspects, optical response is different from and complementary to other probes, such as photoemission and *dc* transport. Accordingly, this review is divided into three parts addressing each of the three aspects mentioned above.

In the first part, we analyzed the interplay between the contributions to the conductivity from normal and umklapp *ee* scattering, both at finite frequency and near the *dc* limit. We discussed the similarities and differences between the optical and *dc* conductivities, and demonstrated that, unlike the *dc* conductivity, the optical one has a finite dissipative part in non-Galilean-invariant systems, even if only normal scattering is present. As a specific example of a non-Galilean-invariant system, we re-visited a two-band model with momentum-conserving inter-band scattering and momentum-relaxing intra-band scattering. A useful lesson from this model is that although its optical conductivity does have a finite dissipative part, it does not obey the Drude form, because the scattering rates of momentum-conserving and momentum-relaxing processes do not add up according to the Matthiessen rule. We also discussed how the Fermi surface geometry affects the behavior of the optical and *dc* conductivities. In particular, we reviewed the theoretical predictions that, for any convex and simply-connected Fermi surface in 2D, the effective scattering rate scales as $\max\{T^4, \Omega^4\}$ rather than $\max\{T^2, \Omega^2\}$, as it is to be expected for a Fermi liquid.

In the second part, we re-visited the Gurzhi formula for the optical conductivity of a Fermi-liquid metal, $\mathrm{Re}\sigma^{-1}(\Omega, T) \propto \Omega^2 + 4\pi^2 T^2$, and showed that a factor of $4\pi^2$ in front of the T^2 term is a manifestation of the 'first-Matsubara-frequency rule' for boson response, which states that a combination of the T^2 and Ω^2 terms must vanish upon analytic continuation to the first boson Matsubara frequency, $\Omega \to \pm 2\pi i T$. We discussed the origin and the accuracy of this rule for the single-particle self-energy and conductivity, both for Fermi and non-Fermi liquids. We then discussed recent experiments in several materials, which showed that, although the conductivity can be fitted to the Gurzhi-like form, $\mathrm{Re}\sigma^{-1}(\Omega, T) \propto \Omega^2 + b\pi^2 T^2$, the coefficient b happens to deviate from the theoretical value of 4 in all cases, except for Sr_2RuO_4 [14]. The discrepancy is especially pronounced in rare-earth Mott insulators and heavy-fermion materials, where b is in general smaller than 2 and remarkably close to 1 in some cases, e.g. in URu_2Si_2 [12]. We proposed that the deviations from Gurzhi scaling may be due to the presence of elastic scattering, which decreases the value of b below 4, with $b = 1$ corresponding to the limit where elastic scattering dominates over inelastic one.

In the third part, we considered the optical conductivity of a metal near quantum phase transitions to nematic and spin-density-wave states (with nesting momentum (π, π)). In the

last case, we reviewed the special role of a 'composite' scattering process, which consists of two consequent (π,π) scatterings. We demonstrated that this effectively small-momentum scattering gives rise to a non-Fermi-liquid behavior of the optical conductivity at the critical point and at $T=0$. We reviewed the results of recent papers [23, 24], which predict that the dissipative part of the conductivity, $\sigma'(\Omega)$, scales as $\Omega^{-1/3}$ at asymptotically low frequencies and as Ω^{-1} at higher frequencies, up to the bandwidth. The $1/\Omega$ scaling of $\mathrm{Re}\sigma(\Omega)$ is consistent with the behavior observed in the superconducting cuprates. We also argued that composite scattering alone cannot render the *dc* conductivity finite–to do so, one needs to invoke some momentum-relaxing process (with scattering rate $1/\tau_{\mathrm{i}}$). Nevertheless, if $1/\tau_{\mathrm{i}}$ is the slowest scattering rate in the problem, one can discuss Ω/T scaling of $\sigma'(\Omega,T)$ at finite T and $\Omega \gg 1/\tau_{\mathrm{i}}$. Within this approximation, we showed that $\sigma'(\Omega,T)$ is of the Fermi-liquid form, $\sigma'(\Omega,T)\propto T^{-2}$, below some T-dependent frequency, but scales in a non-Fermi-liquid way, as $T^{4/3}\Omega^{-5/3}$, above that frequency.

Acknowledgments

We acknowledge stimulating discussions with I L Aleiner, B L Altshuler, D Basov, C Batista, K Behnia, M Broun, G Blumberg, D Dessau, P Coleman, S Dodge, M Dressel, B Fauquè, A Georges, L P Gor'kov, I V Gornyi, D Gryaznov, K Haule, S Hartnoll, K Ingersent, M Kennett, Y-B Kim, G Kotliar, E A Kotomin, P Kumar, I V Lerner, S Maiti, D van der Marel, M Metlitski, A Millis, U Nagel, H Pal, I Paul, M Yu Reizer, T Rõõm, S Sachdev, M Scheffler, B I Shklovskii, D Tanner, T Timusk, A-M Tremblay, D Vanderbilt, and V I Yudson. This work was supported by the National Science Foundation via grant NSF DMR-1308972 (DLM) and NSF-DMR 1523036 (AVC). We acknowledge hospitality of the Center for Non-Linear Studies, Los Alamos National Laboratory, which both of us visited in 2015–2016 as Ulam Scholars.

Appendix A. Diagrams for the optical conductivity

In this appendix, we show that the diagrams for the optical conductivity do not cancel for a system with broken Galilean invariance, even in the absence of umklapp processes. We select five diagrams shown in figure 1. Such a choice can be justified, e.g. within the large-N limit, when each the five diagrams contains a factor of N^2 while the diagrams not included in this group are smaller by a factor of N. The interaction, $U_{\mathbf{q}}$, is static but otherwise an arbitrary function of the momentum transfer $\mathbf{q}$.

First, we consider the self-energy diagrams (a) and (b), whose combined contribution to the current–current correlation function reads

$$\mathcal{K}_{ab} = -\sum_{P} \mathbf{v}_{\mathbf{p}}^2 (G_P^2 G_{P+Q}\Sigma_P + G_{P+Q}^2 G_P \Sigma_{P+Q}). \tag{A.1}$$

As in the main text, $P=(\mathbf{p},p_0)$, $Q=(\mathbf{0},q_0)$, etc, $\sum_P$ stands for $T\sum_{p_0}\int \mathrm{d}^D p/(2\pi)^D$, and $\mathbf{v}_{\mathbf{p}}=\boldsymbol{\nabla}\varepsilon_{\mathbf{p}}$ is the group velocity of Bloch electrons. Notice that Q has only a temporal component. With the help of an identity

$$G(P)G(P+Q) = \frac{1}{\mathrm{i}q_0}(G_P - G_{P+Q}), \tag{A.2}$$

$\mathcal{K}_{ab}$ can be re-written as

$$\mathcal{K}_{ab} = \frac{1}{q_0^2}\sum_P \mathbf{v}_{\mathbf{p}}^2 (G_P - G_{P+Q})(\Sigma_{P+Q} - \Sigma_P). \tag{A.3}$$

Using an explicit form of the self-energy $\Sigma(P) = -\sum_L U_{\mathbf{l}}^2 G_{P+L}\Pi_L$, where $\Pi_L = \sum_K G_K G_{K-L}$ is the particle-hole polarization bubble, we re-write $\mathcal{K}_{ab}$ as

$$\mathcal{K}_{ab} = \frac{1}{q_0^2}\sum_{P,K,L} \mathbf{v}_{\mathbf{p}}^2 U_{\mathbf{l}}^2 (G_P - G_{P+Q})(G_{P+L} - G_{P+L+Q}) G_K G_{K-L}. \tag{A.4}$$

Applying idenitity (A.2) to vertex diagram (c) and adding up the result with equation (A.4), we obtain for the combined contribution of diagrams (a)–(c)

$$\begin{aligned}\mathcal{K}_{ab} + \mathcal{K}_c &= \frac{1}{q_0^2}\sum_{P,K,L} \mathbf{v}_{\mathbf{p}}\cdot\left(\mathbf{v}_{\mathbf{p}} - \mathbf{v}_{\mathbf{p}+\mathbf{l}}\right) U_{\mathbf{l}}^2 \left(G_P - G_{P+Q}\right) \\ &\quad \times \left(G_{P+L} - G_{P+L+Q}\right) G_K G_{K-L} \\ &= \frac{1}{q_0^2}\sum_{P,K,L} \mathbf{v}_{\mathbf{p}}\cdot\left(\mathbf{v}_{\mathbf{p}} - \mathbf{v}_{\mathbf{p}+\mathbf{l}}\right) U_{\mathbf{l}}^2 \left(2G_P G_{P+L}\right. \\ &\quad \left. - G_P G_{P+L+Q} - G_{P+Q}G_{P+L}\right) \times G_K G_{K-L},\end{aligned} \tag{A.5}$$

where we relabeled $P+Q\to P$ in the term $G_{P+Q}G_{P+L+Q}$. Since Q has only a temporal component, this transformation affects neither the velocities nor the interaction.

Now we turn to the Aslamazov–Larkin diagrams, (d) and (e). Applying identity (A.2) twice, we obtain for diagram (d)

$$\begin{aligned}\mathcal{K}_d &= -\frac{1}{q_0^2}\sum_{P,K,L} \mathbf{v}_{\mathbf{p}}\cdot\mathbf{v}_{\mathbf{k}-\mathbf{l}} U_{\mathbf{l}}^2 \left(G_P - G_{P+Q}\right) \\ &\quad \times \left(G_{K-L} - G_{K-L+Q}\right) G_K G_{P+L} \\ &= -\frac{1}{q_0^2}\sum_{P,K,L} \mathbf{v}_{\mathbf{p}}\cdot\mathbf{v}_{\mathbf{k}-\mathbf{l}} U_{\mathbf{l}}^2 \left(G_P G_{K-L} + G_{P+Q}G_{K-L+Q}\right. \\ &\quad \left. - G_P G_{K-L+Q} - G_{P+Q}G_{K-L}\right) G_K G_{P+L}.\end{aligned} \tag{A.6}$$

Now, we relabel $P+Q\to P$, $L-Q\to L$ in the second term and $L-Q\to L$ in the third one. This yields the same combination of the Green's functions as in equation (A.5):

$$\begin{aligned}\mathcal{K}_d &= -\frac{1}{q_0^2}\sum_{P,K,L} \mathbf{v}_{\mathbf{p}}\cdot\mathbf{v}_{\mathbf{k}-\mathbf{l}} U_{\mathbf{l}}^2 (2G_P G_{P+L} - G_P G_{P+L+Q} \\ &\quad - G_{P+Q}G_{P+L}) G_K G_{K-L}.\end{aligned} \tag{A.7}$$

Similarly, diagram *e* reads

$$\mathcal{K}_e = -\frac{1}{q_0^2}\sum_{P,K,L}\mathbf{v_p}\cdot\mathbf{v_k}U_{\mathbf{l}}^2\big(G_P - G_{P+Q}\big)\big(G_K - G_{K+Q}\big)G_{K-L}G_{P+L+Q}$$
$$= -\frac{1}{q_0^2}\sum_{P,K,L}\mathbf{v_p}\cdot\mathbf{v_k}U_{\mathbf{l}}^2\big(G_PG_K + G_{P+Q}G_{K+Q} - G_PG_{K+Q}$$
$$- G_{P+Q}G_K\big)G_{K-L}G_{P+L+Q} \tag{A.8}$$

Relabeling $K+Q\to K$ and $L+Q\to L$ in the second and third terms, and $P+Q\to P$ in the fourth one, we obtain the same combination of the Green's functions as in equations (A.5) and equation (A.7) but with an opposite sign:

$$\mathcal{K}_e = -\frac{1}{q_0^2}\sum_{P,K,L}\mathbf{v_p}\cdot\mathbf{v_k}U_{\mathbf{l}}^2(G_PG_{P+L+Q} + G_{P+Q}G_{P+L}$$
$$- 2G_PG_{P+L})G_KG_{K-L}. \tag{A.9}$$

Collecting all contributions, we obtain the final result for the current–current correlation function

$$\mathcal{K} = \mathcal{K}_{ab} + \mathcal{K}_c + \mathcal{K}_d + \mathcal{K}_e = \frac{1}{q_0^2}\sum_{P,K,L}\mathbf{v_p}\cdot\big(\mathbf{v_p} + \mathbf{v_k} - \mathbf{v_{p+l}} - \mathbf{v_{k-l}}\big)U_{\mathbf{l}}^2$$
$$\times\big(2G_PG_{P+L} - G_PG_{P+L+Q} - G_{P+Q}G_{P+L}\big)G_KG_{K-L}. \tag{A.10}$$

The combination of the velocities in the equation above vanishes in a Galilean-invariant system, where $\mathbf{v_k} = \mathbf{k}/m$ but, in general, is non-zero otherwise.

Appendix B. Accuracy of the first-Matsubara-frequency rule

The first-Matsubara-frequency rule is not exact. In this appendix, we discuss the conditions under which the remainder $R(T)$ in equation (4.1) is indeed subleading to the first term.

B.1. Fermi liquid

Equation (4.6) was derived under the assumption that momentum transfers along the normal to the FS are small, of order T/v_F, whereas the momentum transfers tangential to the FS are determined by the internal scale of the interaction, Λ. It is the breakdown of this (local) approximation that gives rise to corrections to first Matsubara rule. In what follows, we assume that the linear-in-T term in the Matsubara self-energy is already singled out. The next term is obtained by retaining only one dynamic polarization bubble in $\chi(\mathbf{q},\Omega)$, which scales as $|\Omega_n|/q_\parallel$. The lower limit in the integral over $q_\parallel$ is set by the condition condition $q_\parallel \gg q_\perp \sim T/v_F$. For an estimate, we will replace T^2. Then

$$\Sigma(\omega_m, T) - \mathrm{i}\lambda\mathrm{sgn}\omega_m T \sim T\sum_{\Omega_n}\Omega_n\int_{T/v_F}^{\Lambda}\mathrm{d}q_\parallel$$
$$q_\parallel^{D-3} \sim T^2[\Lambda^{D-2} - (T/v_F)^{D-2}]. \tag{B.1}$$

For $D>2$, the T-dependent contribution from the lower limit is subleading, and the local approximation indeed works. The next order term contains a square of the dynamic bubble, which yield a correction to equation (B.1) on the order of

$$T\sum_{\Omega_n}\Omega^2\int_{T/v_F}^{\Lambda}\mathrm{d}q_\parallel q_\parallel^{D-4} \sim T^3(\Lambda^{D-3} - T^{D-3}). \tag{B.2}$$

For $D=3$, the integral diverges logarithmically at the lower limit. This is a well-studied $E^3\ln E$ term ($E=\max\{\omega_m, T\}$) in the self-energy of a 3D FL, which gives rise to a non-analytic, $T^3\ln T$ correction to the specific heat [132–135][12] observed both in ^{3}He [136, 137] and heavy-fermion materials [138]. The correction in equation (B.2) is not nullified at the first Matsubara frequency, and its T-dependent part gives an estimate for the remainder

$$R = \mathcal{O}(T^D). \tag{B.3}$$

For $D=2$, the integral equation (B.1) diverges logarithmically at the lower limit. This gives a familiar $E^2\ln E$ form of the self-energy in 2D FL. Still, this term is nullified at $\omega_m = \pi T$ and the surviving term is of order $T^2 \ll T^2\ln T$. An exact result for the surviving term is [20]

$$\Sigma(\pi T, T) - \mathrm{i}\pi\lambda T = \frac{AT^2}{2\pi v_F^2}\left(K + \frac{\pi\ln 2}{4}\right), \tag{B.4}$$

where A is a coupling constant, which is expressed via the charge and spin components of the forward- and backscattering amplitudes, and $K=0.9160$ is the Catalan constant. To summarize, equation (B.3) works for any $D\geqslant 2$.

B.2. First-Matsubara rule in non-Fermi liquids: Hertz–Millis–Moriya criticality

FMFR holds not only for FLs but also for NFLs, in a sense that the $\Omega_n = 0$ term in the sum (4.2) gives, under certain conditions, the leading contribution to the result. However, in contrast to equation (4.1), the leading term does not scale linearly with T because the coefficient λ depends on T itself. This is related to the fact that the effective mass of a NFL depends on the frequency. In addition, the estimate for the remainder term, equation (B.3), changes.

Below, we demonstrate how FMFR works for a NFL using a Hertz–Millis–Moriya quantum critical point [90–92] as a concrete example. We consider a generic Hertz–Millis–Moriya model with a propagator of critical fluctuations described by

$$\chi(q,\Omega_n) = \frac{1}{q^2 + \xi^{-2}(T) + \frac{\gamma\,|\,\Omega_n|}{q^{z-2}}}, \tag{B.5}$$

where $\xi(T)$ is the correlation length and z is the dynamical scaling exponent. Here, q is measured from the center of the Brillouin zone for $z=3$ (Pomeranchuk transition), and $q=|\mathbf{q}-\mathbf{q}_n|$ for $z=2$, where $\mathbf{q}_n$ is the nesting wavevector of a spin- or charge-density-wave. charge-density-wave. Right at the critical point, ξ is finite but temperature-dependent, and it diverges at $T\to 0$. We assume that $\xi\propto T^{-\beta}$. At the tree level, $\beta = 1/2$ modulo logarithmic renormalizations [91]. The derivation for the leading term in FMFR proceeds in the same

[12] For a more complete list of references on the non-analytic behavior of the specific heat, see: [135].

way as in section 4.1, and we arrive again at equation (4.7). However, $\chi_{\rm loc}(0)$ in this equation depends now on T via $\xi(T)$:

$$\chi_{\rm loc}(0) \propto \int {\rm d}q_{\|} q_{\|}^{D-2} \frac{1}{q_{\|}^2 + \xi^{-2}(T)} \propto \xi^{3-D} \propto T^{-\beta(3-D)}. \quad \text{(B.6)}$$

In the local approximation, the sum in equation (4.6) vanishes at $\omega = \pm\pi T$, and we obtain instead of equation (4.1)

$$\Sigma(\pm\pi T, T) = \mp {\rm i}\ {\rm const} \times T^{1-\beta(3-D)} + \tilde{R}(T). \quad \text{(B.7)}$$

Physically, the modification of the leading term is to due to scattering from static fluctuations of the order parameter. Naturally, the leading term—being entirely static—does not depend on the dynamical exponent z. An immediate consequence of equation (B.7) is that the dHvA amplitude deviates from the Lifshitz–Kosevich form of equation (4.16) and is now given by

$$A(T) = \frac{4\pi^2 T}{\omega_c} \exp\left(-2\pi^2 \frac{T + {\rm const} \times T^{1-\beta(3-D)}}{\omega_c}\right). \quad \text{(B.8)}$$

A non-Lifshitz–Kosevich behavior of this type was observed near a magnetic-field–driven quantum critical point in $CeCoIn_5$ [139].

As in a FL, the remainder term in equation (B.7), $\tilde{R}(T)$, comes from the corrections arising from keeping finite $q_\perp$ in the boson propagator. Since we already singled out the static term, we can put $\xi^{-1} = 0$ in equation (B.5), upon which it is reduced to a scaling form

$$\chi(q, \Omega_n) = |\Omega_n|^{-2/z} f\left(\frac{q}{|\Omega_n|^{1/z}}\right) \quad \text{(B.9)}$$

with $f(x) = x^{z-2}/(x^z + 1)$. Now we expand $q = \sqrt{q_\perp^2 + q_{\|}^2}$ to first order in $q_\perp^2$ and obtain a correction to the propagator

$$\delta\chi(q, \omega) = \frac{q_\perp^2}{2q_{\|}|\Omega_n|^{3/z}} f'\left(\frac{q_{\|}}{|\Omega_n|^{1/z}}\right). \quad \text{(B.10)}$$

The Green's function is given by $G = [{\rm i}\omega_m + \Sigma(\omega_m, T) - v_{\rm F} q_\perp]^{-1}$. Since we are in a NFL regime, $\Sigma \gg \omega_m$ and thus typical $q_\perp \sim |\Sigma|/v_{\rm F}$. Replacing Ω_n by T in equation (B.10) and evaluating the corresponding correction to the self-energy, we obtain an estimate for $\tilde{R}(T)$

$$\tilde{R}(T) \propto T^{1-3/z} |\Sigma|^2 \int {\rm d}q_\perp q_\perp^{D-3} f'\left(\frac{q_{\|}}{T^{1/z}}\right) \sim |\Sigma|^2 T^{(z+D-5)/z}, \quad \text{(B.11)}$$

which itself depends on the self-energy. The self-energy at $\omega_m \sim T$ but $\omega_m \neq \pi T$ contains two contributions: the static one, $\Sigma_s \propto T^{1-\beta(3-D)}$, and the dynamical one, $\Sigma_d \propto T^{(z+D-3)/z}$. If $\beta > 1/z$, $\Sigma_s \gg \Sigma_d$ and Σ in the equation above needs to be replaced by Σ_s and vice versa for $\beta < 1/z$. For $\beta > 1/z$, the ratio of the remainder to the first (static) term in equation (B.7) scales as

$$\tilde{R}(T)/\Sigma_s \propto \Sigma_s T^{(z+D-5)/z} \propto T^{(2z+D-5)/z-\beta(3-D)}. \quad \text{(B.12)}$$

Limiting our consideration to $D = 2,3$ and $z = 2,3$ cases, we notice that the only situation when the ratio in the equation above does not necessarily go to zero at $T \to 0$ is $D = z = 2$ (a spin/charge density-wave phase transition in 2D). In this case, the right-hand-side scales as $T^{1/2-\beta}$ and therefore diverges if $\beta > 1/2$. For $\beta < 1/z$, Σ in equation (B.11) is to be replaced by Σ_s, which gives for the ratio

$$\tilde{R}(T)/\Sigma_s \propto \Sigma_d^2 T^{(z+D-5)/z}/\Sigma_s \propto T^{(2z+3D-11)/z+\beta(3-D)}. \quad \text{(B.13)}$$

Again, the only case when the ratio does not vanish at $T \to 0$ is $D = z = 2$.

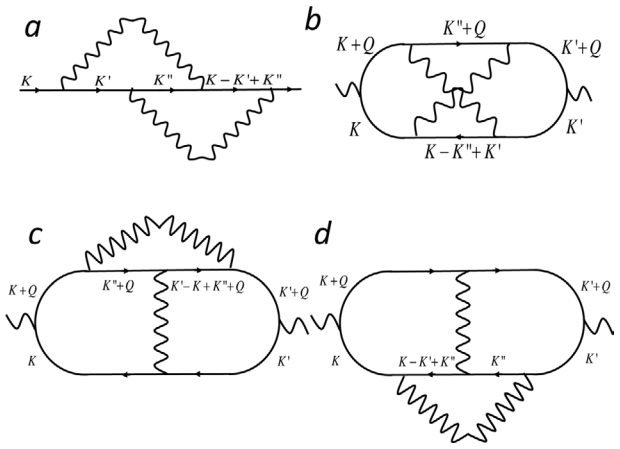

Figure C1. An example of the self-energy diagram (a) and the conductivity diagrams ((b)–(d)), which it generates.

Appendix C. First-Matsubara-frequency rule for vertex corrections to conductivity

In this appendix, we demonstrate how FMFR for the self-energy transforms into an analogous rule for the vertex corrections to the conductivity. This will be done by employing the Ward-type relations between the partial self-energy (as defined by equation (4.12) and (4.13)) and current vertex. As an example, we will consider a particular self-energy diagram (diagram (a) in figure C1):

$$\Sigma_K = \sum_{K',K''} G_{K'} G_{K''} G_{K-K'+K''} U_{\mathbf{k}-\mathbf{k}'} U_{\mathbf{k}'-\mathbf{k}''}. \quad \text{(C.1)}$$

We will actually need the difference between the self-energy in the equation above and the one in which the frequency of the incoming fermion is shifted by the frequency of the external field:

$$\Sigma_{K+Q} = \sum_{K',K''} G_{K'+Q} G_{K''+Q} G_{K-K'+K''+Q} U_{\mathbf{k}-\mathbf{k}'} U_{\mathbf{k}'-\mathbf{k}''}. \quad \text{(C.2)}$$

In the notations of appendix A,

$$\Delta\Sigma_{K,Q} \equiv \Sigma_K - \Sigma_{K+Q} \quad \text{(C.3)}$$

with $Q = (\mathbf{0}, q_0)$. Following [140] and [34], we use an identity

$$x_1x_2x_3 - y_1y_2y_3 = y_1x_3(x_2 - y_2) + y_1y_2(x_3 - y_3) + x_2x_3(x_1 - y_1) \quad \text{(C.4)}$$

to re-write $\Delta\Sigma_{K,Q}$ as a sum of three terms:

$$\Delta\Sigma_{K,Q} = \Delta\Sigma^{(b)}_{K,Q} + \Delta\Sigma^{(c)}_{K,Q} + \Delta\Sigma^{(d)}_{K,Q}, \tag{C.5}$$

where

$$\Delta\Sigma^{(b)}_{K} = \sum_{K',K''} G_{K'+Q}G_{K-K'+K''}(G_{K''} - G_{K''+Q})U_{\mathbf{k}-\mathbf{k}'}U_{\mathbf{k}'-\mathbf{k}''}, \tag{C.6a}$$

$$\Delta\Sigma^{(c)}_{K} = \sum_{K',K''} G_{K'+Q}G_{K''+Q}\big(G_{K-K'+K''} - G_{K-K'+K''+Q}\big)U_{\mathbf{k}-\mathbf{k}'}U_{\mathbf{k}'-\mathbf{k}''}, \tag{C.6b}$$

$$\Delta\Sigma^{(d)}_{K} = \sum_{K',K''} G_{K''}G_{K-K'+K''}\big(G_{K'} - G_{K'+Q}\big)U_{\mathbf{k}-\mathbf{k}'}U_{\mathbf{k}'-\mathbf{k}''}. \tag{C.6c}$$

In equation (C.6*a*), we relabel $K' \leftrightarrow K''$. In (C.6*b*), we also relabel $K' \leftrightarrow K''$ and then $K' + K - K'' \to K'$. Equation (C.6*c*) is left as is. Then

$$\Delta\Sigma^{(b)}_{K,Q} = \sum_{K',K''} G_{K''+Q}G_{K-K''+K'}\big(G_{K'} - G_{K'+Q}\big)U_{\mathbf{k}-\mathbf{k}''}U_{\mathbf{k}'-\mathbf{k}''} = \sum_{\hat{\mathbf{k}}'} \Delta\mathcal{S}^{(b)}_{K,Q;\mathbf{k}'}, \tag{C.7a}$$

$$\Delta\Sigma^{(c)}_{K,Q} = \sum_{K',K''} G_{K''+Q}G_{K-K''+K'+Q}\big(G_{K'} - G_{K'+Q}\big)U_{\mathbf{k}-\mathbf{k}'}U_{\mathbf{k}'-\mathbf{k}''} = \sum_{\hat{\mathbf{k}}'} \Delta\mathcal{S}^{(c)}_{K,Q;\hat{\mathbf{k}}'}, \tag{C.7b}$$

$$\Delta\Sigma^{(d)}_{K,Q} = \sum_{K',K''} G_{K''}G_{K-K'+K''}\big(G_{K'} - G_{K'+Q}\big)U_{\mathbf{k}-\mathbf{k}'}U_{\mathbf{k}'-\mathbf{k}''} = \sum_{\hat{\mathbf{k}}'} \Delta\mathcal{S}^{(d)}_{K,Q;\hat{\mathbf{k}}'}, \tag{C.7c}$$

where $\Delta S^{j}_{K,Q;\hat{\mathbf{k}}'} \equiv S^{j}_{K,\mathbf{k}'} - S^{j}_{K+Q,\mathbf{k}'}$ with $j = b \ldots d$ is the difference of the corresponding partial self-energies, defined by equations (4.12) and (4.13), and $\sum_{\hat{\mathbf{k}}'}$ is a shorthand for an integral over the FS: $\sum_{\hat{\mathbf{k}}'} \equiv (2\pi)^{-D}\int \mathrm{d}a_{\mathbf{k}'}/v_{\mathbf{k}'}$. The sum $\sum_j S^{j}_{K,\hat{\mathbf{k}}'}$ gives the partial self-energy in diagram (a).

Now we observe that the same combinations of the Green's functions and interactions appear in vertex diagrams (b)–(d), figure C1. Indeed, applying identity (A.2) to the two Green's functions adjacent to the right current vertex, we obtain for the sum of diagrams (b)–(d) (as in the main text, we assume a cubic lattice in the D-dimensional space)

$$\mathcal{K}(Q) = -\frac{1}{\mathrm{i}q_0 D}\sum_{j=b\ldots d}\sum_{K} G_K G_{K+Q}\mathbf{v}_{\mathbf{k}}\cdot\mathbf{L}^{(j)}_{K,Q}, \tag{C.8}$$

where

$$\mathbf{L}^{(b)}_{K,Q} = \sum_{K',K''} \mathbf{v}_{\mathbf{k}'}G_{K''+Q}G_{K-K''+K'}(G_{K'} - G_{K'+Q})U_{\mathbf{k}-\mathbf{k}''}U_{\mathbf{k}'-\mathbf{k}''}, \tag{C.9a}$$

$$\mathbf{L}^{(c)}_{K,Q} = \sum_{K',K''} \mathbf{v}_{\mathbf{k}'}G_{K''+Q}G_{K-K''+K'+Q}\big(G_{K'} - G_{K'+Q}\big)U_{\mathbf{k}-\mathbf{k}'}U_{\mathbf{k}'-\mathbf{k}''}, \tag{C.9b}$$

$$\mathbf{L}^{(d)}_{K,Q} = \sum_{K',K''} \mathbf{v}_{\mathbf{k}'}G_{K''}G_{K-K'+K''}\,(G_{K'} - G_{K'+Q})U_{\mathbf{k}-\mathbf{k}'}U_{\mathbf{k}'-\mathbf{k}''} \tag{C.9c}$$

are the renormalized current vertices. Comparing equations (C.7*a*)–(C.7*c*) and (C.9*a*)–(C.9*c*), we obtain the relations between the current vertices and partial self-energies:

$$\mathbf{L}^{(b-d)}_{K,Q} = \sum_{\hat{\mathbf{k}}'} \mathbf{v}_{\mathbf{k}'}\Delta\mathcal{S}^{(b-d)}_{K,Q;\hat{\mathbf{k}}'} \tag{C.10}$$

and thus

$$\mathcal{K}(Q) = -\frac{1}{\mathrm{i}q_0 D}\sum_{K,\hat{\mathbf{k}}'} G_K G_{K+Q}\mathbf{v}_{\mathbf{k}}\cdot\mathbf{v}_{\mathbf{k}'}\Delta\mathcal{S}_{K,Q;\hat{\mathbf{k}}'}. \tag{C.11}$$

Within the local approximation, the current vertices do not depend on the fermion dispersions. Then the product of two Green's functions in equation (C.11) can be integrated over $\varepsilon_{\mathbf{k}}$ with the result

$$\mathcal{K}(Q) = \frac{\pi}{\mathrm{i}q_0^2 D}T\sum_{k_0}\big[\mathrm{sgn}(k_0+q_0) - \mathrm{sgn}k_0\big] \times \sum_{\hat{\mathbf{k}},\hat{\mathbf{k}}'} \mathbf{v}_{\mathbf{k}}\cdot\mathbf{v}_{\mathbf{k}'}\big(\mathcal{S}_{K,\mathbf{k}'} - \mathcal{S}_{K+Q,\mathbf{k}'}\big). \tag{C.12}$$

For $q_0 = 2\pi T$, the Matsubara sum in the equation above contains only one term ($k_0 = -\pi T$), and therefore the first and second partial self-energy are evaluated at $k_0 = -\pi T$ and $k_0 + q_0 = \pi T$, correspondingly. Recalling that $K = (\mathbf{k}, -\pi T)$ and $K + Q = (\mathbf{k}, \pi T)$, and that the partial self-energy obeys FMFR (equation (4.14)), we find that $\mathcal{K}(2\pi T)$ is reduced to a T-independent constant:

$$\mathcal{K}(2\pi T) = \frac{1}{2\pi\mathrm{i}TD}\sum_{\hat{\mathbf{k}},\hat{\mathbf{k}}'} \mathbf{v}_{\mathbf{k}}\cdot\mathbf{v}_{\mathbf{k}'}\big(\mathcal{S}_{(\mathbf{k},-\pi T),\mathbf{k}'} - \mathcal{S}_{(\mathbf{k},\pi T),\mathbf{k}'}\big) = -\frac{1}{D}\sum_{\hat{\mathbf{k}},\hat{\mathbf{k}}'} \mathbf{v}_{\mathbf{k}}\cdot\mathbf{v}_{\mathbf{k}'}\mu_{\mathbf{k},\mathbf{k}'}. \tag{C.13}$$

The corresponding Matsubara conductivity $\sigma(2\pi T, T) = -e^2K(2\pi T)/2\pi T$ scales as $1/T$, in agreement with equation (4.31).

The same procedure can be extended to other vertex-correction diagrams. Namely, one can always find a correspondence between a particular self-energy diagram and a set of vertex diagrams for the conductivity which it generates. FMRF for the conductivity then follows from the analogous rule for the (partial) self-energy.

References

[1] Basov D N and Timusk T 2005 *Rev. Mod. Phys.* **77** 721
[2] Basov D N, Averitt R D, van der Marel D, Dressel M and Haule K 2011 *Rev. Mod. Phys.* **83** 471
[3] Abrikosov A A 1988 *Fundamentals of the Theory of Metals* (Amsterdam: North Holland)
[4] Maslov D L, Yudson V I and Chubukov A V 2011 *Phys. Rev. Lett.* **106** 106403
[5] Patel A A, Strack P and Sachdev S 2015 *Phys. Rev.* B **92** 165105
[6] Eberlein A, Mandal I and Sachdev S 2016 *Phys. Rev.* B **94** 045133
[7] Beach R T and Christy R W 1977 *Phys. Rev.* B **16** 5277

[8] Parkins G R, Lawrence W E and Christy R W 1981 *Phys. Rev.* B **23** 6408
[9] Van Der Marel D, Molegraaf H J A, Zaanen J, Nussinov Z, Carbone F, Damascelli A, Eisaki H, Greven M, Kes P H and Li M 2003 *Nature* **425** 271
[10] Dodge J S, Weber C P, Corson J, Orenstein J, Schlesinger Z, Reiner J W and Beasley M R 2000 *Phys. Rev. Lett.* **85** 4932
[11] Kamal S, Kim D M, Eom C B and Dodge J S 2006 *Phys. Rev.* B **74** 165115
[12] Nagel U *et al* 2012 *Proc. Natl Acad. Sci. USA* **109** 19161
[13] Mirzaei S I *et al* 2013 *Proc. Natl Acad. Sci. USA* **110** 5774
[14] Stricker D, Mravlje J, Berthod C, Fittipaldi R, Vecchione A, Georges A and van der Marel D 2014 *Phys. Rev. Lett.* **113** 087404
[15] Tytarenko A, Huang Y, de Visser A, Johnston S and van Heumen E 2015 *Sci. Rep.* **5** 12421
[16] Reber T J *et al* 2015 arXiv:150901611
[17] Gurzhi R N 1959 *Sov. Phys.—JETP* **35** 673
[18] Fowler M and Prange R E 1965 *Physics* **1** 315
[19] Martin G W, Maslov D L and Reizer M Y 2003 *Phys. Rev.* B **68** 241309
[20] Chubukov A V and Maslov D L 2012 *Phys. Rev.* B **86** 155136
[21] Maslov D L and Chubukov A V 2012 *Phys. Rev.* B **86** 155137
[22] Hlubina R and Rice T M 1995 *Phys. Rev.* B **51** 9253
[23] Hartnoll S A, Hofman D M, Metlitski M A and Sachdev S 2011 *Phys. Rev.* B **84** 125115
[24] Chubukov A V, Maslov D L and Yudson V I 2014 *Phys. Rev.* B **89** 155126
[25] Basov D N, Liang R, Dabrowski B, Bonn D A, Hardy W N and Timusk T 1996 *Phys. Rev. Lett.* **77** 4090
[26] Puchkov A V, Basov D N and Timusk T 1996 *J. Phys.: Condens. Matter* **8** 10049
[27] Norman M R and Chubukov A V 2006 *Phys. Rev.* B **73** 140501
[28] Horowitz G T, Santos J E and Tong D 2012 *J. High Energy Phys.* JHEP11(2012)168
[29] Vegh D 2013 arXiv:1301.0537
[30] Donos A and Gauntlett J P 2014 *J. High Energy Phys.* JHEP5(2014)40
[31] Langley B W, Vanacore G and Phillips P W 2015 *J. High Energy Phys.* JHEP10(2015)163
[32] Davison R A, Goutéraux B and Hartnoll S A 2015 *J. High Energy Phys.* JHEP10(2015)112
[33] Khveshchenko D V 2015 *Lithuanian J. Phys.* **208** 215
[34] Maebashi H and Fukuyama H 1997 *J. Phys. Soc. Japan* **66** 3577
[35] Maebashi H and Fukuyama H 1998 *J. Phys. Soc. Japan* **67** 242
[36] Lawrence W E and Wilkins J W 1973 *Phys. Rev.* B **7** 2317
[37] Lawrence W E 1976 *Phys. Rev.* B **13** 5316
[38] Riseborough P S 1983 *Phys. Rev.* B **27** 5775
[39] Gurzhi R N, Kopeliovich A I and Rutkevich S B 1980 *Sov. Phys.—JETP Lett.* **32** 336
[40] Gurzhi R, Kopeliovich A and Rutkevich S B 1982 *Sov. Phys.—JETP* **56** 159
[41] Gurzhi R N, Kopeliovich A I and Rutkevich S B 1987 *Adv. Phys.* **36** 221
[42] Rosch A and Howell P C 2005 *Phys. Rev.* B **72** 104510
[43] Rosch A 2006 *Ann. Phys.* **15** 526
[44] Pal H K, Yudson V I and Maslov D L 2012 *Phys. Rev.* B **85** 085439
[45] Pal H K, Yudson V I and Maslov D L 2012 *Lithuanian J. Phys.* **52** 142
[46] Briskot U, Schütt M, Gornyi I V, Titov M, Narozhny B N and Mirlin A D 2015 *Phys. Rev.* B **92** 115426
[47] Holstein T 1964 *Ann. Phys.* **29** 410
[48] Gornyi I V and Mirlin A D 2004 *Phys. Rev.* B **69** 045313
[49] Farid A K and Mishchenko E G 2006 *Phys. Rev. Lett.* **97** 096604
[50] Altshuler B L and Aronov A G 1985 *Electron–Electron Interactions in Disordered Systems* ed A L Efros and M Pollak (Amsterdam: North-Holland) p 1
[51] Varlamov A and Larkin A 2005 *Theory of Fluctuations in Superconductors* (Oxford: Oxford University Press)
[52] Hruska M and Spivak B 2002 *Phys. Rev.* B **65** 033315
[53] Andreev A V, Kivelson S A and Spivak B 2011 *Phys. Rev. Lett.* **106** 256804
[54] Gantmakher V F and Levinson Y B 1987 *Carrier Scattering in Metals and Semiconductors* (Amsterdam: North-Holland)
[55] Baber W G 1937 *Proc. R. Soc. Lond.* A **158** 383
[56] Hosur P and Qi X 2013 *C. R. Phys.* **14** 857 and references therein
[57] Müller M and Sachdev S 2008 *Phys. Rev.* B **78** 115419
[58] Tomadin A, Vignale G and Polini M 2014 *Phys. Rev. Lett.* **113** 235901
[59] Forcella D, Zaanen J, Valentinis D and van der Marel D 2014 *Phys. Rev.* B **90** 035143
[60] Narozhny B N, Gornyi I V, Titov M, Schütt M and Mirlin A D 2015 *Phys. Rev.* B **91** 035414
[61] Levitov L and Falkovich G 2006 *Nat. Phys.* **12** 672
[62] Bandurin D A *et al* 2016 *Science* **351** 1055
[63] Lin X, Fauqué B and Behnia K 2015 *Science* **349** 945
[64] Mikheev E, Raghavan S, Zhang J Y, Marshall P B, Kajdos A P, Balents L and Stemmer S 2016 *Sci. Rep.* **6** 20865
[65] Maiti S, Yudson V I and Maslov D L unpublished
[66] Epifanov Y N, Levanyuk A P and Levanyuk G M 1981 *Sov. Phys. Solid State* **23** 391
[67] Epifanov Y N, Levanyuk A P and Levanyuk G M 1981 *Ferroelectrics* **35** 199
[68] Mahan G D 2000 *Many-Particle Physics* 3rd edn (New York: Plenum)
[69] Berthod C, Mravlje J, Deng X, Žitko R, van der Marel D and Georges A 2013 *Phys. Rev.* B **87** 115109
[70] Dang H T, Mravlje J, Georges A and Millis A J 2015 *Phys. Rev. Lett.* **115** 107003
[71] Scheffler M, Dressel M, Jourdan M and Adrian H 2005 *Nature* **438** 1135
[72] Jacobsen C S, Tanner D B, Williams J M, Geiser U and Wang H H 1987 *Phys. Rev.* B **35** 9605
[73] Dumm M, Faltermeier D, Drichko N, Dressel M, Mézière C and Batail P 2009 *Phys. Rev.* B **79** 195106
[74] Dressel M 2011 *J. Phys.: Condens. Matter* **23** 293201
[75] Eliashberg G M 1962 *Sov. Phys.—JETP* **14** 886
[76] Eliashberg G M 1962 *Sov. Phys.—JETP* **15** 1151
[77] Dressel M and Grüner G 2002 *Electrodynamics of Solids* (Cambridge: Cambridge University Press)
[78] Chubukov A V and Maslov D L 2003 *Phys. Rev.* B **68** 155113
[79] Gangadharaiah S, Maslov D L, Chubukov A V and Glazman L I 2005 *Phys. Rev. Lett.* **94** 156407
[80] Chubukov A V, Maslov D L, Gangadharaiah S and Glazman L I 2005 *Phys. Rev.* B **71** 205112
[81] Yang J, Hwang J, Timusk T, Sefat A S and Greedan J E 2006 *Phys. Rev.* B **73** 195125
[82] Schneider M *et al* 2014 *Phys. Rev. Lett.* **112** 206403
[83] Timusk T 2016 private communication
[84] Lifshitz E M and Pitaevskii L P 1981 *Physical Kinetics* (Burlington: Butterworth-Heinemann)
[85] Engelsberg S and Simpson G 1970 *Phys. Rev.* B **2** 1657
[86] Engelsberg S 1978 *Phys. Rev.* B **18** 966
[87] Wasserman A and Springford M 1996 *Adv. Phys.* **45** 471
[88] Varma C M, Littlewood P B, Schmitt-Rink S, Abrahams E and Ruckenstein A E 1989 *Phys. Rev. Lett.* **63** 1996
[89] Varma C M, Nussinov Z and van Saarloos W 2002 *Phys. Rep.* **361** 267
[90] Hertz J A 1976 *Phys. Rev.* B **14** 1165
[91] Millis A J 1993 *Phys. Rev.* B **48** 7183
[92] Moriya T 1985 *Spin Fluctuations in Itinerant Electron Magnetism* (Berlin: Springer)

[93] Allen P B and Mitrovic B B 1982 *Solid State Physics* vol 37, ed H Ehrenreich *et al* (London: Academic Press) pp 2–92
[94] Luttinger J M 1961 *Phys. Rev.* **121** 942
[95] Adamov Y, Gornyi I V and Mirlin A D 2006 *Phys. Rev.* B **73** 045426
[96] Wang Y, Abanov A G, Altshuler B L, Yuzbashyan E A and Chubukov A V 2016 *Phys. Rev. Lett.* **117** 157001
[97] Sulewski P E, Sievers A J, Maple M B, Torikachvili M S, Smith J L and Fisk Z 1988 *Phys. Rev.* B **38** 5338
[98] Katsufuji T and Tokura Y 1999 *Phys. Rev.* B **60** 7673
[99] Scheffler M *et al* 2013 *Phys. Status Solidi* b **250** 439
[100] Hewson A C 1993 *The Kondo Problem to Heavy Fermions* (Cambridge: Cambridge University Press)
[101] Mackenzie A P and Maeno Y 2003 *Rev. Mod. Phys.* **75** 657
[102] Pomeranchuk I J 1958 *Sov. Phys.—JETP* **8** 361
[103] Fradkin E, Kivelson S A, Lawler M J, Eisenstein J P and Mackenzie A P 2010 *Ann. Rev. Condens. Matter Phys.* **1** 153
[104] Borzi R A, Grigera S A, Farrell J, Perry R S, Lister S J S, Lee S L, Tennant D A, Maeno Y and Mackenzie A P 2007 *Science* **315** 214
[105] Hu J and Xu C 2012 *Phys. C: Supercond.* **481** 215
[106] Fernandes R M, Chubukov A V and Schmalian J 2014 *Nat. Phys.* **10** 97
[107] Gallais Y and Paul I 2016 *C. R. Phys.* **17** 113
[108] Cyr-Choinière O, Grissonnanche G, Badoux S, Day J, Bonn D A, Hardy W N, Liang R, Doiron-Leyraud N and Taillefer L 2015 *Phys. Rev.* B **92** 224502 and references therein
[109] Abanov A, Chubukov A V and Schmalian J 2003 *Adv. Phys.* **52** 119
[110] Mathon J 1968 *Proc. R. Soc.* A **306** 355
[111] Kim Y B, Furusaki A, Wen X G and Lee P A 1994 *Phys. Rev.* B **50** 17917
[112] Schofield A J 1999 *Contemp. Phys.* **40** 95
[113] Chubukov A V and Maslov D L unpublished
[114] Mills D and Lederer P 1966 *J. Physi. Chem. Solids* **27** 1805
[115] Rice M 1967 *Phys. Lett.* A **26** 86
[116] Schindler A I and Rice M J 1967 *Phys. Rev.* **164** 759
[117] Kaiser A B and Doniach S 1970 *Int. J. Magn.* **1** 11
[118] Oomi G, Kagayama T and Ōnuki Y 1998 *J. Alloys Compd.* **271–3** 482
[119] Nicklas M, Brando M, Knebel G, Mayr F, Trinkl W and Loidl A 1999 *Phys. Rev. Lett.* **82** 4268
[120] Niklowitz P G, Beckers F, Lonzarich G G, Knebel G, Salce B, Thomasson J, Bernhoeft N, Braithwaite D and Flouquet J 2005 *Phys. Rev.* B **72** 024424
[121] Brando M, Duncan W J, Moroni-Klementowicz D, Albrecht C, Grüner D, Ballou R and Grosche F M 2008 *Phys. Rev. Lett.* **101** 026401
[122] Brando M, Belitz D, Grosche F M and Kirkpatrick T R 2016 *Rev. Mod. Phys.* **88** 025006
[123] El Azrak A, Nahoum R, Bontemps N, Guilloux-Viry M, Thivet C, Perrin A, Labdi S, Li Z Z and Raffy H 1994 *Phys. Rev.* B **49** 9846
[124] Mena F P, van der Marel D, Damascelli A, Fäth M, Menovsky A A and Mydosh J A 2003 *Phys. Rev.* B **67** 241101
[125] Qazilbash M M, Hamlin J J, Baumbach R E, Zhang L, Singh D J, Maple M B and Basov D N 2009 *Nat. Phys.* **5** 647
[126] Bruin J A N, Sakai H, Perry R S and Mackenzie A P 2013 *Science* **339** 804
[127] Hussey N E 2008 *J. Phys.: Condens. Matter* **20** 123201
[128] Hussey N E, Cooper R A, Xu X, Wang Y, Mouzopoulou I, Vignolle B and Proust C 2011 *Phil. Trans. R. Soc.* A **369** 1626
[129] Rosch A 1999 *Phys. Rev. Lett.* **82** 4280
[130] Patel A A and Sachdev S 2014 *Phys. Rev.* B **90** 165146
[131] Hartnoll S A, Mahajan R, Punk M and Sachdev S 2014 *Phys. Rev.* B **89** 155130
[132] Eliashberg G M 1960 *Sov. Phys.—JETP* **11** 696
[133] Eliashberg G M 1963 *Sov. Phys.—JETP* **16** 780
[134] Pethick C J and Carneiro G M 1973 *Phys. Rev.* A **7** 304
[135] Chubukov A V, Maslov D L and Millis A J 2006 *Phys. Rev.* B **73** 045128
[136] Abel W R, Anderson A C, Black W C and Wheatley J C 1966 *Phys. Rev.* **147** 111
[137] Greywall D S 1983 *Phys. Rev.* B **27** 2747
[138] Stewart G R 1984 *Rev. Mod. Phys.* **56** 755
[139] McCollam A, Julian S R, Rourke P M C, Aoki D and Flouquet J 2005 *Phys. Rev. Lett.* **94** 186401
[140] Götze W and Wölfle P 1972 *Phys. Rev.* B **6** 1226
[141] Murzin S S, Dorozhkin S I, Landwehr G and Gossard A C 1998 *Sov. Phys.—JETP Lett.* **67** 113
[142] Klimin S N, Tempere J, van der Marel D and Devreese J T 2012 *Phys. Rev.* B **86** 045113
[143] Lee S S 2009 *Phys. Rev.* B **80** 165102
[144] Chubukov A V 2010 *Physics* **3** 70
[145] Paul I and Maslov D L unpublished
[146] Pfleiderer C, Uhlarz M, Hayden S M, Vollmer R, Lohneysen H V, Bernhoeft N R and Lonzarich G G 2001 *Nature* **412** 58
[147] Smith R P, Sutherland M, Lonzarich G G, Saxena S S, Kimura N, Takashima S, Nohara M and Takagi H 2008 *Nature* **455** 1220
[148] Lee Y S, Yu J, Lee J S, Noh T W, Gimm T H, Choi H Y and Eom C B 2002 *Phys. Rev.* B **66** 041104
[149] Geiger D, Pracht U S, Dressel M, Mravlje J, Schneider M, Gegenwart P and Scheffler M 2016 *Phys. Rev.* B **93** 165131